Cape Peninsula
University of Technology

Effect of synthesis duration and HCl acid concentration on the formation of hydrothermally synthesised TiO$_2$ nanoparticles

by

Jules Lind

Thesis submitted in fulfilment of the requirements for the degree

Master of Technology: Chemical Engineering

in the FACULTY OF ENGINEERING

at the Cape Peninsula University of Technology

Supervisor: Prof. Veruscha Fester

Cape Town Campus

July 2015

DECLARATION

I, Jules Lind, declare that the contents of this thesis represent my own unaided work, and that the thesis has not previously been submitted for academic examination towards any qualification. Furthermore, it represents my own opinions and not necessarily those of the Cape Peninsula University of Technology.

25/08/2015

Signed   **Date**

ABSTRACT

It is known when synthesising nanomaterial on laboratory scale, a variation in a single synthesis parameter may alter the product. Numerous synthesis techniques have been employed in the synthesis of titanium dioxide with varying phase, size and shape. It was found that changes in the phase directly affect their properties and application, such as treating of textile wastewater by photodegradation. However, when synthesising nanoparticles, changes to any reaction parameters and/or kinetics can have a desirable or undesirable effect on titanium dioxide nanoparticles. There is therefore a need to understand how HCl acid concentration (homogeneous catalyst) and shortened gel formation duration affect synthesis of TiO_2 nanoparticles and photocatalytic properties.

A sol-gel followed by hydrothermal treatment was employed to synthesise 2.8 grams of titanium dioxide nanorods for the duration of 96 hours, initially. A systematic study was conducted to exploit reaction kinetics by varying HCl acid concentration (3, 4, 5 molar), water feed for TiO_2 gel formation (72, 24, 12 hours), and hydrothermal treatment time for the transformation of gel to crystalline TiO_2 (1–20 hours). The photocatalytic activity of synthesised TiO_2 nanoparticle was evaluated, when irradiated with a UV-C bulb to degrade an industrial textile dye, methylene blue.

Systematic studies were successful in identifying the effects HCl acid concentration, gel formation time and lengthened hydrothermal treatment time have on TiO_2 nanoparticles' phase, size and shape. Increased HCl concentrations for shortened gel formation times resulted in mixed phases of TiO_2, decreases in particle size and particle shape deformed from nanorods. Increased photocatalytic activity was found for a decrease in the rutile and increase in the brookite phase percentage, but this plateaued after 42% brookite phase. Furthermore, lengthened hydrothermal treatment assisted in phase transformation of particles synthesised at shortened gel formation times for high HCl acid concentrations. Pure rutile TiO_2 was synthesised at a sixth of the initial synthesis time. Furthermore, the effects of changes in nanoparticles on the photocatalytic activity was discussed. Moreover, exploiting reaction kinetics resulted in the synthesis of a more efficient photocatalytically active TiO_2 nanoparticle sample at shortened synthesis time.

Cape Peninsula
University of Technology

DEDICATION

This thesis is dedicated to three family members, for their love and support for the duration of my tertiary studies:

- Hester Lind
- Sheldon Lind
- Garth Lind

I declare all honour and glory to my God, for his love that has guided and upheld me in all my trials faced.

ACKNOWLEDGEMENTS

I would like to thank the following people and organizations for their input and aid in the completion of this thesis:

- Samantha Marais, I thank you and love you for your strength and support.
- Lastly, to my friend, Pieter Wynand du Plessis, for his ongoing advice, inspiration, friendship and support for the past eight years, this helped me throughout my tertiary studies.

TABLE OF CONTENTS

Chapter 1

Chapter 2

Chapter 4

Chapter 5

Appendices

LIST OF FIGURES

Cape Peninsula
University of Technology

Cape Peninsula
University of Technology

Cape Peninsula
University of Technology

Cape Peninsula
University of Technology

Cape Peninsula
University of Technology

LIST OF TABLES

TERMS AND CONCEPTS

- Ageing: first synthesis step of TiO_2 nanoparticles that consists of first the breaking of existing chemical bonds in solution followed by the formation of new chemical bonds by the aid of reagent.

- Agglomeration: the self-assembly of a heaped mass of nuclei suspended in a solution; however these nuclei are unstable as they have not taken on a form as found for aggregation, and can be viewed as a rounded mass suspension in solution; breaking of adhesive forces binding them is termed 'rupturing'.

- Aggregation: the self-assembly of stable nuclei that constitute the forming of nanoparticles, which can resist compression stress; breaking of adhesive forces binding them is termed 'milling'.

- Amorphous: refers to nanoparticles that lack form and specific chemical structure with regard to the atom orientation.

- Anatase: one of the three phases that TiO_2 nanomaterial possesses. Anatase is the second thermally stable of the TiO_2 nanomaterials; however the lack of thermal stability is compensated for by the photocatalytic properties that this phase possesses.

- Batch system: a process where no material is removed from or charged to the system during operations.

- Brookite: Brookite is the least thermally stable of TiO_2 nanomaterial; however the lack of thermal stability is compensated for by the photocatalytic properties that this phase possesses. Furthermore, this phase is one commonly found in nature and possesses a complex phase.

- Coalescence: a process of particles coming into contact and fusing together.

- Condensation: also referred to as polycondensation (Yoldas, 1986); the instantaneous second stage of the sol-gel reaction that is observed during the formation of the gel; the chemical reaction of two molecules that binds to form one molecule.

- Crystalline: nanoparticles that possess a distinct geometric shape and chemical structure orientation of atoms.

- Deprotonation: a chemical process that often follows protonation, whereby protons are removed, often by dehydration of metal oxide molecules, resulting in structural changes.

- Dissolution: A process by which a solid is dissolved into a solvent in making up a solution, can be referred to as solvation.

- Hydrolysis: first reaction that is observed after the sol is formed; the addition of water for decomposition of titanium isopropoxide in the presence of a homogeneous catalyst.

- Hydrothermal synthesis: technique used in crystallization by means of elevated temperatures or vapour pressure; crystallization step of the final stage for TiO_2 rutile nanoparticles.

- Nanomaterial sciences: the study of the field of material sciences, of which nano-sized material and their morphologies are the focus.

- Nucleation: the change in physical state induced by changes in temperature of pressure of natural or unnatural systems. This can be explained by the formation of water droplets in clouds for gaseous water to liquid water droplets.

- Phase: the use of phase in this research makes reference to the geometric arrangement of molecules in a crystalline material formed by TiO_2 nanoparticles synthesised; such physical phases are brooktite, anatase, and rutile.

- Precursor: the initial chemical compound that is used in a chemical reaction in the formation of a desired product.

- Protonation: a chemical process by the addition of a proton (H^+) to a molecule.

- Reaction kinetics: the study of the rate at which a reaction takes place, by varying experimental conditions.

- Reaction parameters: the physical parameter of the system that can be altered to vary reaction kinetics.

- Rutile: one of three phases that TiO_2 nanomaterial possesses. Rutile is the desired phase as it is the most thermally stable phase.

- Surface chemistry: the interaction of two phases on surfaces by physical and chemical properties simulated by chemical reactions.

LIST OF SYMBOLS

Symbols	Name of Symbol	Unit
E_a	Activation energy	J/mol
A	Agitation frequency	s^{-1}
α	Alpha	mol/m^2
v	Atomic volume of solute	m^3
A_{length}	Average particle length	nm
k	Boltzmann constant	J/K
dC_B	Change in concentration of chemical B	mol/m^3
dt	Change in time	sec
C_A	Concentration of chemical A	mol/m^3
$R*$	Critical radius	nm
S	Degree of supersaturation	Unit less
C	Difference between C - C_{eq}	mol/m^3
R	Gas Constant	J/(kg.K)
ΔG^*	Gibbs free energy	J
$-r'_A$	Reaction rate of chemical A consumed in the presences of a catalyst	s^{-1}
k_A	Reaction rate constant of chemical A	s^{-1}
$k_A(T)$	Specific rate constant at a given temperature	s^{-1}
C	Solute concentration	mol/m^3
C_∞	Solute concentration at infinity	mol/m^3
C_{eq}	Solute concentration at equilibrium	mol/m^3
σ_{SL}	Surface tension of solid-liquid interface	N/m
T	Temperature	K

LIST OF SYMBOLS

Symbols	Name of Symbol	Unit
t_{gel}	Gel formation time	hrs

This chapter provides background information on the synthesis of TiO_2 (titanium dioxide) bulk and nanoparticles, identifies the research problem and states the aims and objectives and the expected research outcomes.

1.1   Background

The production of the semiconductor, photocatalyst metal oxide, titanium dioxide (TiO_2), started in 1948; its initial use was in military aircraft, thereafter studies of this material led to wider applications (Kroschwitz & Seidel, 2007: 94-98). Titanium dioxide was given the name 'titan', after the Titans of Greek mythology, by a German chemist in 1975 (Kroschwitz & Seidel, 2007: 94). Titanium dioxide was originally mined and processed to form TiO_2 and used as pigments; the ore containing the element titanium is ilmenite ($FeTiO_3$) (Kroschwitz |& Seide: 94). This ore was treated with sulphuric acid, where digestion of the ore and crystallisation took place, resulting in the extraction of iron found in the ore in the form of iron sulphate; hence the process name, sulphate process (Kroschwitz & Seidel, 2007: 94). The raw product of the digestion underwent hydrolysis, filtration and washing to remove waste sulphuric acid and to retrieve the desired TiO_2 material. Furthermore, the TiO_2 was treated by calcination and surface treatment (Kroschwitz & Seidel, 2007: 94). Thereafter usable TiO_2 bulk material was formed (Kroschwitz & Seidel, 2007). The sulphate process was developed to produce a higher grade of TiO_2 in the early years of the 1900s; in the years that followed a purer form of TiO_2 and titanium metal, which was used to form alloys (Kroschwitz & Seidel, 2007: 94). As sciences evolved, so did the process used for retrieving a higher grade of TiO_2 from mined ore: this process was known as the chloride process (Kroschwitz & Seidel, 2007: 94).

Twenty to forty years later a secondary process was developed to obtain a purer form of TiO_2 bulk material with the possibility of being able to synthesis the metal titanium for applications. This process was given the name 'chlorine' process; this is where the natural or synthesised TiO_2 raw material was treated with chlorine and carbon in a chlorination step of the process, whereby the reaction taking place occurs as follows (Kroschwitz & Seidel, 2007: 97):

$$TiO_2 + 2C + 2Cl_2 \rightarrow 2CO + TiCl_4$$
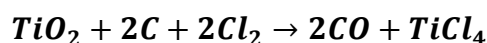
Equation 1.1

After the chlorination the waste chlorine is removed by purification and oxidation resulting in the formation of TiO_2 which is surface treated (Kroschwitz & Seidel, 2007: 98). Bulk TiO_2 material has been synthesised at 85% purity by oxidisation of $TiCl_4$ intermediate formed when using the chlorination process (Kroschwitz & Seidel, 2007: 98). Furthermore, greater controls over synthesis processes have been investigated to the point of being able to

control the molecular arrangement and chemical structure formed by TiO_2. It is at this point in the scientific evolution of synthesising TiO_2 nanoparticles that this research wishes to contribute to the knowledge of reducing synthesis time and controlling shape, size and phase.

The most viable choice of TiO_2 synthesis routes identified in the literature is a sol-gel synthesis producing amorphous material, followed by some form of heat treatment (Matthews, 1976; Wu et al., 2002; Cushing et al., 2004; Kolen'ko et al., 2006; Tahir et al., 2006; Su et al. ,2006; Ryu et al., 2006; Chen and Mao, 2007; Chen et al., 2011; Wu et al., 2011). Its properties, uses, and applications in day-to-day life have been highlighted in studies (Mogyorosi et al., 2003; Pavasupree et al., 2006; Nagarajan and Alan Hatton, 2008: 125; Dong et al., 2010; Gupta and Tripathi, 2011; Chen et al., 2011; Yang et al., 2012; Ede et al., 2012). However the fundamentals such as hydrothermal synthesis temperature (Yu et al., 2007) , ageing time (Yu et al., 2007), acids used (Wu et al., 2002), reaction pressure, precursor (Vorkapic and Matsoukas, 1998), and molarity of homogenous catalyst still require further investigation (Li et al., 2003).

When synthesising nanomaterial on laboratory scale, a variation in a single synthesis parameter may alter the product (Nagarajan and Alan Hatton, 2008). The alteration of the product can occur with regard to the size, shape, and type of phase, however still producing TiO_2.

Two precursors, titanium (IV) butoxide, and titanium (IV) isopropoxide were found to be favourable in the production of TiO_2 (Vorkapic and Matsoukas, 1998; Wu et al., 2002; Ryu et al., 2006; Chen and Mao, 2007; Bandyopadhyay, 2008: 1-2; Chen et al., 2011). Titanium isopropoxide precursor was favoured for synthesising TiO_2 nanoparticles due to the mean particle size distribution obtained (Vorkapic and Matsoukas, 1998), high reactivity by hydrolysis (Mahshid et al., 2007), and costs (Yoldas, 1986).

The hydrolysis temperature was varied for sol (initial stage) synthesis stages (Vorkapic and Matsoukas, 1998). The peptization temperature was varied in gel and crystallization (final stages) stages (Vorkapic and Matsoukas, 1998). The hydrothermal treatment temperature (Chen et al., 2011) and hydrothermal treatment duration (Chen et al., 2011), was also investigated.

Hydrothermal treatment in an acidic medium yielded the formation of rutile and/or anatase nanoparticles depending on the type of acid used (Andersson et al., 2002), and its concentration (Tahir et al, 2006 Chen et al, 2011, Yu et al, 2012). Furthermore, three acids were used repeatedly in the studies for synthesising TiO_2, namely, nitric acid, hydrochloric acid and sulphuric acid (Lakshmi et al., 1997; Andersson et al., 2002; Wu et al., 2002; Kim et al., 2005; Tahir et al., 2006; Wang et al., 2007; Chen et al., 2011; Yu et al., 2012) (Chen et al., 2011, Wu et al., 2002, Wang et al., 2007, Yan et al., 2012, Kim et al., 2005, Tahir et al., 2006, Lakshmi et al., 1997, Andersson et al., 2002). The hydrothermal treatment temperature and the duration varied between 100 °C to 220 °C and 1 to 24 hours respectively (Ryu et al., 2006; Chen et al., 2011).

However, a systematic study relating to the reaction parameters for the ageing process in the optimisation of the formation of TiO_2 nanoparticles was not conducted.

Cape Peninsula
University of Technology

1.2 Aim and objectives

This study aims to exploit reaction kinetics to reduce the synthesis time for TiO_2, by increasing HCl acid concentration, decreasing gel formation time and increase hydrothermal treatment time, in order to evaluate the effects to phase, shape, size and photocatalytic activity, for changes made.

1.3 Significance

This research will provide manufacturers with knowledge of how to decrease the synthesis duration, which will lead to decreased costs and higher productivity. The knowledge attained from experiments will be used in developing a continuous hydrothermal synthesis strategy, to scale up production of these particles. The application of TiO_2 in hydrogen fuel cells (Gupta and Tripathi, 2011), expansion of TiO_2 applications for treating cancer (Arora et al., 2010), and the treatment of wastewater (Ilyas et al., 2011, Yang et al., 2012, Ede et al., 2012)) could be facilitated, as it is known that the high cost of TiO_2 has been the limiting factor to this research and the effective employment of these techniques.

1.4 Delineation

The use of other acids, other than hydrochloric acid, will not be studied and the concentration studied shall not be less than 3 molar. A set stirring speed of 220 RPM will be used. The variations in titanium precursor volume, concentration, and hydrothermal temperature have been researched; thus these variations will not be studied in this research.

1.5 Thesis layout

- Chapter 2 provides a detailed literature review of TiO_2 synthesis.

- Chapter 3 presents the technique followed for the synthesis and exploiting reaction kinetics of TiO_2.

- Chapter 4 presents the results obtained and the discussion thereof.

- Chapter 5 presents conclusions and contributions made of this study.

C_{hapter 2}

This chapter gives the background of the widely used titanium dioxide, chemical reaction kinetics (factor affecting rates) and particle nucleation and crystal growth fundamentals. Furthermore, it introduces nanoparticles and the techniques used to synthesise them, which incorporate the use of a catalyst. It gives an overview of the effects on TiO_2 nanoparticles' phase, size, shape and application, for changes made to sol-gel synthesis and hydrothermal treatment time. Furthermore characterisation techniques for investigating synthesised TiO_2 nanoparticles are also provided. The effect of synthesis parameters on particle phase, shape and size is reviewed as well as its affects on the photocatalysis of textile effluent.

2. Literature review

Titanium dioxide, otherwise denoted as TiO_2, is a white crystalline powder that has been used in the generation of hydrogen in hydrogen fuel cell applications (Fujishima & Honda, 1972, Gupta & Tripathi, 2011), and shows promising applications in both the medical field (Arora et al., 2010) and wastewater treatment (Han et al., 2009). TiO_2 is a metal oxide that has four commonly known chemical structures: rutile, anatase, brookite, and TiO_2 (B) (Gupta & Tripathi, 2011); despite these polymorphs, an additional two rutile high-pressure polymorph forms have been synthesised, namely TiO_2 (*II*) and TiO_2 (H).

TiO_2 nanoparticles of the phase rutile are the most thermodynamically stable. These nanoparticles possess a tetragonal structure that contains 6 atoms per the unit cell; they act poorly as a photocatalyst, but are more stable for most temperatures and pressure below 60 kbar (Bandyopadhyay, 2008: 1-2). Transformation of TiO_2 nanoparticles from both brookite and anatase polymorphs is possible at elevated temperatures and if the pH of the solution is decreased (Matthews, 1976; Gupta &Tripathi, 2011). Rutile and anatase phases of TiO_2 share a similar structure and same number of atoms per unit cell. Furthermore, differences in their structure result in differences in applications and properties they possess.
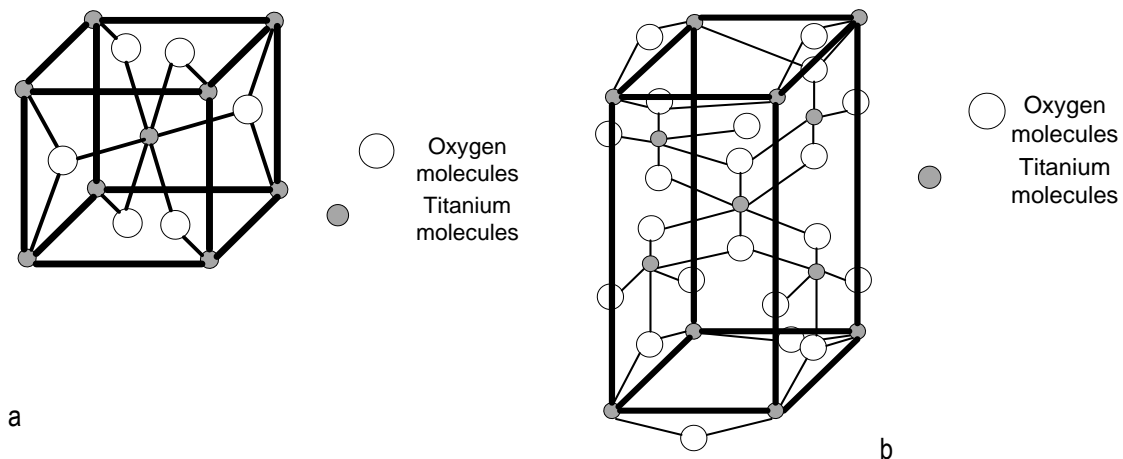
Figure 2.1: Structural arrangement of TiO$_2$: a) rutile and b) anatase (Gupta & Tripathi, 2011)

For the synthesis of TiO$_2$ nanoparticles, a synthesis route has been devised so that the greatest control over reaction kinetics will be possible. According to Nagarajan and Alan Hatton (2008) and Niederberger and Pinna (2009), an aqueous sol-gel chemistry approach for synthesising amorphous nanoparticles allows for greatest control over the reaction kinetics. Furthermore it allows for interaction between the aqueous Ti precursor and homogeneous catalyst, in the primary stages of the synthesis of TiO$_2$ nanoparticles (Nagarajan & Alan Hatton, 2008: 7). According to Kim et al. (2005), hydrothermal treatment of amorphous TiO$_2$ will enable the nanoparticles to interchange between the three phases of TiO$_2$. Therefore reaction kinetics is vital according to Fogler (1999), to optimise the operations, since the concentration of catalyst (Chen et al., 2011) and Ti precursor (Li et al., 2003) will affect the reaction rate and temperature at which the reaction takes place, and will impact the rate of reaction. For optimising the synthesis of TiO$_2$ nanoparticles, it is crucial to note that when altering synthesis parameters to molecularly alter a material's structure on a nanoscale, any changes to synthesis parameter, however small, can have a detrimental effect on the nanoparticle synthesised.

Manipulation on a molecular level allows these molecules then to take on varying structures and can yield a large number of forms of materials. Nanomaterial was introduced in 1959 by Professor Richard Feynman; it was hypothesised that it should be possible to directly manipulate individual atoms, in effect enabling a more powerful control of the synthesis chemistry and chemical structure (Bandyopadhyay, 2008: 1-2).

A nanometer (1 nm) is equal to 10 Å or 10^{-9} meter. The nanoscale is within 0.1–100 nm. For metal oxides, the diameter of a single oxygen ion is about 1.4 Å, and TiO$_2$ consists of six atoms per unit cell, of which two are titanium ions (Bandyopadhyay, 2008; 1-2; Gupta & Tripathi, 2011). Bond spacing for most crystalline materials is estimated to be 3 Å (Ramesh, 2010), thus the smallest size in angstrom that a TiO$_2$ nanomaterial can be is 30.6 Å which equates to 3.06 nm in diameter. Nanotechnology is a division of technology whereby material is engineered by controlling the material synthesised on a nanoscale, otherwise referred to as molecular manipulation (Ramesh, 2010). The world of nanotechnology has infused mechanics, physics, and materials which has provided advancements such as the ability to control structure and observe these nanoscale materials within small lengths and duration scales (Ramesh, 2010).

It is this control that is needed to develop and synthesise new chemical species with direct application functions. Such chemical species are nanomaterials that have functionalised growth properties (Tahir et al., 2006), or where other materials have doping and capping properties (Gupta & Tripathi 2011).

Not only is the challenge daunting of finding a means of meeting the increased demand for titanium dioxide; the challenge incorporates synthesising this crystalline material on a nanoscale (Kolen'ko et al., 2006; Ismagilov et al., 2009; Gupta & Tripathi 2011; Arora et al., 2010; Chen et al., 2011).

The ability to refine material up to its finest constituent is currently one of the primary goals in materials research (Bandyopadhyay, 2008: 1-2), as the finer the material, the greater the purity. This allows for greater properties to be exhibited and a greater number of applications (Barrañón, 2009). The fineness is twofold: fineness in how fine the particle size is, and how chemically pure the material is. The finest degree to which materials can be refined with respect to size is within the range of 1 to 100 nm by means of mechanical reduction or by synthesis (Bandyopadhyay, 2008: 1-2). The greater the fineness of the material, the greater the surface area; this in turn means higher reactivity and better mechanical performance (Edelstein & Cammarata, 1998; Bandyopadhyay, 2008: 1-2; Ramesh, 2010: 9).

The phenomenon which makes nanotechnology an ever-advancing technology is the direct impact which the manipulations of a chemical nature and structure on a micro and nano scale have on the material behaviour and mechanical performance at a centimetre to hundred metre range (Ramesh, 2010).

2.1. Fundamental kinetics of chemical reactions

Reaction kinetics is the study of chemical reaction rates and the mechanisms they follow (Levenspiel, 1972: 2; Fogler, 1999: 5). The rate of a reaction is a measure of how 'fast' or 'easily' a chemical species loses its identity, kind, number or configuration in a space of time (Levenspiel, 1972: 3; Fogler, 1999: 5). TiO_2 can consists of three phases- anatase, rutile and brookite and altering between the three is possible by thermal treatment (Kim et al., 2005). The effects of varying reaction kinetics in the synthesis of TiO_2 has been investigated extensively, but not necessarily systematically (Bischoff & Anderson, 1995; Vorkapic & Matsoukas, 1998; Wu et al., 2002; Oskam et al., 2003; Su et al., 2006; Ismagilov et al., 2009; Megawati et al., 2011; Chen et al., 2011).

2.1.1. Reaction rates

For a chemical product to be generated on industrial scale to be profitable, a factor to consider is the rate of synthesising the desired chemical. Synthesising a new product or determining a new reaction path, to achieve a reduced synthesis rate, is achieved by laboratory experimentation. Four main factors affecting the rate of reaction as given by (Masterton et al., 2011: 329-333) is concentration, synthesis technique used, temperature, use of a catalyst and reaction mechanism.

2.1.1.1. Effects of concentration on rate of reaction

Concentration, by definition, is strength of a substance per unit volume (Farlex, 2012). The effects of increasing concentration in solution will increase the chances of a greater number of molecular collisions between reacting

reagents (Masterton et al., 2011: 332-334). The concentration of reagents plays a significant role in the rate of the reaction. In the case of TiO_2 , the formation of a sol by the addition of titanium isopropoxide at set concentration of 0.25 molar, favours formation of rutile phase and rod shape of TiO_2 (Wu et al., 2002).

It has been found for using HCl (catalyst) has two functions firstly for the conversion of gel synthesised to crystalline nanoparticles (Su et al., 2006); secondly as catalyst to decrease the energy barrier needed to complete the reaction (Oskam et al., 2003; Chen et al., 2011). Owing to the high reactivity of metal alkoxides, the use of HCl concentration to control the hydrolysis stage of the sol-gel process is vital. The use of HCl in a high Ti ratio experiment was needed to avoid the formation of large aggregated primary nanoparticles (Wu et al., 2002; Oskam et al., 2003; Barnard & Zapol, 2004; Kim et al., 2005). When the homogeneous catalyst, HCl, concentration is increased controls the hydrolysis and polycondensation rates, that in turn affects the reaction rate, sizing and phase of the nanoparticles synthesised (Wu et al., 2002).

2.1.1.2. Effects of temperature on reaction rate

Temperature induces kinetic energy and therefore affects the reaction kinetics of molecules in chemical reactions (Masterton et al., 2011: 348). Moreover, these reacting molecules are also held together by strong chemical bonds, which need to be broken for a reaction to take place (Masterton et al., 2011: 348-349). In higher temperatures, reacting molecules have greater amounts of energy needed to break existing chemical bonds, but also possess more kinetic energy which allows these molecules to move more vigorously within the solution (Masterton et al., 2011: 349). With increasing kinetic energy, there is a greater probability of effective collision. The minimum energy required for a reaction to take place is known as activation energy (Masterton et al., 2011: 349-350), which is explained in greater detail later.

2.1.1.3. Reaction rates using catalysts

Catalysts to aid reactions have been used by mankind for over 2000 years, in making bread, wine and cheese (Fogler, 1999: 6). The catalyst redirects the natural chemical reaction mechanism to a new reaction mechanism at which the reaction will take place at lower activation energy (Masterton et al., 2011: 352). For catalysed reactions, two or more steps in the reaction path are found, as presented in Figure 2.2:
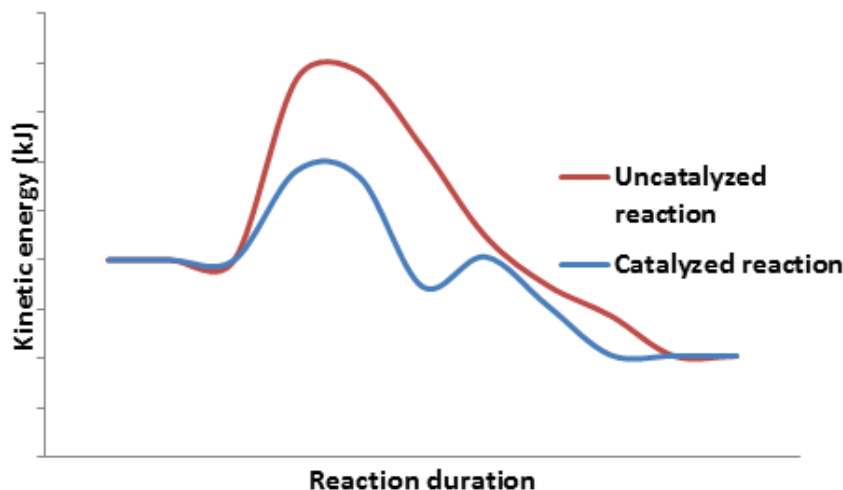
Figure 2.2: Kinetic energy required and alternative reaction path taken for catalysed reactions vs. un-catalysed reactions (Masterton et al., 2011: 353)

The use of a catalyst in chemical reactions can promote higher selectivity, higher yields, lower reaction times, and lower activation energy (Fogler, 1999: 92-93). The type of catalyst selected to achieve one or more of the above simultaneously is thus vital. The types of catalysts that can be used in chemical reactions are either homogeneous or heterogeneous (Fogler, 1999: 87-88).

2.1.2. Reaction rate laws

Reactions can vary with regard to chemical phase, order and type (Fogler, 1999: 4). Thus it can be deduced that the rate of reactions will vary for different reaction types. Reactions can be heterogeneous or homogeneous and can be reversible or non-reversible (Fogler, 1999: 88). Mathematically, rate law is the kinetic expression of concentration of a chemical species that is being consumed or generated (Fogler, 1999: 5).

Zero order reaction expression in terms of concentration and time (Masterton et al., 2011: 349):

$$[A]_o - [A] = kt$$

Equation 2.1

First order reaction expression in terms of concentration and time:

$$ln\frac{[A_0]}{[A]} = kt$$

Equation 2.2

Second order reaction expression in terms of concentration and time:

$$\frac{1}{[A_0]} - \frac{1}{[A]} = kt$$

Equation 2.3

Where $[A]_o$ is the initial concentration, $[A]$ is the concentration after time t and k is the reaction rate constant, of species A. With the use of a balanced stoichiometric equation, it can be possible to determine the order of reaction with the use of the exponents of chemical species' concentrations in the rate law equation.

2.1.3. Reaction rate constant

Reaction rate constant is not a true constant, but merely quantifies the rate at which a chemical reaction takes place (Fogler, 1999: 82, Farlex, 2012). The reaction rate constant can be driven by the changes in temperature of chemical species. With regard to the reaction rate constant for liquid phase reactions, a number of parameters such as solvents used can drive the reaction rate constant (Masterton et al., 2011: 328).

The reaction rate constant is determined with the use of the Arrhenius equation; for simplicity it is assumed that the reaction rate constant is temperature dependent only (Fogler, 1999: 92) as given in Equation 2.4 where k_A is the specific rate constant at a given temperature.

$$k_A(T) = Ae^{-\frac{E}{RT}}$$

Equation 2.4

Activation energy is the minimum energy required for chemical bonds to be broken and for the formation of new chemical bonds in a chemical reaction to occur between two reacting chemicals (Fogler, 1999: 92; Masterton et al., 2011: 345). The activation energy can be minimised by introducing a catalyst surface (Fogler, 1999: 18).

2.2. Nucleation and crystal growth kinetics

Nucleation dictates the interaction between molecules of reactions whereby slightly soluble species in high supersaturated conditions result in the formation of material via a reaction process. Furthermore, for homogenous nucleation and crystal growth does not occur simultaneously in the whole mass (Bandyopadhyay, 2008: 208). However this starts at single point within the substances and over times progresses to the full extends of the substance mass (Bandyopadhyay, 2008: 208). For homogeneous reaction types, the formation of nuclei occurs in the condensation stage. The formation of nuclei within this reaction stage allows for control over the particle size distribution and phase formed (Nagarajan & Alan Hatton, 2008: 7).

Nuclei constitute a group of atoms bound together in a central structure, and resist changes by chemical reactions (Farlex, 2012). These particles are formed by thermal excitation that can fluctuate from point to point within the substance, resulting in different size formation. According to Svishchev and Nahtigal (2008) and Porter et al. (2009), nucleation rate is defined as the number of nuclei that are generated per unit volume, per unit time,

that are larger than the critical size. The starting point size of a nucleus is referred to as to the critical size to undertake a new crystalline phase mass (Bandyopadhyay, 2008: 208). Furthermore for the change in physical state to take place, a number of reaction conditions are needed to initiate such a reaction (Cushing et al., 2004, Kelton & Greer, 2010: 1-2)

Change in physical state is a result of the reaction parameters of the chemical reaction, and most noted parameters used to induce such reactions are system, and temperature and pressure; however, inducing a precipitation reaction does not ensure that material yielded is of a nanoscale (Cushing et al., 2004; Kelton & Greer, 2010: 1-2).

If reference is made to the reaction rate constant, there are two activation energies that influence the rate of nucleation: first, the activation energy barrier to be overcome to produce critical-sized nuclei; second, activation energy is required for atom migration between the central matrix and the nucleus (Porter et al., 2009). Nucleation is the working of two opposite forces. One resists the creation of a new interface, and the other grows a more stable phase (Porter et al., 2009). The generation of larger nuclei is due to the coagulation of the smaller nuclei on one another (Nagarajan and Alan Hatton, 2008: 6). According to Porter et al. (2009), temperature has a large impact on nucleation and on growth kinetic nanoparticles. Gibbs free energy has been determined with Equation 2.5, for the formation of nanoparticles (Cushing et al., 2004, p 3896).

$$\Delta G^* = \frac{4\pi\sigma_{SL}R^{*2}}{3} = \frac{16\pi\sigma_{SL}^3 v^2}{3k^2T^2 \ln S^2}$$

Equation 2.5

2.3. Nanoparticles synthesis

The significance of nanoparticle properties is highly influenced by their chemical nature and particle size, as these properties control ionic potential and the high fraction of molecule/atom surface area rather than internal surface area (Nagarajan & Alan Hatton, 2008: 4). The synthesis route will affect final properties and sizing of the nanoparticles that originate from these phenomena (Nagarajan & Alan Hatton, 2008: 4-5).

Nanoparticles are sensitive to synthesis. This can result in diverse nanoparticles forming, with regard to their phase, size, reaction parameters, synthesis route followed, and most importantly, the reagents used in the synthesis (Vorkapic & Matsoukas, 1998; Wu et al., 2002; Ryu et al., 2006; Nagarajan & Alan Hatton, 2008: 5-7; Bandyopadhyay, 2008: 1-2; Gupta & Tripathi, 2011). The large surface area of the synthesised nanoparticles is the reason for the growing number of applications (Nagarajan & Alan Hatton, 2008: 5, 10). Figure 2.3 presents the possibilities for manipulating of nanoparticles, which can be engineered by variations to synthesis routes.

Chemical Nature:

Metals

Metal oxides

Semiconductors

Shape:

Spheres, Cylinders, Needles

Hollow tubes

Dispersion state:

Individual dispersed

Agglomerated reversibly

Engineered

Nanoparticles

Dispersion Medium:

Gases

Liquids

Surface Modifications:

Unmodified

Surface coating
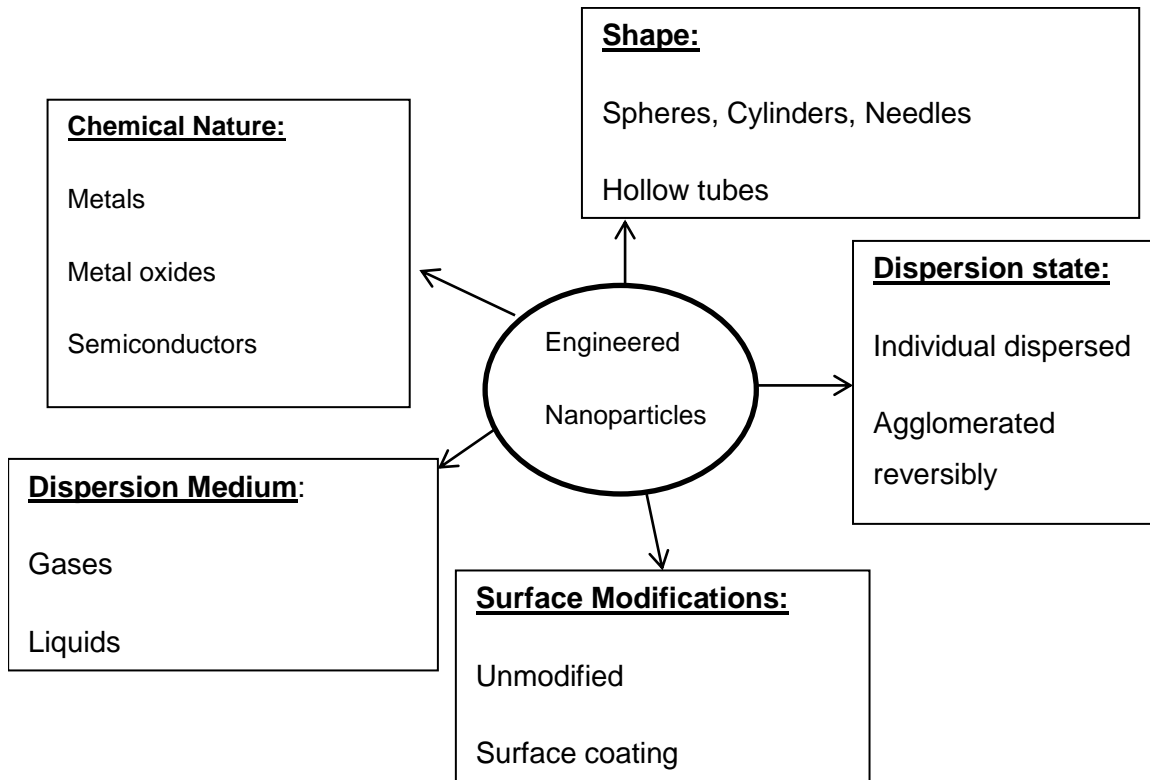
Figure 2.3: Diverse types observed in nanoparticles that are engineered by variations to synthesis routes (adapted from Nagarajan & Alan Hatton, 2008: 3)

Nanoparticles can be synthesised using a number of methods such as gas, liquid, and solid phase processes(Nagarajan & Alan Hatton, 2008, Gupta & Tripathi, 2011). Two approaches to the synthesising nanomaterial can be taken: top-down approach and bottom-up approach (Rotello, 2004: 32).

2.3.1. Top-down synthesis approach

A top-down approach is where large materials are physically modified to generate a finer particle by processes such as lithographic techniques, mechanical techniques, or laser beam processing (Rotello, 2004: 32). However, if this method of generating nanoparticles is used, a colloidal stabiliser is needed to avoid aggregation of nanoparticles (Nagarajan & Alan Hatton, 2008). This type of synthesis approach is expensive with regard to energy and equipment costs; it also permits a high level of impurities to contaminate the bulk mass (Gupta & Tripathi, 2011).

2.3.2. Bottom-up synthesis approach

The bottom-up approach is the synthesis of ultra-fine material on a molecular level; this is achieved by self-assembly and direct assembly when using a bottom-up approaches (Rotello, 2004: 32). This approach is, however, constrained by the complex nature of how chemicals interact, which limits this technique for large-scale production (Rotello, 2004: 32). With the use of this synthesis approach, material can be tailor made, and the development of new materials is endless (Gupta & Tripathi, 2011, Gupta & Tripathi, 2012).

Cape Peninsula
University of Technology

2.3.3. Gas phase synthesis

According to Goossens et al. (1998), gas phase entails two means of particle formation: firstly by a homogeneous method of synthesis that is based on nucleation of a supersaturated vapour followed by particle growth via condensation, and secondly by a heterogeneous method (Nagarajan & Alan Hatton, 2008: 6-7). The heterogeneous differs from the homogeneous nucleation method by the supersaturated vapour nucleating on a contact surface, and thereafter condensing (Nagarajan & Alan Hatton, 2008: 6-7). One means of the gas phase process is flame pyrolysis, a high- reaction temperature synthesis in the presence of flames (Nagarajan & Alan Hatton, 2008: 6; Wiggers, 2009), a method based on high-temperature reaction by gasification of the chemical precursor (Granqvist et al., 2004: 2). Hydrolysis of the precursor rarely occurs with synthesis of nanoparticles (Wiggers, 2009); however reacting in the presence of flames supplies sufficient energy by exothermic combustion of the precursor (Wiggers, 2009). Fluctuating parameters have immense control over size and morphologies, depending on the heating and cooling used. This synthesis technique provides control over such parameters; however costs and safety hazards of operation following synthesis procedures are limiting factors (Edelstein & Cammarata, 1998: 36).

2.3.4. Electro-deposition synthesis

Electro-deposition synthesis of nanoparticles is a process that uses the electrochemical properties of the desired material to be synthesised (Fendler, 2007: 56). Electrodeposition can be viewed as electroplating, as both processes incorporate a current applied to close current in solution (Fendler, 2007: 566). The current applied creates dissolution of ions in solution, and these ions react and are deposited onto the surface on the electrode (Fedlheim & Foss, 2001: 237).

2.3.5. Liquid phase and colloidal interaction synthesis

The liquid method of synthesising nanoparticles is a favoured synthesis technique used. Liquid phase synthesis of nanoparticles refers to a number of processes, according to the literature: colloidal methods (Nagarajan & Alan Hatton, 2008: 7), solution process (Gogotsi, 2006: 21-22), and sol-gel process (Sakka, 2005: 3-4; Akurati, 2008).

At this stage it will be referred to as the colloidal method; this is a method by which chemical reactions take place in solvents, leading to the formation of colloids (Nagarajan & Alan Hatton, 2008: 7). The synthesis path that the colloidal method follows can be best described by Figure 2.4. Furthermore, the methods of synthesis differ as to how starting particle are generated; however the formation of the nanoparticle remains consistent (Nagarajan & Alan Hatton, 2008: 6). As presented in Figure 2.4, the two types of nanoparticles found are aggregated orderly synthesised nanoparticles, and agglomerated ones, meaning heaped conjunction (Farlex, 2012).

Cape Peninsula
University of Technology
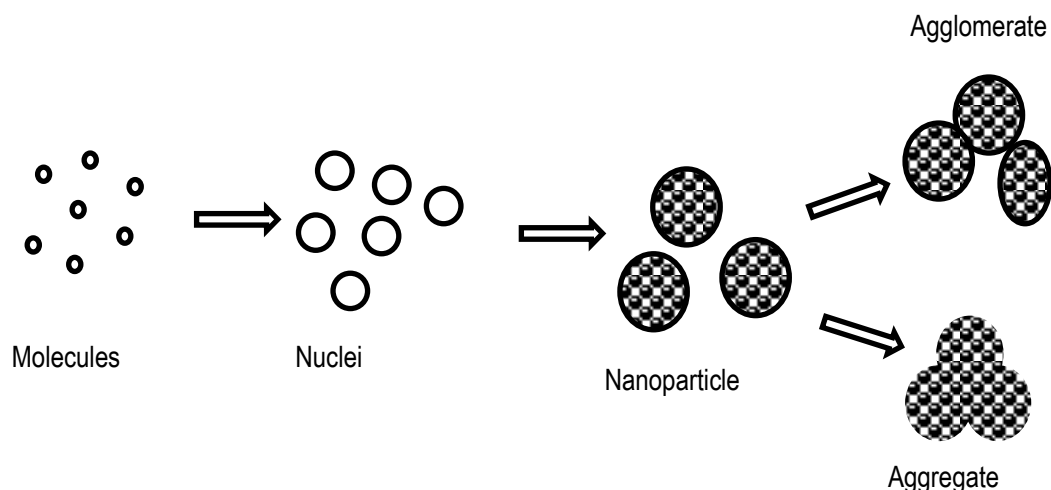
Figure 2.4: Nanoparticle synthesis mechanism (Nagarajan & Alan Hatton, 2008: 8)

The colloidal method is the precipitation of the molecules formed by the chemical reaction in solution (Nagarajan & Alan Hatton, 2008: 8); moreover the nuclei growth by collision and condensation will control the distribution of particle size and phase (Gopal et al., 1997). This method of generating nanoparticles allows for great control of synthesis parameters. Such parameters are: temperature, pressure, and concentration (Nagarajan & Alan Hatton, 2008: 7). Related past work shows the direct effects that variations in synthesis parameters [temperature] (Vorkapic & Matsoukas, 1998, Chen et al., 2011), concentration (Lakshmi et al., 1997; Vorkapic & Matsoukas, 1998; Oskam et al., 2003; Nian and Teng, 2006; Wang et al., 2007; Ismagilov et al., 2009), precursor (Mogyorosi et al., 2003), reagents (Bischoff & Anderson, 1995; Vorkapic & Matsoukas, 1998; Tahir et al., 2006), and reaction duration have on the nanoparticle size, phase and shape. The above method has been applied to both bulk solutions and smaller-scale systems, and to a range of nanoparticles (Nagarajan & Alan Hatton, 2008: 7).

2.3.6. Sol-gel synthesis of TiO_2

Synthesising metal oxides in bulk has traditionally been done using a ceramic technique (Sakka, 2005: 3-4). With an increased knowledge of and interest in nanoparticle synthesis, various means of synthesis have been proposed (Bischoff & Anderson, 1995; Moritz et al., 1997; Oskam et al., 2003; Bandyopadhyay, 2008: 138; Nagarajan & Alan Hatton, 2008; Monreal. et al., 2009). Every synthesis procedure has its own set of limitations; however it is the control over the synthesis parameters and the influence this has on the nanoparticles synthesised, this is why the sol-gel synthesis technique is highly favoured (Sakka, 2005: 3).

 It was thus proposed that if the nanoparticles were synthesised by a liquid-liquid route, greater control over the size and shape of these nanoparticles could be obtained, as this method offers greater molecule transformation of the precursor species to the final product. In each synthesis pathway forming the nanoparticles, reaction parameters of the solvents (hydrolysis and condensation rate of the metal oxide precursor, pH, temperature, and rate of oxidation) should be strictly controlled as this will have a direct influence on the nanoparticles (Niederberger & Pinna, 2009: 11). Sol-gel synthesis procedures are divided into two main groups: those that

involve hydrating the metal oxide precursor/the production of water from the reaction, and the non-hydrated metal oxide precursor (Niederberger & Pinna, 2009: 10).

These are reactions of metal precursor solutions to form inorganic solids via polymerisation reactions induced by water (Niederberger & Pinna, 2009: 10). The use of metal alkoxides as precursors has been found to be the most reactive and commonly used (Vorkapic & Matsoukas, 1998; Wu et al., 2002; Cozzoli et al., 2003; Oskam et al., 2003; Limmer et al., 2004; Zhang, 2004; Kim et al., 2005; Kolen'ko et al., 2006; Ryu et al., 2006; Tahir et al., 2006; Pavasupree et al., 2006; Livraghi et al., 2006; Niederberger & Pinna, 2009: 10; Monreal et al., 2009; Chen et al., 2011). Water is used because of the metal alkoxides' reactivity with water (Cushing et al., 2004; Niederberger & Pinna, 2009: 10). Titanium alkoxides (Ti-OR) are used for their simplicity of reaction path, and low cost (Niederberger & Pinna, 2009: 10-11). The sol-gel process consists of the following steps, which are illustrated in Figure 2.5.
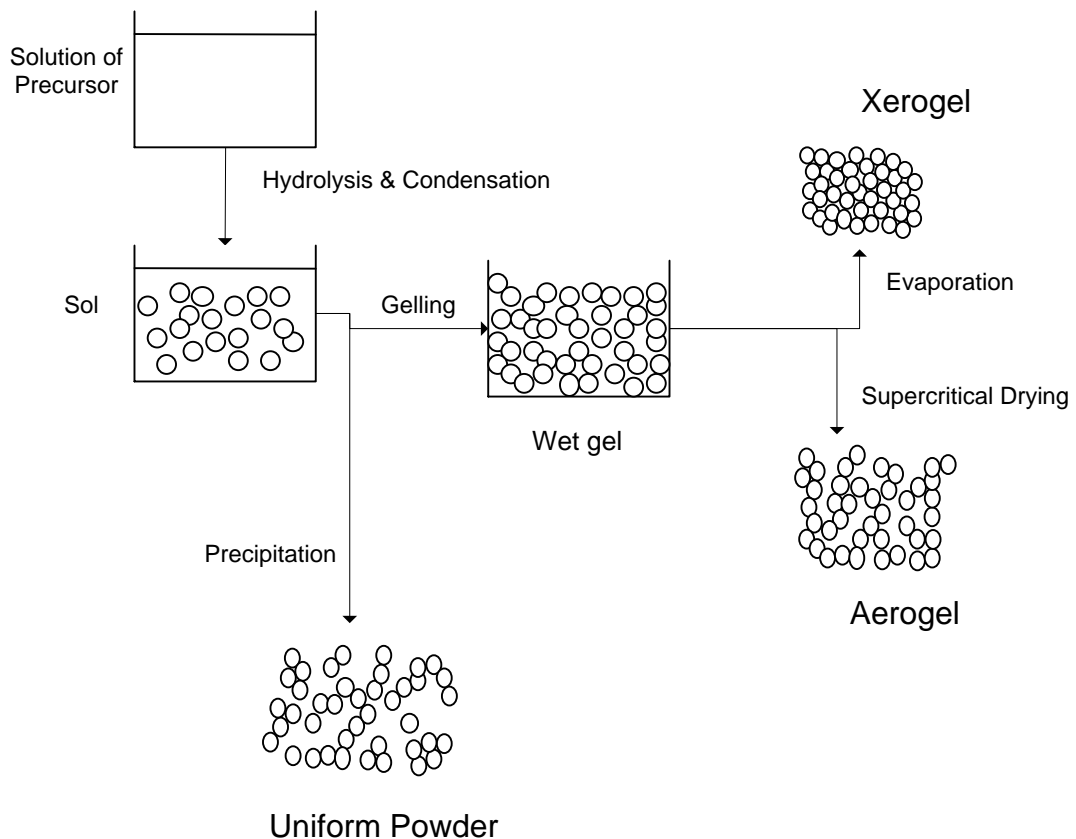
Figure 2.5:Superstructure of methods and means of synthesising TiO$_2$ nanoparticles, using an aqueous sol-gel chemistry approach (Niederberger & Pinna, 2009: 11)

First, a homogenous solution is formed by dissolving a metal organic (alkoxide) precursor in a solvent that is miscible with water. In this step of the sol-gel reaction, the formation of an inorganic polymer occurs due to the hydrolysis and condensation reactions that occur instantaneously (Machesky et al., 2008; Niederberger & Pinna, 2009: 11). This entails that the metal precursor is forced to take on a highly cross-linked solid structure (Barnard & Zapol, 2004). Secondly a conversion of this solution to a sol is prepared with a suitable reagent, predominantly water. Hydrolysis of the precursor leads to the formation of the sol as the alkoxide group is replaced by a hydroxide ion via nucleophilic attack of an oxygen atom (Barnard & Zapol, 2004; Niederberger & Pinna, 2009: 10-

11). Condensation forms the gel by the inter-reaction of the metal hydroxide species formed in hydrolysis, leading to the formation of M-O-M bonds (Niederberger & Pinna, 2009: 11).

Thereafter the process follows the order of: ageing, shaping (if needed) and thermal treatment (Niederberger and Pinna, 2009). The use of a metal alkoxides avoids the formation of a large number of oligomeric species, and provides high homogeneity in solvents. Equation 2.6 and 2.7 express the general hydrolysis and condensation reactions that take place in the synthesis of a metal alkoxide in the formation of a metal oxide. However, as the thesis is focused on the synthesis of metal dioxide, specifically TiO_2, the following reaction equation can be used to describe the chemistry of generating TiO_2 from an alkoxide (Bischoff & Anderson, 1995):

$$\equiv M\text{-}OR + H_2O \rightarrow \quad \equiv M\text{-}OH + R\text{-}OH$$

$$\equiv M\text{-}OH + \equiv M\text{-}OH \rightarrow \quad \equiv M\text{-}O\text{-}M \equiv + H_2O$$

Equation 2.6

Hydrolysis

Cape Peninsula
University of Technology

$$\text{IsoO} - \underset{\underset{\text{OIso}}{|}}{\overset{\overset{\text{OIso}}{|}}{\text{Ti}}} - \text{OIso} \ + 4\ H_2O \longrightarrow \text{HO} - \underset{\underset{\text{OH}}{|}}{\overset{\overset{\text{OH}}{|}}{\text{Ti}}} - \text{OH} \ + 4\ \text{Proponal}$$

Condensation

$$\text{HO} - \underset{\underset{\text{OH}}{|}}{\overset{\overset{\text{OH}}{|}}{\text{Ti}}} - \text{OH} \ + \text{HO} - \underset{\underset{\text{OH}}{|}}{\overset{\overset{\text{OH}}{|}}{\text{Ti}}} - \text{OH} \longrightarrow \text{HO} - \underset{\underset{\text{OH}}{|}}{\overset{\overset{\text{OH}}{|}}{\text{Ti}}} - \text{O} - \underset{\underset{\text{OH}}{|}}{\overset{\overset{\text{OH}}{|}}{\text{Ti}}} - \text{OH} \ + H_2O$$

Further Condensation

$$\text{HO} - \underset{\underset{\text{OH}}{|}}{\overset{\overset{\text{OH}}{|}}{\text{Ti}}} - \text{O} - \underset{\underset{\text{OH}}{|}}{\overset{\overset{\text{OH}}{|}}{\text{Ti}}} - \text{OH} \longrightarrow 2\ TiO_2 \ + \ 3\ H_2O$$
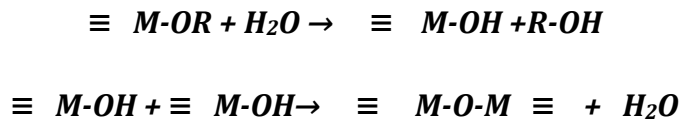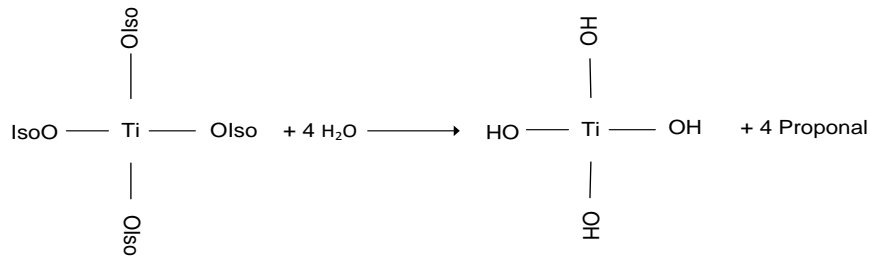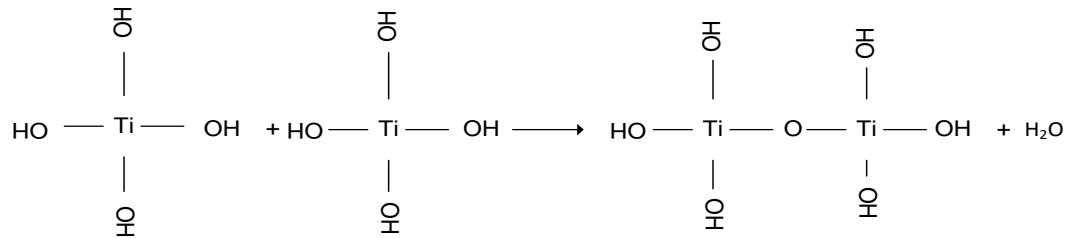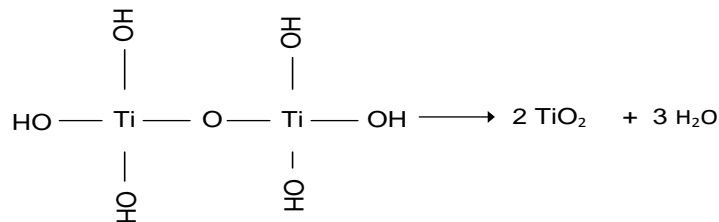
Equation 2.7

2.4. TiO$_2$ synthesised by sol-gel techniques, incorporating hydrothermal treatment

Process parameters such as Ti precursors, catalyst, reagent concentrations, reaction temperature and hydrothermal treatment duration and temperature affecting the sol-gel process of TiO$_2$ are discussed in this section. Since subtle differences in methods exist amongst researchers, a brief review of the synthesis method in addition to the findings.

2.4.1. Titanium precursor used for sol-gel technique

Vorkapic and Matsoukas (1998) studied the effects of temperature and concentration of the reagents in the preparation of TiO$_2$ from titanium alkoxides. The aim of the research was to report the effects of alkoxide type, temperature, and use of alcohol for peptisation of a sol, which promoted the formation of stable TiO$_2$ nanoparticle synthesis. As previously mentioned, various titanium alkoxides were used: ethoxide, propoxide, isopropoxide, and butoxide. It was proposed that TiO$_2$ particles size increased with increasing the alkoxide group chain the larger the TiO$_2$ nanoparticles shall be formed. Four alcohols were used as solvents: ethanol, propanol, isopropanol, and butanol. This was done to ascertain the effects that the alcohol group size has on the size of TiO$_2$ nanoparticles also. Nitric acid was used as homogeneous catalysts and to control hydrolysis and peptisation respectively.

Experiments were performed by synthesising a sol in either purified water or a water-alcohol mixture, in a warm bath, with temperature varying between 0 °C – 90 °C. Titanium alkoxides were added dropwise into the mixture under magnetic stirring, until a molar ratio of $[H_2O]$: $[Ti]$ was reached. The results obtained showed that titanium ethoxide formed the largest nanoparticles, while titanium isopropoxide synthesised the smallest nanoparticles in diameter. This was the rationale for the use of titanium isopropoxide as the titanium precursor. The effects of synthesis duration on the nanoparticle size were recorded in this article as well. Archana et al. (2013) found that for increased synthesis duration, larger nanoparticles were synthesised. The effects of temperature on hydrolysis and peptisation have a direct impact on nanoparticle size, and optimum temperatures for smallest particle size were 25 °C and 50 °C respectively. Alcohol present in the initial mixture resulted in larger nanoparticles being synthesised, and nanoparticles grew as the concentration of alcohol increased. How these nanoparticles grew and developed was explained, and it was found that the limitations to shortening synthesis duration presented themselves in the peptisation stage of the synthesis procedure. The limitation found in this research was that amorphous TiO_2 nanoparticles were formed and only one acid was studied.

2.4.2. Selection of catalyst for sol-gel synthesis

The work of Hsu and Nacu (2003) showed HCl concentration (at 0.15 M and 0.77M) affects TiO_2 nanoparticles. The catalyst concentration affects the hydrolysis rate. The titanium precursor was added dropwise in ethanol and then added to acidified water to produce the sol. HCl acid concentrations were varied and the mixture was under constant magnetic stirring. The sol formed was then fed using a micro feed pump into a double-walled glass reactor; this started the gel formation stage. Then left to gel overnight in dilute alcohol. No hydrothermal treatment was used in this study. However, it was stated that calcination would lead to an increase in crystal size and further agglomeration. TiO_2 particles decreased in size with increasing HCl concentration, and decreasing standard size deviation of particle size distribution. Furthermore, the effects of phase were not documented in this study (Hsu & Nacu, 2003).

The seminal research of Wu et al. (2002) studied the use of an acidic medium for sol-gel synthesis of pure rutile and anatase TiO_2 nanoparticles. This study focused on phase transformation and particle sizes obtained for the variations in the homogeneous catalysts (acids) used their concentrations, and variation in reaction temperatures and duration, at the hydrothermal stage of the synthesis. In addition, adding NaCl (salt) to gel before being hydrothermally treated was studied to see the effects the addition would have on the particle size during hydrothermal treatment. Titanium (IV) n-butoxide, as the Ti precursor, was used and added dropwise under magnetic stirring for the formation of the sol; the homogeneous catalysts (acids) used were: hydrochloric acid, nitric acid, sulphuric acid, and carboxylic acid. Catalyst concentration varied between 0.5 – 1.5 molar for each acid in formation of the sol. It was found that for hydrochloric acid at 1.5 molar, pure rutile TiO_2 rod-shaped nanoparticles were formed and for nitric acid, that a mixture of rutile and anatase nanoparticles formed. Furthermore pure anatase nanoparticles were synthesised for both sulphuric and carboxylic acid homogeneous catalysts of 1.5 molar. Moreover, variations in the titanium precursor concentration were studied, and findings

concluded that varying the titanium precursor affected the nanoparticle phase. Titanium precursor concentration was varied of 0.25 to 0.5 molar was tested and showed that; 0.25 molar was the optimum for rutile synthesis.

2.4.3. Effects of precursor ratio and temperature for sol-gel synthesis

Bischoff and Anderson (1995) used different ratios of hydronium ion to titanium ethoxide precursor (0.1 – 0.5 H^+/Ti), in the presence of ethanol at a 1:1 ratio. Formation of gels was promoted when using acids and heated at 80 °C. For increased peptisation times of 0.25 - 11 hours, anatase and traces of brookite nanoparticles were formed. It was concluded that increasing the acid to precursor ratio increased the solubility of the gel resulting in slow dissolution and rutile formation.

So et al. (1997) studied the molar ratio of H^+/TTIP and H_2O/TTIP (titanium tetraisopropoxide), for synthesising stable and unstable sols via a sol-gel technique. Stable sols were found in the range of 0.1 - 0.45 H^+/TTIP and 50 - 190 H_2O/TTIP. White precipitate formed was transferred to a beaker, where nitric acid was added and the mixture was peptised at 80 °C for 12 hours. These gels were transferred to an autoclave and treated at a temperature range of 160 °C – 240 °C for treatment times that varied from 3 to 12 hours. The research found that in general, formation of a stable sol is likely to form when the H^+/TTIP molar ratio is decreased and an increase in H_2O/TTIP molar ratio is used. Stable sols did not change phase after hydrothermal treatment; the sol and gel formed were anatase. However, unstable sols formed changed phase after hydrothermal treatment (anatase to rutile), and formed rod-like particles with a high tendency to aggregate. The explanation given for stable sol formation with respect to aggregate size and H^+/TTIP was due to interparticle distancing caused by strong ion repulsion in dilute solutions. With increasing H^+/TTIP ratio, an increase in aggregation was found, and rod-like aggregates were formed at 0.67 molar ratio. An increase in particle size was found when increasing hydrothermal treatment duration (So et al., 1997).

Gopal et al. (1997) studied the synthesis of TiO_2 of varying phases at reaction temperatures of 35 °C to 100 °C. Reagents for the synthesis of TiO_2 crystalline powder were: titanium (IV) isopropoxide as the Ti precursor, nitric acid and isopropanol (used as the catalyst), and distilled water. Large water to titanium alkoxide ratio of 1000:1 was used. A mixture of nitric acid to distilled water was first prepared; thereafter isopropanol was slowly added dropwise to this mixture. Once the solution was well mixed, titanium isopropoxide was added dropwise, with a white precipitate formed instantaneously. This mixture was then sonicated for five minutes and became clear, indicating the formation of the sol. The sol was formed at initial synthesis temperatures of 35 °C, holding temperatures of 35 °C to 90 °C, with heating performed at different rates (0.5 °C/min, 5 °C/min), for varied durations. Thereafter it was left to settle for 24 hours and dried using an infrared lamp at about 90 °C. It was concluded in this study that controlling the reaction temperature and heating rates that either rutile or anatase can be formed below 100 °C. Furthermore, slow heating rates resulted in the formation of rutile, while for faster heating rates formed anatase (Gopal, 1997).

2.4.4. Effects of pH, and reactivity of other reagents in sol-gel synthesis

Nian and Teng (2006) studied the formation of anatase titanium dioxide nanorods, incorporating a two-stage hydrothermal synthesis technique approach. Titanium dioxide nanorods were synthesised from commercially available titanium dioxide powder comprised of nanotubes with an average size of 21 nm. The first stage of the synthesis comprised of treating 5g of TiO_2 nanotubes hydrothermally, in 70 ml of concentrated NaOH at 130 °C for duration of 20 hours. Thereafter samples were filtered and washed with varying concentrations of nitric acid added. Using HNO_3 to control the pH of the mixtures (pH 2.2 - 8.2), the first stage was thus repeated at 175 °C for duration of 48 hours. Varying pH of the mixture resulted in changes to shape and phase, forming nanorods and anatase respectively. The nanoparticles were to undergo hydrothermal treatment in an acidic environment. Furthermore, a trend of increasing particle size with a decrease in pH of solution was found for set hydrothermal duration. In this study it also appeared that the synthesis of single crystalline anatase nanorods formed easily in an acidic environment. To enhance peptisation in the synthesis of TiO_2, it was stated this could be done with the use of an acidic environment and induced heat. Nanorods synthesised varied between 10 – 120 nm in length. Furthermore, the use of HNO_3 as a homogeneous catalyst proved to synthesise anatase nanorods of average dimensions of 10 nm at a low pH.

Mahshid et al. (2006) studied the sol-gel synthesis of titanium isopropoxide (TTIP) in the presence of isopropanol and acidified distilled water. This work was aimed at studying the effects by varying pH of solution on the size and phase of nanoparticles synthesised. Heating of the solution was performed at 60 °C – 70 °C for 18 – 20 hours. After this process it was observed that a white blue suspension started to form and this resulted in the mixture solution's decreasing in volume. The material was not hydrothermally treated, however, was washed with ethanol and dried for three hours at 100 °C. Thereafter it was thermally treated for 2 hours at temperatures ranging from 200 °C – 800 °C. It should be noted in the discussion of the results obtained that it was made clear why the intermediate $Ti(OH)_4$ previously mentioned was unable to form; this was due to the high acidity (pH of 2) of the solution, thus nucleation of stable $Ti(OH)_4$ was unable to form. Furthermore reaction parameters which will be varied in this research found that the synthesis temperature, pH, and use of titanium isopropoxide as the Ti precursor have had an impact on particle shapes.

Tahir et al. (2006) studied the control of polymorph growth with the aid of different surface ligands and reagents. With growing energy costs and more environmentally friendly operations to synthesise these materials at lower temperatures has emerged; however synthesising rutile nanoparticles at lower temperatures poses a greater problem than the polymorph anatase. Therefore the aid of a functionalisation agent would be needed to compensate for the kinetic growth control with regard to these polymorphs. TiO_2 nanoparticles were synthesised by mixing titanium chloride into ice-cooled water; thereafter the addition of sodium carbonate was added as catalyst. Dopamine was then added and left to age, then hydrothermally treated for 13 hours at 150 °C. Limitations of this study were that the cost of reagents was too high. Collectively, the above literature provides insight into the concentrations of reagents to be used, why acid media were used, and ratios of water to titanium

precursor, and acid to titanium precursor. Furthermore, a greater understanding of how the generated sol interacts with the deionised water for gel formation emerges from the above.

2.4.5. Effect of calcination and hydrothermal treatment for phase transformation

Two means of general techniques for the transformation of nanomaterial from amorphous to crystalline has been achieved with the used of calcination and hydrothermal treatment. TiO_2 nanoparticles are hydrothermally treated to synthesise a desired phase, shape, and size, as this influences the application. There is a growing need to better understand TiO_2 nanoparticles in these industrial and domestic applications. Limitations by hydrothermal treatment for the phase transformation of TiO_2 have been studied (Matthew,1976; Wu et al., 2002; Hu et al., 2003; Zhang & Banfield, 2005; Nian & Teng, 2006; Su et al., 2006; Pavasupree et al., 2006; Ryu et al., 2006; Chen et al., 2011).

Hu et al. (2003) studied the phase transformation of TiO_2 nanoparticles synthesised at varying pHs by calcination from 300 °C – 1000° C. This included the effects synthesis pH value on the phase transformation, and the relationship between phase transformations of the three phases of TiO_2. TiO_2 crystalline powder was synthesised using titanium (IV) chloride as the Ti precursor, hydrochloric acid and isopropanol as the catalysts and distilled water hydrolysis agent. Titanium (IV) chloride was dissolved in chilled water in a glove box with a filled argon environment, to a concentration of 0.1 molar. Thereafter HCl and isopropanol were added to the solution to a concentration and ratio of 0.1 molar and 3:1 respectively. On forming the white precipitate, the solution's pH was varied with the addition of ammonia, and then heated to 50 °C for 1 hour. Initially it was found that for nanoparticles dried and heated to 450 °C there was no change in the phase, below the synthesis pH of 4 was reached. With a drop in pH, the formation of mixed anatase and brookite nanoparticles was found for calcination at 450 °C. A change in anatase phase to brookite was justified by strain taken by the lattices under hydrostatic pressure, and the decomposition of hydroxyl groups on heating. TiO_2 nanoparticles synthesised at a pH of 2 were then heated and treated for two hours, at a temperature range of 300 °C to 750 °C. It was noted that anatase to rutile transformation initiated first, with brookite to rutile following. However, brookite to rutile transformation was noted to be size dependent, and was found to transform more easily at high temperatures than anatase to rutile particles (Hu et al., 2003).

The cost for calcination of these materials' is too high, this results in safety issues and energy costs becoming factors to bear in mind. Hydrothermal treatment is of great importance as it provides gel material with the needed kinetics for easy transformation in phase, with an added benefit of controlling particle size (Matthews, 1976; Wu et al., 2002; Zhang & Banfield, 2005). At stated earlier, So et al. (1997) explain how stable sols that are hydrothermally treated at low temperatures will behave, and how unstable sols when hydrothermally treated form rod-like particles. Therefore hydrothermal treatment at lower temperatures is used to transform amorphous TiO_2 gels. An increasing number of studies have been performed on the duration of hydrothermal treatment. One of these is that of Chen et al. (2011). In this study they demonstrated how increasing hydrothermal duration impacted, the particle sizes of rutile nanoparticles as shown in Figure 2.6.
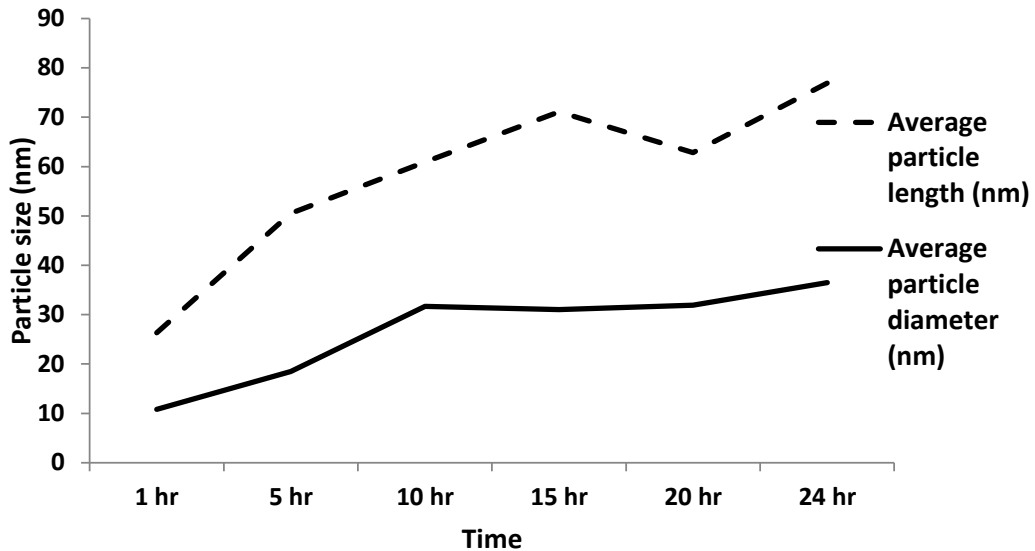
Figure 2.6: Data taken from Chen et al. (2011) showing effects of hydrothermal treatment time on TiO₂ nanorod size

Figure 2.6 shows the effect to particle size with increase in hydrothermal treatment. However at 20 hours, particle length and diameter deviate from this growth pattern, with greater change in particle length occurring. Therefore more needs to be understood about increasing the duration of hydrothermal treatment. Hydrothermal synthesis techniques allow for a greater control over the reaction parameters, and thus provide in-depth insight into the effects of individual parameters. Such parameters that are referred to are duration, temperature, and pH.

Wu et al. (2002) as previously mentioned studied hydrothermal treatment temperatures of 100 °C, 140 °C and 220 °C, and reaction durations of 5, 10, 20, and 72 hours. Limitations found in this research were the effects on nanoparticles in the initial stages of sol-gel synthesis that suggests that more work should be done to decreasing the overall synthesis duration.

Reyes-Coronado et al. (2008) studied the synthesis conditions to form pure phase TiO₂, where the three phases were formed by hydrothermal treatment with the use of relevant reagents. The mechanism for formation and growth of the three phases were proposed. Gel TiO₂ material was synthesised using a set method, but reagents and reaction parameters were altered for the hydrothermal treatment stage of the synthesis. Hydrothermal treatment conditions were varied to achieve pure phase TiO₂ nanoparticles to be synthesised. Pure anatase phase was achieved for 1.5 M acetic acid and hydrothermally treated at 200 °C for 6 hours. Pure rutile structure was structure was achieved for 4 M hydrochloric acid and hydrothermally treated at 200 °C for 8 hours. Pure brookite obtained for 3 M hydrochloric acid and hydrothermally treated at 175 °C for 7 hours. Two growth mechanisms were established for the sudden increase in rutile nanoparticle size; they were orientated attachment and aggregation-recrystallisation. Increased hydrothermal treatment of brookite nanoparticles commonly resulted in phase transformation to rutile phase. It was stated that anatase possesses a low agglomerative force, whereas brookite and rutile are higher. Orientated aggregation best describes the formation of large rutile nanorods.

Anatase synthesis was found to be insensitive to the reagent use; this was due to the anatase phase having the lowest total energy for this phase formation (Reyes-Coronado et al., 2008).

Kolen'ko et al. (2006) studied the formation of titanium dioxide and other titanates by the means of hydrothermal synthesis. A titanium precursor of $TiCl_4$ was used for synthesising raw amorphous TiO_2 gel. A set hydrothermal duration was used with variations in reactor temperature of 110 °C, 160 °C, and 200 °C. Nanoparticle sizes synthesised were too large (0.4 – 15 µm in length and 70 – 1400 nm in diameter); however this might have been due to the reaction times used to hydrothermally treat the amorphous gel, which led to particles adhering to one another and in turn becoming one. Furthermore, increasing the time of the hydrothermal treatment will cause an increase in nanoparticle size (Kolen'ko et al., 2006).

Su et al. (2006) studied sol-hydrothermal synthesis of TiO_2 and found that anatase was initially synthesised and then shift in phase to forming rutile as hydrothermal durations were increased. The sol was hydrothermally treated at 150 °C and 200 °C for 1 – 7 hours respectively. Extended heat treatment times (3 - 7 hours) lead to phase transformation of anatase to rutile, simultaneously resulting in particle growth. It explains primary particles formed in gel formation can contain a large number of defect sites, for which high temperature treatment can assist in phase transformation. It is this breaking of bonds that allows atoms to rearrange. It was found that hydrothermal treatment can facilitates initially formed unstable anatase being transformed to rutile on a twin interface [112]; this interface possesses a similar structure of rutile. It was found that spherical anatase particles tend to coagulate just before the changing phase, to be ellipsoids. A strange phenomenon for the changes in particle size was again found with respect to hydrothermal treatment time, as presented in Figure 2.7.
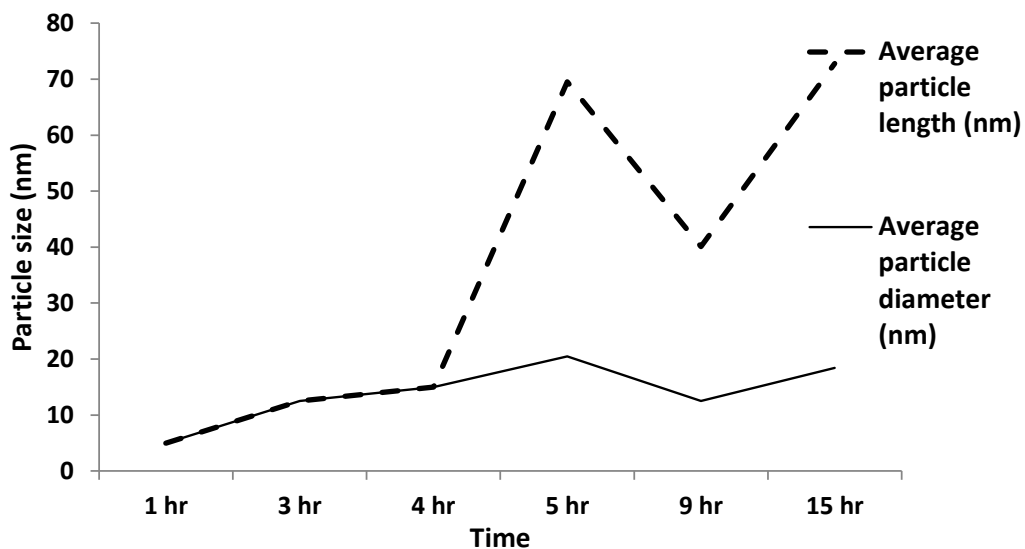
Figure 2.7: Data taken from Su et al. (2006) showing effects of hydrothermal treatment time on TiO_2 nanoparticle size

Spherical particles were formed for the experiments 1 – 4 hours. However after 9 hours particle length and diameter deviated from this growth pattern and were found for which greater change in particle length occurring.

Therefore more needs to be understood about lengthening the duration of hydrothermal treatment. These data were taken for a set temperature of 200 °C (Su et al., 2006).

Yu et al. (2007) studied the effects to TiO_2 microstructures and photocatalytic activity by varying hydrothermal temperature and time. The effects of hydrothermal treatment temperature were studied at temperatures varying from 100 °C – 200 °C for a duration of 3 hours, and then duration was studied at a set temperature of 180 °C for a durations of 1, 3, 5, 10 and 24 hours. Small changes in average nanoparticle size were found for an increase in hydrothermal temperature, and standard size distribution for increasing temperature was no greater than 2 nm. The increase in hydrothermal duration resulted in an increase in degree of crystallinity. These results were justified by longer hydrothermal treatment durations promoting Ostwald ripening (Yu et al., 2007).

Ryu et al. (2006) studied the effects of synthesis temperature calcination on nanosized TiO_2 physical properties. The total duration for synthesis of TiO_2 anatase needle-shaped nanoparticles was 7 hours, for which the temperature of hydrothermal treatment was in the range of 120 °C – 200 °C. Results obtained from this study showed the possibility of synthesising anatase TiO_2 nanoparticles at relatively low temperatures via hydrothermal ageing. It was observed that increasing the synthesis temperature of the hydrothermal treatment will increase the particle size, for a set duration. Results obtained with regard to nanoparticles synthesised at varying hydrothermal temperatures indicate an effect on the shape (Ryu et al., 2006).

Jiang et al. (2006) studied the effects of carboxyl and hydroxyl modifiers for the hydrothermally synthesised TiO_2 nanoparticles. Organic modifiers were used with the aim of controlling the phase of TiO_2 nanoparticles formed at low pH and low hydrothermal treatment temperatures. Gel formed was washed and nitric acid was added to the suspension until a pH of 0.7 was attained. This mixture was then hydrothermally treated at 220 °C for 18 hours. It was found that low pH mixtures that were hydrothermally treatment favoured synthesis of protonated TiO_6 octahedra surfaces that resulted in an edge-sharing rutile phase. The results suggest rutile is synthesised by rearrangement by solvated TiO_6 octahedra under highly acidic conditions, instead of phase transformation of brookite and anatase phase under hydrothermal treatment. Additional organic modifiers impacted the size distribution of rutile TiO_2 nanoparticles (Jiang et al., 2006).

Oskam et al. (2003) studied the growth kinetics of TiO_2 nanoparticles. Particles were synthesised using high water to titanium ratios. A light blue gel heated to 160 °C and 200 °C, for 4 – 300 hours in an autoclave. This found that there was an increase in standard size distribution and a change in phase with hydrothermal treatment time. Stability of rutile particles is size dependent; where particle size is smaller than 14 nm, anatase is viewed to be more stable (Oskam et al., 2003).

Chen et al. (2011) used a batch hydrothermal synthesis route to produce pure rutile nanorods. TiO_2 nanoparticles were used in the generation of thin films for their application as a photocatalyst in dye-sensitive solar cells. Titanium (IV) n-butoxide, as the Ti precursor, was used and added dropwise under magnetic stirring for the formation of the sol; the homogeneous catalyst used in generating the sol was hydrochloric acid. From the results it was found that at a peptisation concentration of 3-molar HCl, pure nanorod rutile nanoparticles were obtained.

Cape Peninsula
University of Technology

A hydrothermal temperature of 220 °C, with variations in hydrothermal treatment duration, from 1 – 24 hours, was studied. It was concluded that for shorter hydrothermal treatment durations, smaller nanorods were synthesised; these increased in particle size with increasing synthesis duration.

Table 2.1 provides a summary of the work done to evaluate the effects of various process parameters of sol-gel process on TiO_2 nanoparticle characteristics. The phase was found to be temperature and catalyst dependant and HCl was used frequently as catalyst and the temperature ranged between 150 and 200 °C. Hydrothermal treatment times ranged from 1 to 10 hours. Less than 40% of cases studied peptised the sol prior to thermal treatment. Table 2.1 shows an overview of the changes in synthesis parameters for the synthesis of TiO_2 studied.

Table 2.1: Literature review for sol-gel, catalyst, peptisation treatment temperature and time, hydrothermal treatment temperature and time for the synthesis of TiO_2

Author	Catalyst used	Peptisation temperature (°C)	Peptisation treatment time (hours)	Hydrothermal treatment temperatures (°C)	Hydrothermal treatment times (hours)	Resulting phase
Chen et al. (2011)	HCl	-	-	220	1-24	Rutile
Reyes-Coronado et al. (2008)	HCl, acetic acid and 1 isopropanol	-	-	175 and 200	6, 7 and 8	Anatase, Brookite and Rutile
Yu et al. (2007)	-	-	-	100, 120, 150, 180 and 200	1-24	Anatase
Yu et al. (2007)	-	-	-	100, 120, 150, 180 and 200	3	Anatase
Nian and Teng (2006)	NaOH	-	-	130 and 175	20 and 48	Anatase
Mahshid et al. (2006)	HNO_3, isopropanol and NH_4OH	60 - 70	18 - 20	Calcination: 200 - 800	-	Anatase
Kolen'ko et al. (2006)	HCl and NH_3	-	-	110, 160 and 200	20	Anatase
Tahir et al. (2006)	Na_2CO_3 and dopamine	-	-	150	13	Rutile
Jiang et al. (2006)	HCl and Na_2CO_3, including surface modifiers	60	1	220	18	Anatase, Brookite and Rutile
Su et al. (2006)	Acetylacetone and Isopropanol	-	-	150 and 200	1, 3, 5 and 7	Anatase, Brookite and Rutile

Jiang et al. (2006)	HCland Na_2CO_3	-	-	220	18	Anatase, Brookite and Rutile
Ryu et al.(2006)	Trimethylamine	-	-	120-200 Calcination: 200 - 800	4	Anatase
Zhang and Banfield (2005)	-	-	-	375-500	3	Anatase
Hu et al. (2003)	HCl, isopropanol and NH_4OH	50	1	Calcination: 300 - 1000	2	Anatase and Rutile
Hsu and Nacu (2003)	HCl and ethanol	25 - 60	-	-	-	-
Oskam et al. (2003)	HNO_3	-	-	160 and 200	4-300	Anatase, Brookite and Rutile
Wu et al. (2002)	H_2SO_4, HNO_3,HCl and CH_3COOH	-	-	200	10 and 72	Anatase, Brookite and Rutile
Vorkapic and Matsoukas (1998)	HNO_3	10 - 100	6 - 72	-	-	-
So et al. (1997)	HNO_3 and isopropanol	80	12	160 – 240	3 - 12	Anatase and Rutile
Gopal et al. (1997)	HNO_3 and 2-propanol	35, 62, 79 and 90	7.5, 75, 29 and 16 min	-	-	Anatase and Rutile
Bischoff and Anderson (1995)	H_2SO_4, HNO_3 and HCl	80	0 - 11	-	-	Anatase and trace brookite

In the three-stage synthesis pathway used, limitations were seen as: the effects of temperature in the initial stages of the sol-gel synthesis; the shortening of synthesis duration without altering the nanoparticles synthesised; and the effects on the nanoparticles by compensating pH and reaction temperature in the attempt to shorten the synthesis duration. A major limitation found in the study of Chen et al. (2011) was the synthesis time of 96 hours. From Vorkapic and Matsoukas' (1998) study it was evident that titanium tetra isopropoxide can be selected over the titanium tetra butoxideas used by Chen et al. (2011), owing to cost. Furthermore, the reason for using titanium alkoxides was because of their high reactivity with water (Vorkapic & Matsoukas, 1998).

Cape Peninsula
University of Technology

2.5. TiO$_2$ nanoparticles as a semiconductor and photocatalyst

A photocatalyst is the combination of two chemical reaction mechanisms that work together simultaneously (Novikov, 2010); A photon is defined as a quantum of electromagnetic (light) energy, and a catalyst is a homo/heterogeneous substance that increases the rate at which a reaction takes place (Farlex, 2012). Photocatalytic reactions thus mean that both light and a catalyst are needed for a reaction to take place (Patil et al., 2008: 189). A range of different semiconductor photocatalysts has been used and studied. The various photocatalysts and their respective band gaps are given in Table 2.2.

Table 2.2: Band gaps of semiconductor photocatalysts, at a pH of 1 (Gupta & Tripathi, 2011)

Photocatalyst	Band gap (eV)
TiO$_2$	3.2
SiC	3.0
SnO$_2$	3.8
WO$_3$	3.2
ZnO$_2$	3.2
CdS	2.5

A photocatalyst that has received considerable attention in industrial and domestic applications is TiO$_2$ (Gupta & Tripathi, 2011). With TiO$_2$ being able to be manipulated at a nanoscale, it has been established that photocatalytic activity is affected by changes in phase (Liao & Liao, 2007).

TiO$_2$ has the potential to be excited by the use of different light energies; photons with energy equal or higher than TiO$_2$ band gap will initiate the photo oxidation and reduction reactions on the TiO$_2$ nanoparticle surface (Chen et al., 2011; Gupta & Tripathi, 2011). The growing demand for research in using TiO$_2$ for environmentally friendly photocatalytic applications is because they are chemically inert (Yu et al., 2007), they have strong oxidizing power (Chen et al., 2011), are inexpensive (Su et al., 2006), photostable, and non-hazardous to humans (Gupta & Tripathi, 2011). TiO$_2$'s three phases have different band gaps: rutile (3.02 eV), anatase (3.2 eV), brookite (2.96 eV) (Gupta & Tripathi, 2011). Difference in phase relates to the photo-stability and the photo-reactivity (Gupta & Tripathi, 2011). This band gap range of TiO$_2$ can be excited when radiated with UV light of the wavelength of ~387.5 nm (Ehrampoosh et al., 2011). This limits TiO$_2$ to be activated by solar radiation beginning at a wavelength of 300 nm; thus TiO$_2$ can only use 3–4% of the solar radiation on the earth's surface (Ehrampoosh et al., 2011).

Photocatalysts have been used in a number of studies for the degradation of organic pollutants from water (Patil et al., 2008: 194).The process of a semiconductor photocatalyst is a simple exchange of electrons at the surface of the photocatalyst (Chen & Mao, 2007). This exchange is created by the absorption of photons radiated with larger energies than that of the TiO$_2$ band gap; this results in excited electrons to be exchanged between the valence and conduction band (Chen & Mao, 2007). When the electrons are exchanged, electron-hole pairs are

created that react and degrade the unwanted pollutant (Chen & Mao, 2007). Photodecomposition reactions are driven by radicals generated by the electron-hole pairs created; some of the radicals formed and their oxidation potentials are listed in Table 2.3 (Chen & Mao, 2007; Patil et al., 2008: 191).

Table 2.3: Oxidation potential of radicals formed during photocatalytic electron-hole pairs creation (Patil et al., 2008: 191)

Species	Oxidation potential (V)
Hydroxyl radicals	2.80
Atomic oxygen	2.42
Perhydroxyl radicals	1.70

The mechanism followed by the TiO_2 photocatalytic process is given in Equation 2.8 (Patil et al., 2008: 191)

$$TiO_2 + hv \rightarrow h^+_{VB} + e^-_{CB}$$
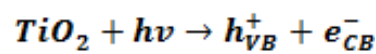
Equation 2.8

Where hv is the photon energy radiated from light (eV), e^-_{CB} is the electron released from conduction band and h^+_{VB} is the electron received to valence band.

Figure 2.8 presents a general representation of the photocatalytic mechanism in operation, and how the radicals are formed at the surface of the photocatalyst (Patil et al., 2008: 192).
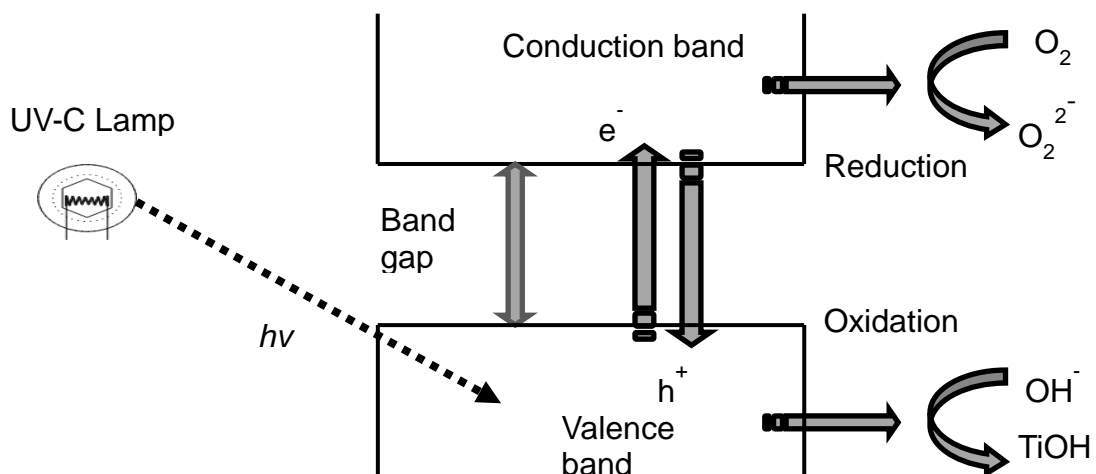
Figure 2.8: Representation of general mechanism for establishing electron transfer over band gap for TiO₂ photocatalytic activity (Patil et al., 2008)

After electron transfer between band gap has been established, electron-hole pairs at the conduction and valence band can become trapped at the surface of TiO_2. Electron-hole pairs trapped at the surface of the valence band will come into contact and react with water or hydroxide ions to form hydroxyl radicals (Patil et al., 2008: 192):

$$h_{VB}^+ + 2OH^- \rightarrow OH^- + OH^\bullet$$

$$H_2O + h_{VB}^+ \rightarrow H^+ + OH^\bullet \ [H_2O \leftrightarrow H^+ + OH^-]$$
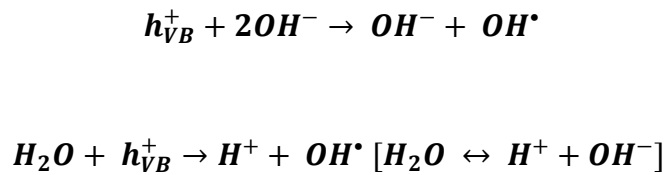
Equation 2.9

$OH^\bullet$ -   Hydroxyl radical

On the conduction band side, electron-hole pairs trapped at the surface will come into contact and react with reducible species such as oxygen (Patil et al., 2008: 192):

$$e_{CB}^- + O_2 \rightarrow O_2^{\bullet-}$$

$$O_2^{\bullet-} + 2H_2O \rightarrow 2OH^\bullet + 2OH^- + O_2$$
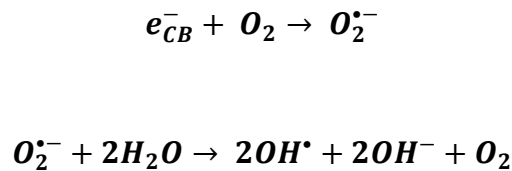
Equation 2.10

The hydroxyl radicals released by oxidation and reduction reactions taking place at the valence and conduction band attack and degrade the organic pollutant (Patil et al., 2008: 192):

$$R + 2OH^\bullet \rightarrow R^{'\bullet} + 2H_2O + O_2$$

Equation 2.11

$R^{'\bullet}$ -   Organic radical

The organic radical released by reaction presented in Equation 2.11, undergoes complete oxidation to carbon dioxide (Patil et al., 2008: 192).

2.5.1. TiO$_2$ photocatalytic application

Coloured organic dyes in wastewater streams can result in a number of medical complications; furthermore they have a great impact on the environment and aquatic life (Thomas & Burgess, 2007). These coloured organic dyes are compounds that can be of an acidic or basic nature, and can absorb UV light (Thomas & Burgess, 2007). Organic dyes generally contain organic one cyclic ring or more; chromophores (conjugated bonds) give these

dyes their colouration (Thomas & Burgess, 2007). A common coloured dye family is that of azoic dyes; these dyes are known for their N=N bond (azo bond) (Thomas & Burgess, 2007).

Chen et al. (2011) studied the impact on photocatalytic activity of pure rutile TiO_2 synthesised via the sol-gel technique with prolonged hydrothermal treatment. It was found that particles produced under increased hydrothermal duration (up till 15 hours), increased the rate of degradation of methylene blue dye, this was found to be due to increase in crystallinity domain. Ryu et al. (2006) studied the impact on photocatalytic activity of pure anatase and mixed anatase-rutile phase TiO_2. It was found for pure anatase phase TiO_2 that rate of degradation of methylene orange was greater than for pure rutile. In this case they found that the reaction rate decreased for mixed phase of anatase and rutile compared to pure anatase. Tzikalos et al. (2013) studied the degradation of a reactive red with the use of mixed anatase and brookite compared to commercially available anatase/rutile (Degussa P25) phase; this study showed that the anatase/brookite mixture had similar photodegradation potential to that of P25.

Liao and Liao (2007) studied the impact of TiO_2 photocatalytic activity on changes in average particle size and the shape of TiO_2 nanoparticles. It was found that cubic-shaped TiO_2 nanoparticles' reaction rate of degradation was fastest. Testino et al. (2007) studied the effects of phase on the photocatalytic degradation of phenol. It was found that size, phase, and shape alone did not constitute an optimum photocatalyst; however, a combination of size, shape, and phase produced an optimum photocatalyst for the degradation of phenol (Testino et al., 2007). Shape and sizes was found to change the wavelength at which excited the surfaces of particles.

From the review of work done on photocatalytic behaviour of synthesized TiO_2, it was evident that TiO_2 photocatalytic activity is not only dependant on concentrations of material to be photodegraded and type of material degraded, but also on the phase, shape and size of particles. It was found that the degree of crystallinity of a pure phase increased the rate of photodegradation. Furthermore, pure phases showed to be less efficient than mixed phases.

2.6 Characterisation techniques for nanomaterial

Solid material can be classed into two groups: amorphous, where solid atoms have the same random disordered arrangement as found in liquids, and crystalline, where solid atoms have a more ridged structure (Bandyopadhyay, 2008: 129). Characterisation is crucial, as this will provide the necessary information of the materials, such as chemistry, phase (architecture) and shape.

As stated earlier, TiO_2 nanoparticles have a large number of applications and properties (Gupta & Tripathi, 2011). Because of these various properties of TiO_2, different characterisation approaches are needed. In this research, the effects of synthesis parameters on nanoparticles synthesised was studied with the use of these three analytical approaches:

2.6.1 XRD

X-Ray Diffraction (XRD) is a powerful and frequently used means of characterisation which is used to determine solid powder samples' composition and phase (Nayak & Singh, 2007, Leng, 2009: 58-59). XRD equipment comprises an X-ray diffractometer; in the diffractometer a single X-ray beam is shot on the surface of the sample. The beam of a single wavelength (for which the incident angle is varied between angles selected) comes into contact with the surface of the sample and is diffracted off the surface. The diffracted X-ray beam, referred to as the diffractometry of the X-ray beam, enables exposure of samples' composition and phase (Leng, 2009: 59).

Using this means of characterisation is non-destructive to samples, and furthermore provides information on samples' impurity, therefore this method of characterisation will shed light on the purity and phases formed of the sample synthesised for alterations made to synthesis parameters (Belin & Epron, 2005). Furthermore XRD analysis distinguishes the phase of the sample, even if the sample is in multi-mixed phase (Nayak & Singh, 2007). This means of characterisation provides information on the crystal size by samples' peaks recorded. The width of the peak recorded is related to crystal size; an increase in peak width relates to a decrease in particle size (Leng, 2009: 64).

A database of over 60 000 known diffractometries has been complied for the powder diffraction file. Once the sample has undergone XRD analysis, the sample phase can be determined by making reference to the powder diffraction file (Leng, 2009: 66). Figure 2.9 provides an example of XRD pattern.
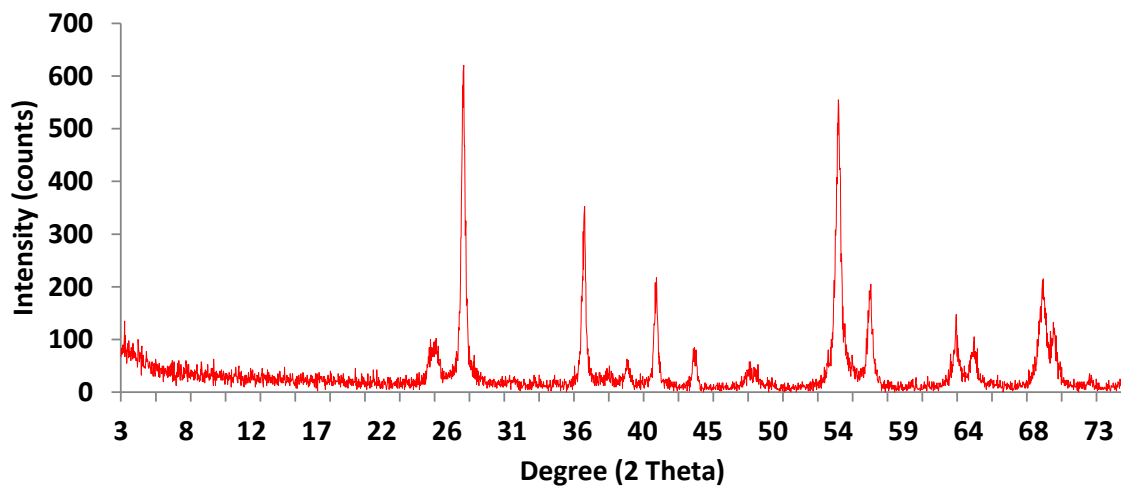
Figure 2.9: XRD pattern of TiO₂ sample presenting the major peaks of Rutile and Anatase phase

This method of characterisation was one of the techniques used to characterise clay composition, which provided the researcher with the phase present in the clay (Nayak and Singh, 2007). XRD analysis has been previously used to study effects on nanoparticle size and phase for changing pH of a reaction (Mahshid et al., 2006). It was also used to quantify effects on particle size and phase by calcination at varying temperatures (Mahshid et al., 2006). XRD has been used to further understand the effects on TiO₂ nanoparticle shape, size and phase, varying in catalyst concentration and catalyst used (Wu et al., 2002). Kuzmany et al. (2001) used XRD to determine

sample particle diameter, using a general formula that could be applied to XRD data obtained. The use of XRD by Chen et al. (2011) was to determine domain size of rutile TiO_2 nanoparticles and they found that for shorter hydrothermal treatment duration, a smaller particle size would be obtained.

Limitations of using this characterisation technique are: it is incapable of differentiating structural detail of samples; moreover overestimations of sample particle diameter can occur for non-spherical particles. For more accurate structural information results pertaining to sample particle, the use of TEM analysis is advised (Belin & Epron, 2005).

2.6.2 TEM

Transmission Electron Microscopy (TEM) is a powerful means of studying nanomaterial samples by recording the interactions with an incident electron beam passing through the sample (Novikov, 2010: 168; Agostini & Lamberti, 2011: 133).

TEM characterisation obtains chemical information at an atomic level; furthermore TEM surpasses XRD characterisation as it takes electron diffracted signals used to characterise samples to form an image of the samples (Agostini & Lamberti, 2011: 133). Two images obtained from using TEM characterisation are presented in Figure 2.10 (Chen et al., 2011).
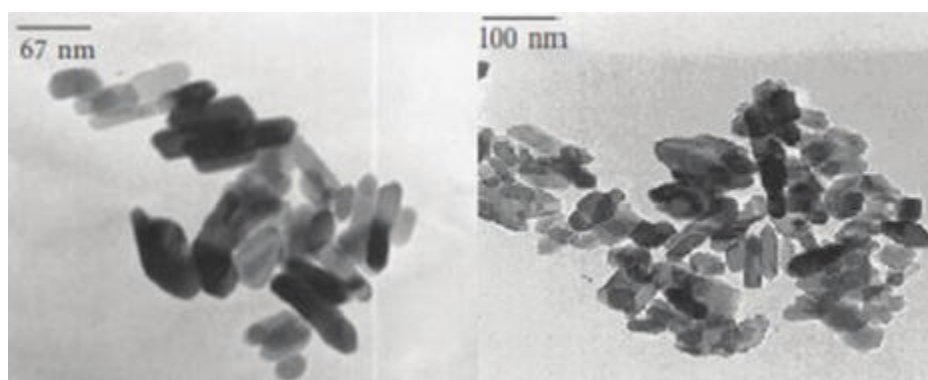
Figure 2.10: TEM characterisation image showing shapes of TiO$_2$ nanoparticles (Chen et al., 2011: 5).

TEM characterisation supplies information on crystal lattice, fringe analysis, textual analysis, and interplanar spacing, plus crystallographic planes of the crystal (Francisco et al., 2001). A TEM microscope comprises an electron gun (source of electrons used in characterisation), followed by a number of magnetic lenses and condensers that are assembled in the following order (Agostini & Lamberti, 2011: 134-135):

The arrangement of an electron microscope is presented in Figure 2.11.
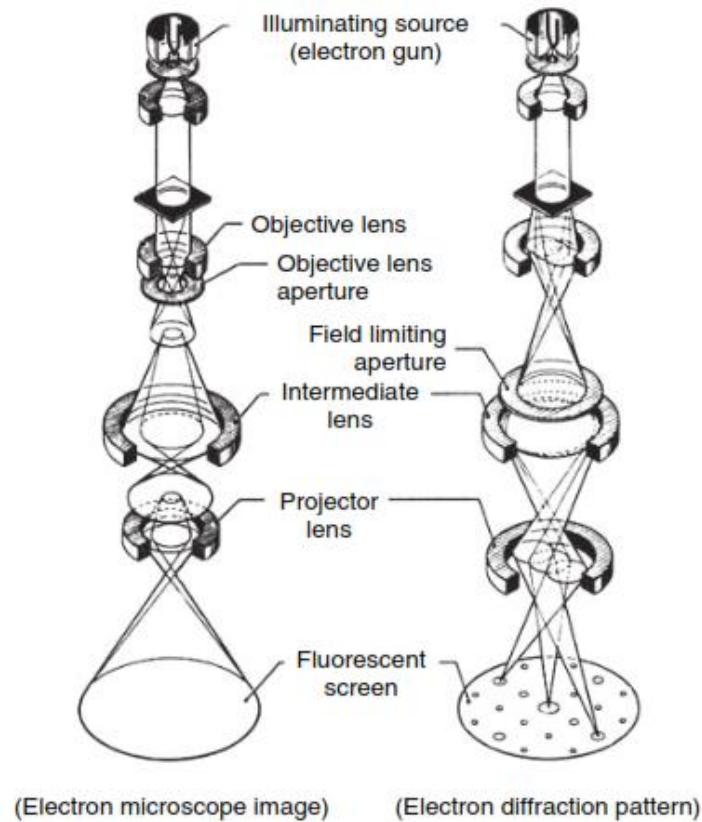
Figure 2.11: TEM microscope assembly, which shows the method followed in formation of an image and the formation of the diffraction pattern (with permission from Elsevier (Agostini & Lamberti, 2011: 134)

This means of characterisation has been used to characterise multi-walled nanotubes, for which the images were used to develop an analysis methodology. This was made possible by TEM's flexibility in image projection and electron diffraction for studying the carbon nanotubes' structure (Belin & Epron, 2005).

TEM was used in studying structural changes to the surface area observed by the capping of TiO_2 nanoparticles when used as catalysis (Francisco et al., 2001). A high-resolution TEM was used to obtain the data relating to structural information of particles synthesised and capped, structural information obtained, and fringes and spacing of crystal (Francisco et al., 2001). The TEM equipment used was equipped with an EDS characterisation tool.

2.6.3   EDS

Energy dispersive X-ray spectroscopy (EDS) is a technique used for the evaluation of chemical composition, by the energy emitted when a sample is radiated with a high-energy electron beam (Novikov, 2010). EDS can be used for quantitative and qualitative evaluation of the chemical composition of a sample. This characterisation technique was studied simultaneously when performing TEM characterization. The high-energy electron beam is used to radiate the sample. This causes X-ray fluorescent rays to be radiated from the sample (Leng, 2009: 121). These X-rays are counted and analysed with the use of a fixed-energy dispersive counter, to give the sample's energy spectrum. The energy spectrum determined is then associated with an element or elements (Leng, 2009: 123-124; Novikov, 2010: 53).

2.6.4   Colorimetry and UV-Vis spectrophotometry

Colorimetry is a term developed by a chemist that refers to changes in a system's colour due to changes in the concentration of a component (Vogel & Jeffery, 1989: 645). These colour changes can be desirable changes with respect to components formed. Moreover, the change in colour is an indication of a change in matter (Vogel & Jeffery, 1989: 651 - 652).

The visual colorimeter was invented in 1870 by Jules Duboscq, a French inventor (Hannavy, 2013: 445). Chemists found a margin of error for classifying the change in colour of a sample from chemist to chemist; therefore the photoelectric calorimeter replaced the visual colorimeter (Vogel & Jeffery, 1989: 653). Furthermore, a photoelectric colorimeter was introduced in 1905 (Rocco, 2005), which allowed for a larger range of wavelengths to be analysed. This then led to the development of a spectrophotometer (Vogel and Jeffery, 1989: 673). Spectrophotometers allow analysis of matter and components that employ even smaller wavelengths and bandwidths (Thomas & Burgess, 2007: 34).

UV-Visible spectrophotometers were constructed on the basis of two laws regarding colour, light, and concentration of components in water; the two laws are Lambert's and Beer's laws (Vogel & Jeffery, 1989: 651). Lambert's law states that when monochromatic light passes through a material, the decrease in light intensity leaving the material is proportional to the material's thickness (Vogel & Jeffery, 1989: 653). The reason for the decrease in light entering the material and then passing through the material, is due to a fraction of light being absorbed by the material (Vogel & Jeffery, 1989: 651).

Beer's law furthers that which was stated in Lambert's law; Beer's law studies the effect of concentration with respect to coloured material in solution on the light transmission and/or adsorption (Vogel & Jeffery, 1989: 651). The relationship of light entering and being emitted decreased proportionally with an increase in concentration of material in solution found (Vogel & Jeffery, 1989: 651).

UV-Visible spectrophotometry is widely used to determine and identify matter found in water samples by measuring the interaction of artificial light passing through the water sample (Thomas & Burgess, 2007: 1). The passing light will interact with matter that is visible or invisible to the naked eye (Thomas & Burgess, 2007: 1). The spectrophotometer determines the interaction of atoms and material within the sample with the use of electromagnetic radiation supplied by the artificial light passing through (Thomas & Burgess, 2007: 2 - 3).

We as humans are able to see colours; this is made possible by a detector within the eye that can distinguish the different wavelengths of colours observed (Thomas & Burgess, 2007: 3). The electromagnetic spectrum known thus far is presented in Figure 2.12 and the approximate wavelengths of colour ranges are summarised in Table 2.4.
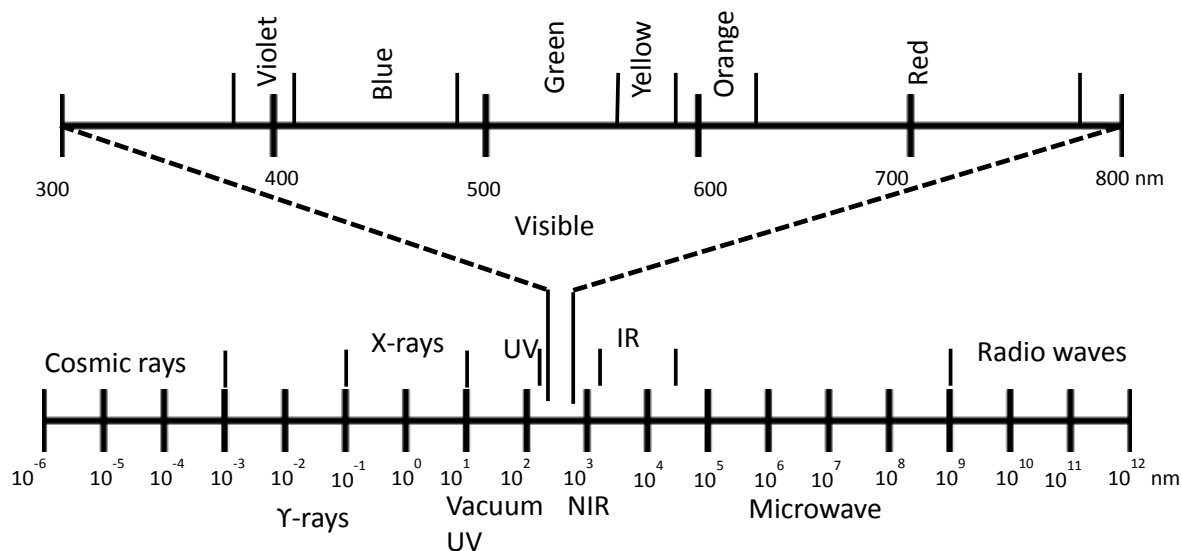
Figure 2.12:Electromagnetic light spectrum (Thomas & Burgess, 2007: 3)

Table 2.4: Wavelength approximates of colour for the electromagnetic light spectrum (Vogel & Jeffery, 1989)

Ultraviolet	<400 nm	Yellow	570–590 nm
Violet	400–450 nm	Orange	590–620 nm
Blue	450–500 nm	Red	620–760 nm
Green	500–570 nm	Infrared	>760 nm

2.7 Conclusion

The fundamental factors affecting reaction rates with the use of catalysts and their laws were reviewed. From the understanding for the optimisation of reaction rates, nucleation and crystal nanoparticles growth of metal oxide was then reviewed. It was found that nucleation and growth of metal oxide proposed a challenge when optimising, dependent on the synthesis technique used. It was found that two distinct techniques were used for the synthesising TiO_2 nanoparticles. A sol-gel synthesis techniques was found to be flexible for varying properties of the metal oxide (TiO_2), with a simplex synthesis route. It was found that a two stage, batch sol-gel synthesis technique could be used. Bischoff and Anderson (1995) found synthesising a gel using sulphuric acid was more complicated than when using hydrochloric. For low concentrations of sulphuric acid, porous gels were formed, however increasing acid concentration resulted in nonporous gels forming (Bischoff & Anderson, 1995). The use of HCl for the synthesis of TiO_2 nanoparticles has been used for a number of studies (Wu et al., 2002; Reyes-Coronado et al., 2008; Hsu & Nacu, 2003; Mogyorosi et al., 2003; Wu et al., 2011; Chen et al., 2011). Sol-gel studies using a homogeneous catalyst performed by Wu et al. (2002), Hsu and Nacu (2003) and Chen et al. (2011), showed that the use of HCl acid as catalyst was vital and favour the formation of rutile TiO_2. A major limitation found in the study of Chen et al. (2011) was the synthesis time of 96 hours to produce pure rutile, even with the use of a catalysts. Furthermore, understanding impacts to crystal size and size distribution is needed for

morphology control. It was found increased concentration of HCl can be used to reduce standard particle and size distribution.

Vorkapic and Matsoukas (1998), showed the effects of titanium precursor on synthesised TiO_2. From Vorkapic and Matsoukas' (1998) study it was evident that. titanium tetra isopropoxide can be selected over the titanium tetra butoxide as used by Chen et al. (2011), owing to cost and a number of studies were performed using this titanium alkoxide (So et al., 1997; Zhang et al., 1998; Mahshid et al., 2006; Kim et al., 2011). Furthermore, the reason for using titanium alkoxides was justified by the high reactivity with water (Vorkapic & Matsoukas, 1998). Synthesis of gel TiO_2 needed to undergo thermal treatment for the formation of a crystalline product. Two thermal treatment techniques were reviewed, where it was found that the use of hydrothermal synthesis technique allowed for a greater control over the reaction parameters and thus provides in-depth insight to the effects of individual parameters. Hydrothermal treatment times ranged from 1 to 10 hours and temperature ranged between 150° and 200 °C. An increase in particle size was found when increasing hydrothermal treatment duration (So et al., 1997). Characterization techniques used for TiO_2 were reviewed. Furthermore applications and techniques for applying TiO_2 were reviewed and the characterisation of these applications. For the different synthesis techniques used and reagents, no consensus was found in literature for TiO_2 particle shape, size and phase, and therefore a systematic study of reaction parameters for the sol ageing process a reduction in synthesis time is required.

C**hapter 3**

This chapter provides information on the experimental methodology used for synthesis of TiO_2 nanoparticles. A sol-gel synthesis technique that incorporated hydrothermal treatment was used. The TiO_2 final product after characterisation was used for the application as a photocatalyst, to degrade an organic dye.

3. Methodology

It was observed that by altering reaction parameters, the phase, particle shape, and size of TiO_2 nanoparticles could be changed. The effects of HCl concentration and gel formation time on the phase, shape and size of TiO_2 nanoparticles synthesised via the sol-gel method needs further investigation, as this affects the efficiency various applications. The reaction parameters studied are the concentration of HCl (homogeneous catalyst), gel formation time and the prolonging of the hydrothermal treatment time to account for shortened gel formation time.

Appendix A shows the pump curves used to determine the flow rate used for the addition of dropwise water. A summary of the systematic approach to studying the effects of HCl concentration and gel formation time on TiO_2 is shown in Figure 3.1 and 3.2.
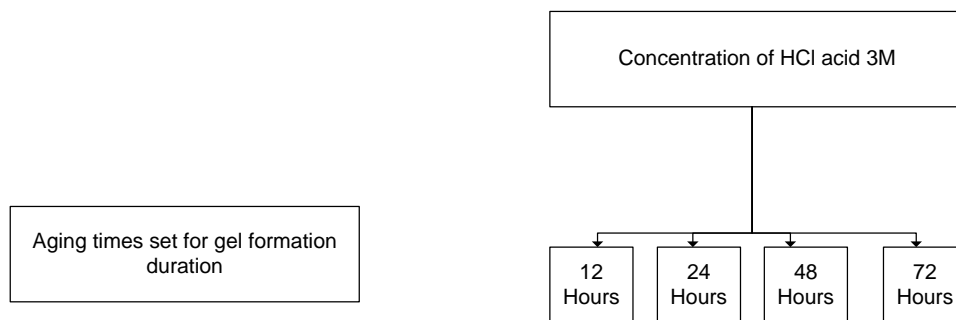
Figure 3.1: Flow chart summary of systematic approach to evaluate the effects of HCl acid concentration and shortened gel formation time

Figure 3.1 presents a flow chart for the shortening gel formation time taken using a sol-gel synthesis technique of TiO_2 amorphous gel, in 3 molar HCl.

Cape Peninsula
University of Technology
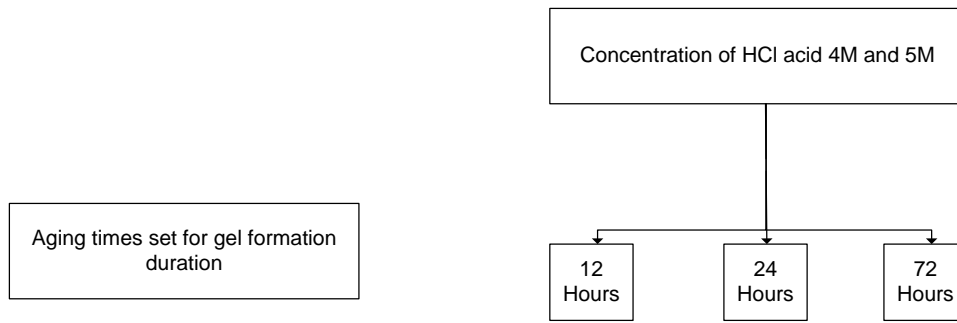
Figure 3.2: Flow chart for systematic approach to evaluate the effects of HCl acid concentration and shortened gel formation time, for 4 and 5 molar

Figure 3.2 illustrates the approach to increasing HCl concentration to 4 and 5 molar, as it was found to change the TiO_2 nanoparticle phase, shape and size favourably.

Figure 3.3 shows the hydrothermal treatment times used at shortened gel formation time, to evaluate their effects on the growth of TiO_2 nanoparticles and transformation between phases.
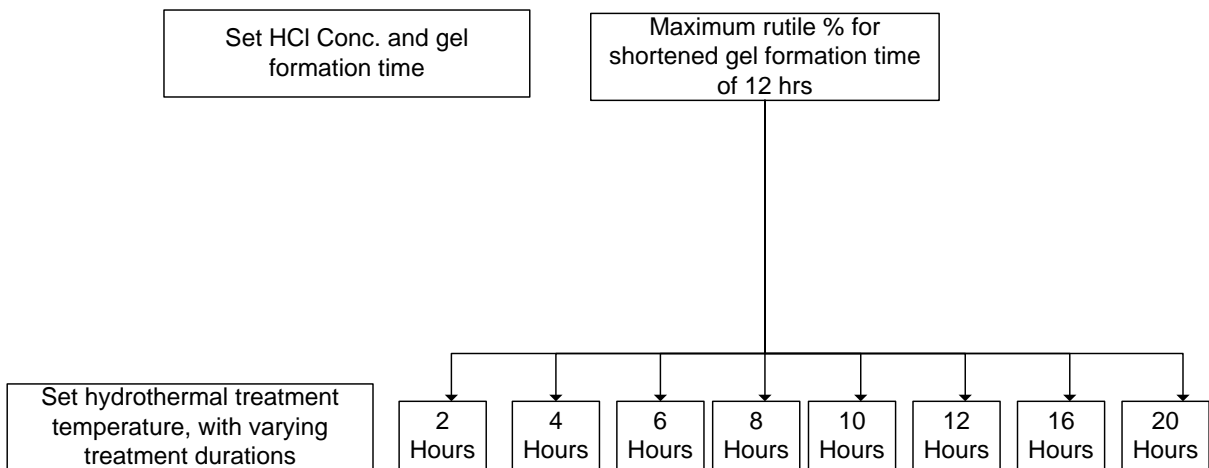
Figure 3.3: Flow chart to evaluate the effects of shortened gel formation time, with prolonged hydrothermal treatment time

Figure 3.4 presents the experimental setup for sol-gel synthesis of amorphous TiO_2 nanoparticles. The experiments consisted of the synthesis of TiO_2 from titanium (IV) isopropoxide precursor, in a batch reactor containing 50ml of concentrated hydrochloric acid. The experiments were performed in a 250ml glass beaker. The ageing step was conducted under continuous magnetic stirring. Changes to HCl concentrations were made at the sol stage of the sol-gel synthesis. A one litre Teflon®-lined autoclave was used for hydrothermal treatment. Different hydrothermal synthesis times were studied for a set hydrothermal temperature, according to Chen et al. (2011).
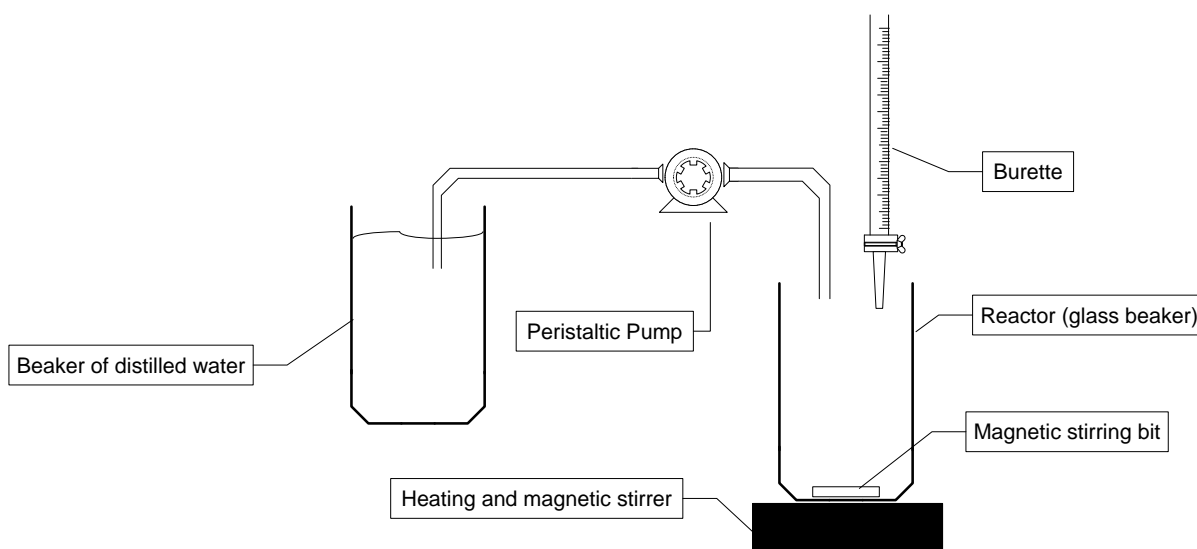
Figure 3.4: Experimental setup of sol-gel synthesis of TiO$_2$

The nanoparticles synthesised were analysed using the following analytical methods: X-ray diffraction (XRD), Transmission Electron Microscopy (TEM) and Electron Diffraction Spectroscopy (EDS). The use of these analytical methods provided information with regard to the particle phase, shape, and size. After characterisation, the TiO$_2$ nanoparticles' photocatalytic efficiencies were evaluated, for the photodegradation of methylene blue. An open-batch system with a fixed UV light source was used for the photodegradation of methylene blue. Waste material synthesised was collected in waste drums, labelled and given to EnviroServ for disposal.

3.1. Sol-gel synthesis procedure

Sol-gel chemistry for the synthesis of TiO$_2$ nanoparticles consists of a two-stage synthesis: firstly the formation of the sol (addition of precursor to HCl) and thereafter the formation of the gel (by adding water dropwise). However to obtain nanoparticles of specific phase, shape and size, thermal treatment was required. Therefore, gel formed was added to a Teflon®-lined hydrothermal reactor; here the amorphous gel was transformed to crystalline nanoparticles. The finalised treatment of the nanoparticles then took place. In this research, only aqueous sol-gel chemistry was studied. The procedure followed for synthesis of TiO$_2$ nanoparticles was based on a previous sol-gel synthesis procedure of Chen et al. (2011), with slight modifications.

3.1.1. Sol synthesis

For synthesising the sol, 11 ml of titanium (IV) isopropoxide (Ti (O-Iso)$_4$, ACROS), as Ti precursor, was added 1 ml per second with a peristaltic pump (Watson Marlow, 505S) into a set volume of 50ml of hydrochloric acid (HCl, C.J.LABS), as HCl homogenous catalyst, under magnetic stirring (SCILOGEX, MS7-H550-Pro), until a clear solution or sol was formed. The above-mentioned experiment was a standard one used as reference. The HCl concentrations used for sol synthesis were 3, 4, and 5 molar.

3.1.2. Gel synthesis

After forming the sol, it was vital to commence with the second stage of the synthesis, otherwise the sol would undergo hydrolysis with the ambient moisture in the air. The pH of the solution was not altered after the sol was formed. The TiO_2 gel was formed by hydrolysis, followed by simultaneous polycondensation. Previous work showed that the smallest nanoparticles were obtained for a [Ti^+] to water ratio of 0.25:1 M (Chen et al., 2011). Thus 150 ml of distilled water (Lasec, Purewater300) was added using a peristaltic pump under constant stirring for gel formation times, of 12, 24, 48 and 72 hours. An opaque white layer was observed when the gel formed, as presented in Figure 3.5.
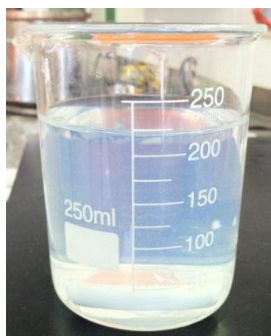
Figure 3.5: Amorphous TiO$_2$ gel before hydrothermal treatment

3.1.3. Hydrothermal treatment procedure

Gel formation was followed by hydrothermal treatment because it promotes crystallisation. It was essential that once the gel had formed, hydrothermal treatment commenced, as the gel should not be left to age. The reason for this was that white, paste-like sediment starts to form. This procedure was taken from Chen et al. (2011); however a set hydrothermal treatment time of 1 hour, and a temperature of 220 °C was used in this study. The 250ml glass beaker was emptied into a one-litre Teflon® liner. The change in Teflon® liner volume differed from that used by Chen et al. (2011). The temperature controllers (GEFRAN 800P, AND 600) were set to increase the temperature of the gel mixture by 2 °C per minute, until a reaction temperature of 220 °C was reached. An oscillation band of two degrees above and below reaction temperature was set, to avoid runaway temperatures and to ensure the most ideal conditions. The reaction temperature was recorded using a data logger (Testo 176T2 logger). Figure 3.6 presents the hydrothermal reactor used for the transformation from amorphous to crystalline TiO_2 and vital components of the reactor.
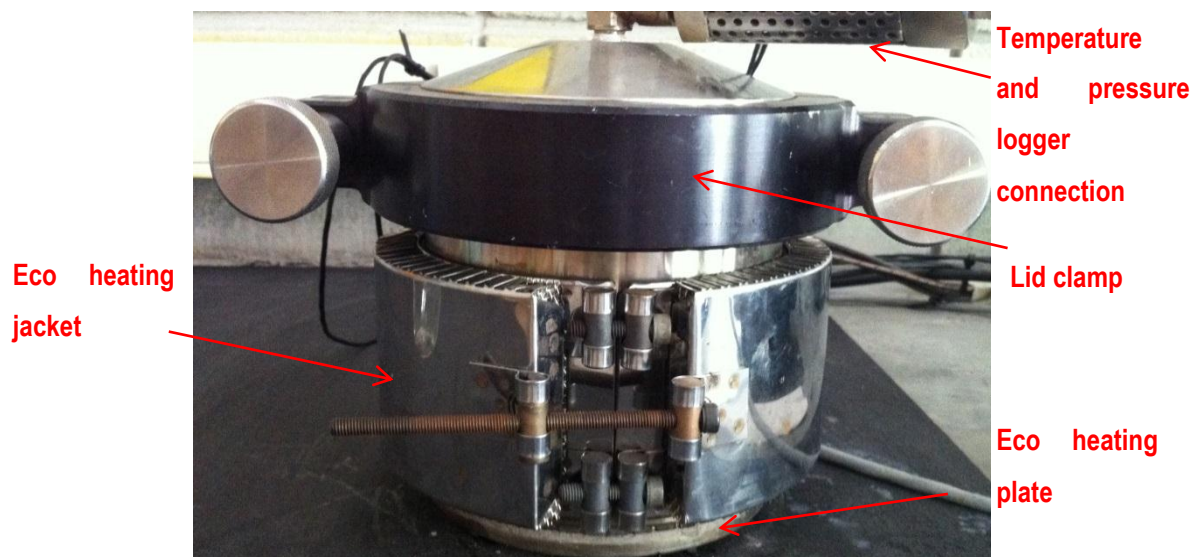
Figure 3.6: Hydrothermal reactor used in transforming amorphous TiO₂ nanoparticles to crystalline TiO₂ nanoparticles

After the gel mixture had undergone hydrothermal treatment, a supernatant liquid was decanted and the residual solids washed several times with water and ethanol and dried in air/oven at a low temperature. Hydrothermal treatment time was varied to favour the growth as used by to support phase transformation to rutile (Zhang & Banfield, 2000; Zhang & Banfield 2005; Chen et al., 2011).

3.1.3.1. Temperature profile

Figure 3.7 illustrates the actual temperature profile versus the ideal temperature profile for the standard operations of the hydrothermal reactor. The vessel was heated to a set point of 220 °C, maintained at this temperature, and thereafter allowed to cool to room temperature. The average reactor temperature and the standard deviation over treatment time is presented in Table 3.1. It was measured with a temperature data logger (Testo, T 176T2); the temperature profiles were obtained for each hydrothermal treatment. The hydrothermal reactor temperature controller was set to ramp the temperature by 2 degrees per minute.
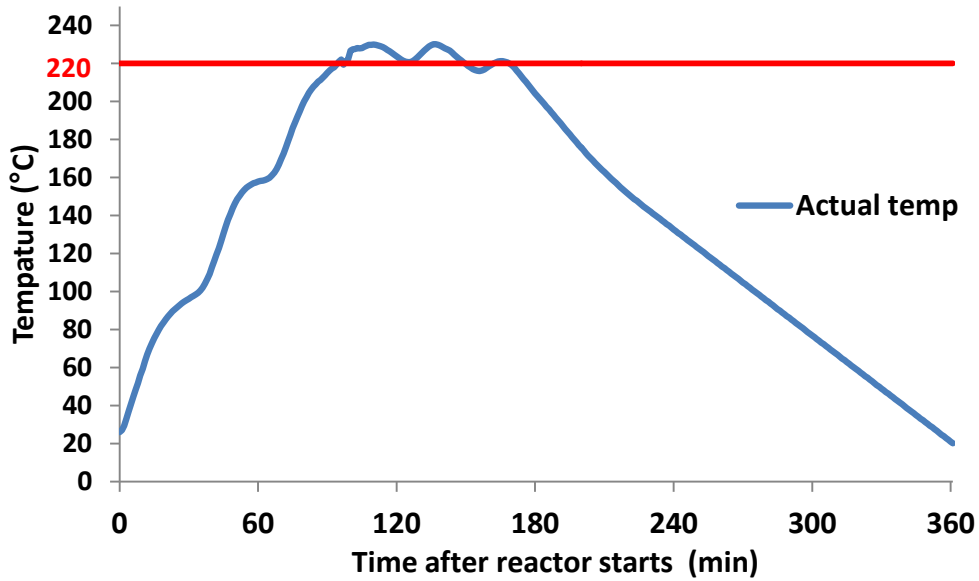
Figure 3.7: Standard temperature profile for hydrothermal reactor operating at a set point of 220 °C

Table 3.1 presents the maximum and average temperature within the reactor vessel, with respect to different HCl concentrations.

Table 3.1: Summary of temperature data logged

HCl concentration	Average Temp. (ºC)	Max Temp. (ºC)
3M	227.25	228.68
4M	224.57	225.81
5M	228.63	230.1

3.1.3.2. Pressure profile

Figure 3.8 shows the actual pressure profile versus the ideal pressure profile for the standard operations of the hydrothermal reactor. The pressure profile was measured with a pressure data logger (Testo, T175). If any changes occurred during the hydrothermal treatment stage with regard to reactor pressure, these would be observed by the pressure profile obtained. From the pressure profile obtained it was clear that the operation of the hydrothermal reactor was functioning as designed. It was determined that the average reactor pressure and standard deviation in reactor pressure over treatment time was 24.95 MPa and plus/minus 1.73 MPa respectively.
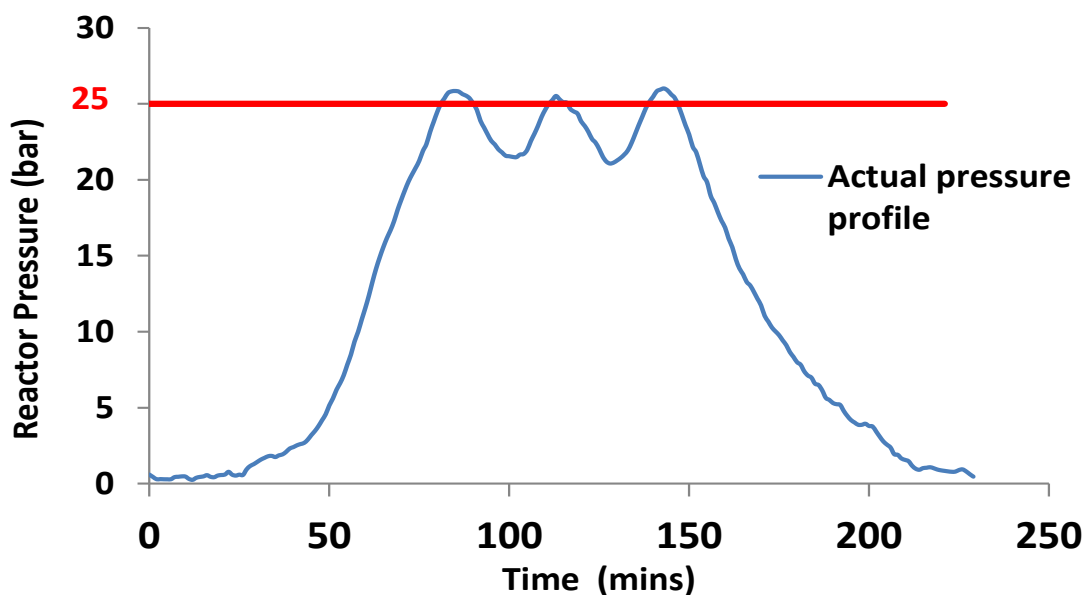
Figure 3.8: Standard pressure profile for hydrothermal reactor operating at a set point of 220 °C; average reactor pressure obtained was 25 bar

Table 3.2 presents the maximum and average pressure within the reactor vessel for the treatment time of x minutes for different HCl concentrations.

Table 3.2: Summary of pressure data logged

HCl concentration	Average Pressure (bar)	Max Pressure (bar)
3M	25.32	26.09
4M	24.41	24.85
5M	25.12	25.81

3.1.4. Final treatment of nanoparticles

The final treatment of TiO_2 nanoparticles was the stage of retrieving the crystalline product. The white TiO_2 sediment collected from the Teflon® liner was then washed with distilled water (Lasec, Purewater300) and ethanol mixture (J.C. Labs), followed by a centrifuging process (Heraeus, Megafuge 1.0). This was repeated several times. After washing, these particles were transferred to a Petri dish and placed in a drying oven (LABCON, 2085K) at a temperature of 150 °C for one hour. The nanoparticles synthesised were weighed after drying.

3.2. Photocatalytic properties and characterisation

The photocatalytic properties and effectiveness to degrade unwanted organics in wastewater streams were tested. Photocatalytic properties of TiO_2 synthesised for shortened gel formation time were studied and compared

with P25 (titanium tetra oxide, industrial grade TiO_2, Degussa Company), as a standard. These experiments were performed on a laboratory scale using methylene blue (methylene blue, Protea Chemicals). Methylene blue was used for comparison of results, as done by Chen et al. (2011). A standard solution of 0.0025 g/ 100 ml methyl blue solution was made up. The solution was then ultrasonically (MRC, CLEAN-01) treated for 30 minutes, to ensure uniformity. The pH was measured (Lasec SA, CRISON, GLP21), and then the solution was stirred at 350 RPM (SCILOGEX, MS7-H550-Pro) for 30 minutes for the solution to be at absorption equilibrium. One ultraviolet lamp (9W UV-C, OSRAM) was used as the source of ultraviolet light. The glass beaker was covered with tinfoil for optimum ultraviolet radiation, and for safe operation. Samples of 1 ml volume were taken at 30-minute intervals and diluted with milliQ water (Lasec, Purewater300) to a ratio 1:3. The experimental matrix is given in Table 3.3.

Table 3.3: Experimental matrix of sol-gel hydrothermally synthesised TiO_2 nanoparticles used to photodecompose methylene blue dye

Catalyst TiO_2 (Catalyst load 0.25 g/L)		Concentration of Dye	Time
HCl conc.	Gel ageing time		
3M	12 hr		
4M	12 hr		
5M	12 hr		
3M	24 hr		
4M	24 hr		
5M	24 hr	0.025 g/100 ml	120 min
P 25			
100 % rutile			
100 % anatase			
Catalyst with no light			
No catalyst			

3.3. Analysis of nanoparticles

Solid material can be classed into two groups: amorphous, where solid atoms have the same random disordered arrangement found for liquids; and crystalline, where the solid atoms have a more ridged structure (Novikov, 2010: 31). The details of the instruments used for XRD, TEM, EDS and UV-Vis characterisation are provided in this section.

3.3.1. XRD

X-ray diffraction was used to study the phase of the TiO_2 synthesised and tests were conducted at the University of Cape Town's (UCT) Department of Geological Sciences. A small amount (less than 1g) of each sample was

prepared by fine grinding with a mortar and pestle into a powder. The powdered sample was placed in a sample holder and loaded into the XRD for analysis. The instrument used was a Philips PW 1390 XRD, which uses a copper K-αα x-ray tube with x-ray wavelength of 1.542 A, accelerating voltage of 40kV and current of 25mA. Bragg 2θ angles between 3° and 70° were used for analysis. A continuous scan step size of 0.025° was applied with a scan step time of 0.5 seconds.

3.3.1.1. X'pert Highscore software

With the use of X'pert HighScore software, with a Joint Committee on Powder Diffraction Standards (JCPDS) database, qualitative analyses of these particles were possible. Furthermore X'pert HighScore provided quantitative studies that determined the sample's phase mixture percentage. The X'pert software was used to calculate the d-spacing of the most intense peaks from the resultant XRD pattern of 2θ vs. counts or counts per second. The software was further used to match the identified peaks and their d-spacing with minerals in the JCPDS database.

3.3.2. TEM and EDS

TEM and electron diffraction spectroscopy (EDS) was characterised at the University of the Western Cape (UWC) Electron Microscope Unit (EMU). This method of analysis provided the researcher with vital knowledge of the nanoparticles: grain size, size distribution, phase, and determining the composition of TiO_2. The following was the instrument used and method of performing the characterisation: HR TEM unit, Tecnai G2 F20 X-Twin Mat200 kV Field Emission HRTEM (operated at 200 kV). The powdered sample was placed in a vial, and 10ml of ethanol added. The mixture was then sonicated for 20 minutes and 1ml of the milky white solution was pipetted onto the TEM scan grid. EDS scans were performed to determine the composition of the nanoparticles that were synthesised.
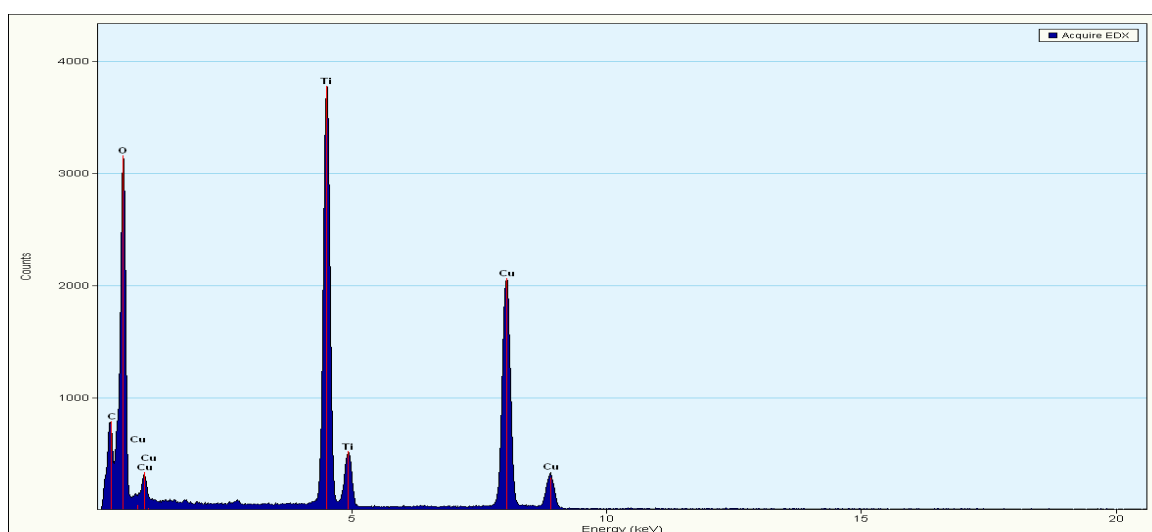
Figure 3.9: EDS scan, identifying the element composition of sample

Figure 3.9 shows the composition of the material that was studied using the TEM unit. There are no impurities from the titanium alkoxide precursor. However from the EDS, the phase of TiO_2 nanoparticles formed was unclear. In Appendix B, two EDS scans can be found, as two TEM sample grids of different material were used.

3.3.2.1. ImageJ software

ImageJ software is an image processing program. It was possible to determine TiO_2 nanoparticle length, diameter and lattice spacing. Several TEM images were taken of each sample and an average of 200 nanoparticles was measured with the use of ImageJ software. This provided the average TiO_2 nanoparticle length and diameter size per sample. In Appendix B, a summary of data collected using ImageJ software for the different reaction parameters used can be found.

3.3.3. UV-Vis spectrophotometer

UV-Vis measurements were performed at CPUT's Chemistry Department. After all samples had been taken every 30 minutes and diluted, they were centrifuged for 5 minutes at a speed of 5600 RPM (Centrifuge, Heraeus, Megafuge1.0). Of the 4 ml samples prepared, only 3 ml were pipetted into a quartz cuvette, for UV-Vis spectrophotometry (UV-Vis spectrophotometer, Cari, Cari 300) characterisation. For methylene blue, a lambda max was determined by the wavelength scan function of the UV-Vis spectrophotometer (UV-Vis spectrophotometer, Cari, Cari 300). Characterisation curves were constructed by characterising change in concentration of dilute samples of the initially prepared methylene blue concentrated solution of 0.0025 g/100 ml. Dilute samples were prepared by adding 1 ml of concentrated methylene blue to 200, 100, 50, 25, 10, 5 ml volumetric flasks; the remaining volume of the flasks was filled with water.

3.4. Conclusion

The experimental methodology of sol-gel hydrothermal synthesises of TiO_2 nanoparticles was explained. The modifications to the sol-gel synthesis technique used by Chen et al. (2011) were: shortening gel formation time, increasing HCl concentration and hydrothermal treatment time. The characterisation techniques used were also explained, as well as the procedure for testing photocatalytic activity for the degradation of methylene blue.

C_{hapter 4}

This chapter provides the results obtained and discussion for TiO_2 nanoparticles when reducing the gel formation time, varying HCl acid concentration, combining shortened gel formation time with varying HCl acid concentration and prolonged hydrothermal treatment times. Furthermore, it provides the test results of the photocatalytic performance of these catalysts synthesised. Effects to phase, shape and size of TiO_2 nanoparticles changed with shortened gel formation time, increased HCl concentration and prolonged hydrothermal treatment times were discussed. The behaviour of TiO_2 nanoparticles with different phases, shapes and sizes that favoured photocatalytic activity is also discussed here.

4. Results and Discussion

For changes made in the sol-gel synthesis technique, the results are presented as the effects observed to changes in phase, shape and size. Further modifications were made to the work of Chen et al. (2011) by increasing HCl concentration from 3 M to 5 M and shortening gel formation time. The effects of HCl concentration and gel formation time on the phase, shape and size of TiO_2 nanoparticles synthesised are presented and discussed. It is followed by the effects by prolonging hydrothermal treatment and the effects on photocatalytic activity for selected synthesised nanoparticles were studied and discussed.

4.1. Effect of acid concentration and gel formation time on TiO_2 nanoparticles phase

According to Wu et al. (2002), where several homogenous acids were used to synthesise TiO_2, it was found that synthesis in an HCl medium forms pure rutile nanoparticles. However, the formation of pure rutile was dependent on the concentration of HCl greater than 1.5M at a constant gel formation time of 72 hours. Figure 4.1 presents which phase is allocated to which peaks, with respect to TiO_2 (Winkler, 2003: 22).
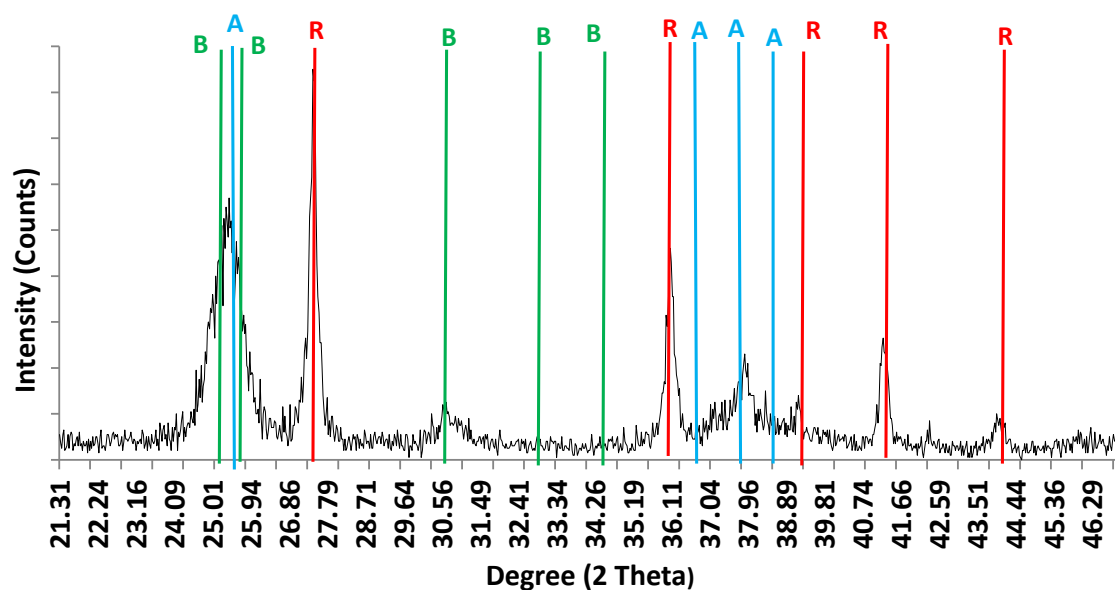
Figure 4.1: XRD patterns of TiO$_2$ nanoparticles for shortening gel formation time for 3 M HCl.

Table 4.1 presents peak Intensities of the three TiO$_2$ morphologies studied.

Table 4.1: Three TiO$_2$ polymorphs peak intensities and location of 2 Theta X ray diffraction spectrum

	Anatase	**2 Theta**	Rutile	**2 Theta**	Brookite	**2 Theta**
Peak intensity (%)	100	25.289	100	27.436	100	25.255
	10	36.949	50	36.087	76.7	25.578
	20	37.791	8	39.183	88.5	30.679
	10	38.566	25	41.226	3.5	32.705
	35	48.052	10	44.048	0.5	34.337

Further modifications were made to the work of Chen et al. (2011) by increasing HCl concentration to 3 M to 5 M. From results obtained by 3 M 24- and 12-hour experiments, the effect the shortening of gel formation duration had on TiO$_2$ nanoparticles was clear. Figure 4.2 presents the transformation of TiO$_2$ nanoparticles for gel formation time ranging from 72 to 12 hours in the presence of 3M HCl. Pure rutile was formed at 72 and 48 hours. Additional peaks were observed in the XRD pattern at 25 °, 37 °, 48 ° (2 Theta), for 24 and 12 hours, indicating the presence of both brookite and anatase.
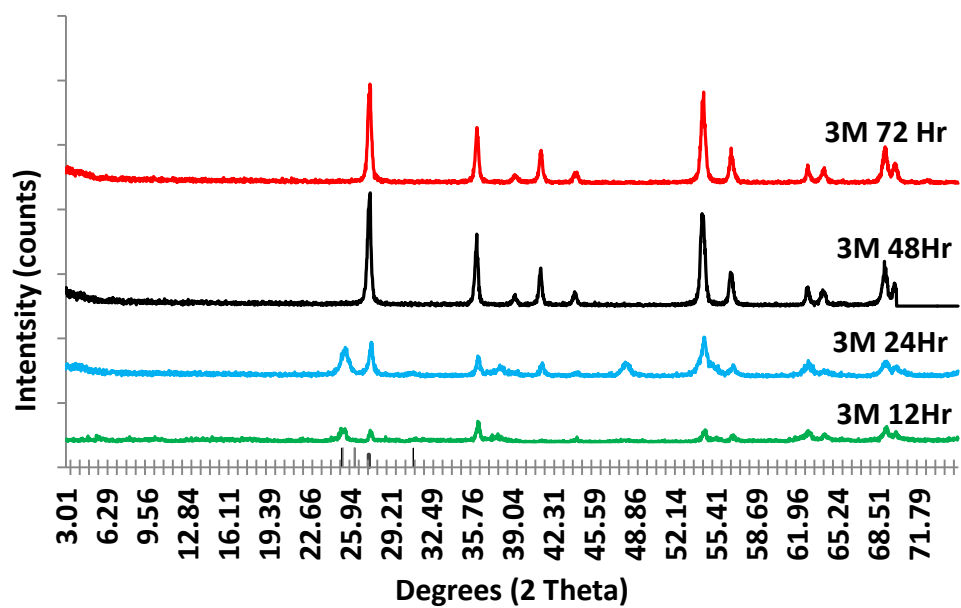
Figure 4.2: XRD patterns of TiO$_2$ nanoparticles for shortening gel formation time for 3 M HCl.

Experiments were performed at increased HCl concentrations for 72, 24 and 12 hours gel formation times, to ascertain if these would favour rutile formation. Pure rutile was formed at 72-hour gel formation time, while all three phases were observed for 24 and 12 hour gel formation times in the presence of 4 and 5 molar HCl as shown in Figure 4.3.
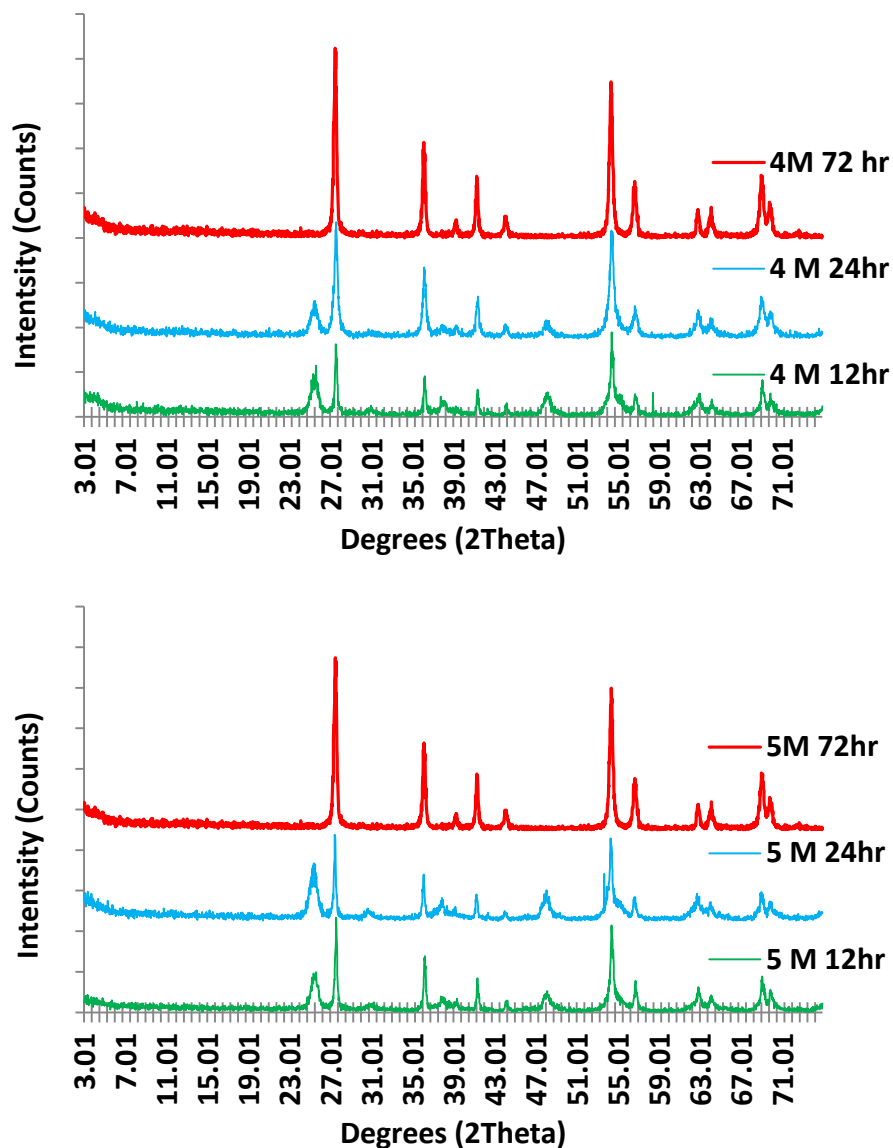
Figure 4.3: XRD patterns of TiO$_2$ nanoparticles formed for shortened gel formation time in the presence of 4 and 5 molar HCl concentrations

Increasing the HCl concentration to 4 and 5 molar did not suppress the formation of other TiO$_2$ phases at gel formation times of less than 72 hours. Nevertheless, the intensity of peaks was analysed for each HCl concentration at different gel formation times, to quantify the percentage of each phase formed in the sample.

Cape Peninsula
University of Technology
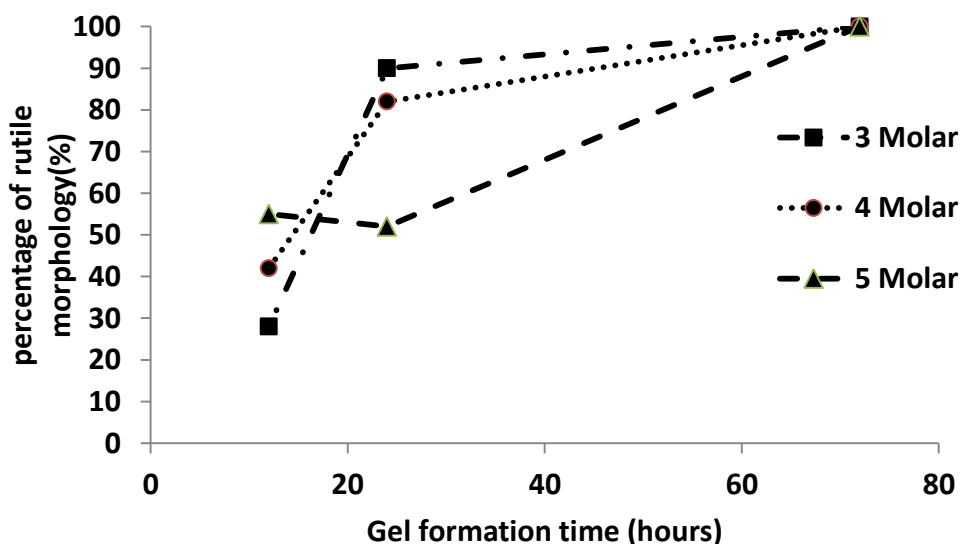
Figure 4.4: Percentage of rutile formed on increasing HCl acid concentration and gel formation time

Figure 4.4 presents the quantity of rutile formed for 72 to 12 hour gel formation time for the three HCl concentrations used. At 72 hours, only pure rutile was formed, regardless of the HCl concentration. This agrees with the findings of Wu et al. (2002), that pure rutile will be formed at HCl concentration greater than 1.5M, even though they only tested up to 2M HCl, and Chen et al. (2011), who extended the HCl range to 3M. The trend for rutile formation for 3 and 4 molar HCl is very similar. The percentage of rutile obtained at 24 hours was 90% and 82% respectively for 3M and 4M HCl. A further reduction in gel formation time to 12 hours led to a significant drop in the percentage rutile of 28% and 42% for 3M and 4M respectively. A contrast was observed for 5 molar HCl concentration. At 24 hours the percentage of rutile obtained was only 52%, a significant drop from that produced at 72 hours, but remained approximately constant towards 12 hours.

Figure 4.5 presents the evolution of TiO_2 polymorphs formed with increasing HCl concentration for a gel formation time of 24 and 12 hours respectively. It is evident that brookite and rutile were dominant, with anatase percentages of up to 15%.
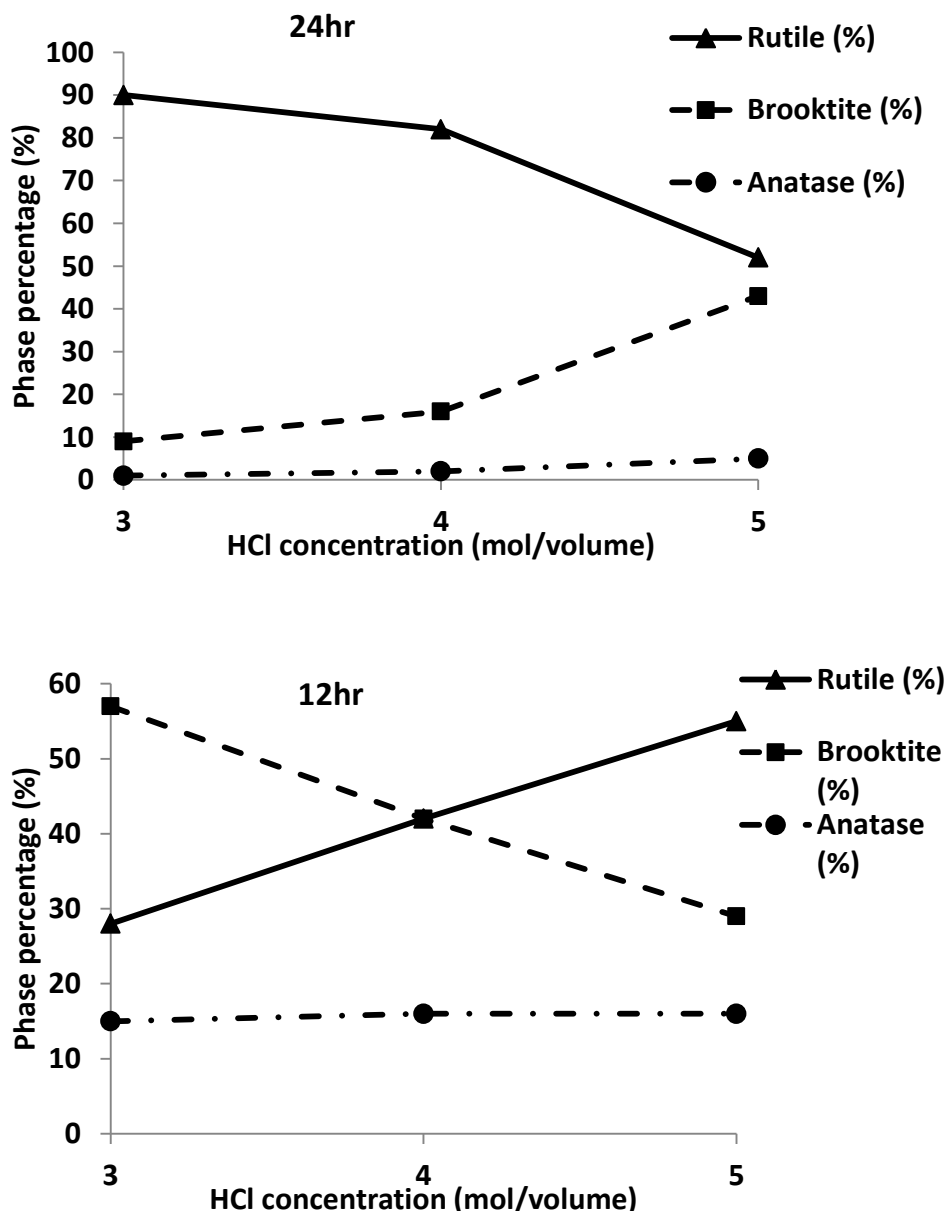
Figure 4.5: Changes in phase of TiO₂ for altering HCl acid concentration at gel formation times of 24 and 12 hours, respectively

Li et al. (2003) suggested that brookite was an intermediate phase of anatase and rutile, depending on the energy available. Brookite, when hydrothermally synthesised, can deform from rutile when too little energy is supplied or solution pH is too high, and deform from anatase where too much energy is supplied or solution of pH is too low (Li et al., 2003). However, situations were described where brookite is not only an intermediate phase, but become more dominant, as in this study. Pottier et al. (2001) found that high Cl⁻ ion concentration and high acidity of solution will favour brookite formation to that of anatase, which is favoured by sulphate ions and lower acidity. In this work, at 12 hours for 3 M HCl, a brookite-rich sample was obtained which transformed into a rutile-rich sample at 24 hours. This is supported by the work of Hu et al. (2003) that stated that large volumes of brookite provide more nucleation sites which give a higher reaction rate and assist in anatase and brookite transformation to rutile. Increasing the HCl concentration to 4M resulted in the same transformation mechanism

Cape Peninsula
University of Technology

but with a 5% reduction in the final percentage of rutile obtained. However, a significant reduction of 30% rutile is observed at 5 M HCl. Reyes-Coronado et al. (2008) proposed that, in contrast to anatase formation that is dominated by surface energy effects, the rutile and brookite formation is driven by continuous dissolution and precipitation which is favoured by highly acidic conditions. This may very well be the reason for the significant reduction in rutile and increase in brookite in this work at 5M HCl, and this mechanism warrants further research which was investigated in this work by prolonged hydrothermal treatment.

Using acid concentration as a means for polymorph manipulation is only effective at gel formation times less than 72 hours. With an increase in HCl concentration at 24-hour gel formation time, a reduction in the initially rutile rich sample was observed. Furthermore, virtually equal proportions of rutile and brookite were observed for 5M HCl. At 12-hour gel formation time, rutile growth is dependent on acid concentration; however with increased gel formation time a reduction in the dependency of acid concentration was observed. This provides a mechanism to prepare either brookite-rich, rutile-rich or equal proportions of rutile and brookite. However, anatase growth is independent of the acid concentration for 24 and 12 hour gel formation time with a maximum yield of 5% and 15% respectively. This work suggests that a much greater HCl concentration than 5M will be needed to suppress anatase growth and formation, compared with 1.5M suggested by Chen et al. (2011).

Transformation and stability of phase have been found to be dependent on particle size in the ranges of 11–35 nm (Zhang and Banfield, 2000), therefore particle shape and size will be presented next.

4.2. Effect of gel formation time and HCl concentration on particle shape

Changes to the shape of TiO_2 nanoparticle were observed for changes in HCl concentration and gel formation time. In Figure 4.6 the lattice spacing of TiO_2 nanoparticles was determined and confirmed to be rutile (A), anatase (B) and brookite (C) nanoparticles. The lattice spacing was found to be 3.25 Å, 3.41Å and 2.5 Å respectively.
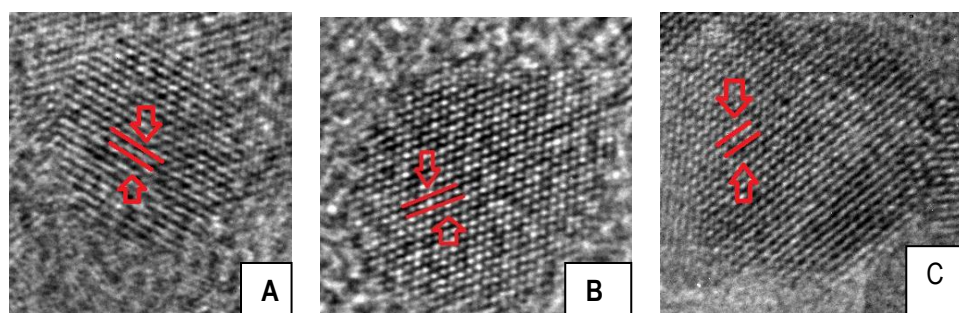
Figure 4.6: Three magnified TEM images of TiO₂ nanoparticles prepared in 3M concentration of HCl and 72- (A), 24- (B), 12-hour (C) gel formation time

In Appendix C, D and E additional TEM images taken can be found, for 3, 4 and 5 molar HCl with varying gel formation times, respectively.

Figure 4.7 presents the change in particle shape with change in gel formation time. Shapes identified in order of decreasing gel formation time are nanorods at 72 and 48 hours; at 24 hours large rodlike and smaller mixed-shaped particles were observed; thereafter a mixture of elliptic and spherical particles formed. It is evident that only gel formation time affects particle shape. Similar results were found for the work performed by So et al. (1997), using titanium isopropoxide, isopropanol, and nitric acid to alter the H_2O/titanium isopropoxide ratio with varying hydrothermal times.

With increasing HCl concentration, particles were shown to possess high aggregative force. Similar results were found by Bischoff and Anderson (1995), where when heat treatment was used in HCl, large aggregated particles broke to form small aggregates. Increasing HCl concentration causes an increase in the hydrolysis reaction rate and a change in the hydroxyl state of TiO_2 octahedra, and this is in agreement with work done by Fogler (1999) and Masterton et al. (2011). Therefore, the shortened gel formation time and higher HCl acid concentration resulted in spherical nanoparticles and a low percentage of nanorods, similar to findings observed by Su et al. (2006), who stated that the spherical particles coagulate to transform to large rod-like phase particles. Furthermore, a similar growth mechanism was found by Ethayaraja and Bandyopadhyaya (2007), where nanodots coagulated on one another to form nanorods.

A growth mechanism was identified for TiO_2 as the formation of spherical and elliptic-shaped particles at 12 hours, thereafter growing a round-headed cube at 24 hours, and finally growing to form rodlike particles at 72 hours. For changes to the shape of TiO_2 nanoparticles, changes in size were also observed. Small changes in average particle diameter were obtained; therefore the changes in particle length are discussed.

Cape Peninsula
University of Technology
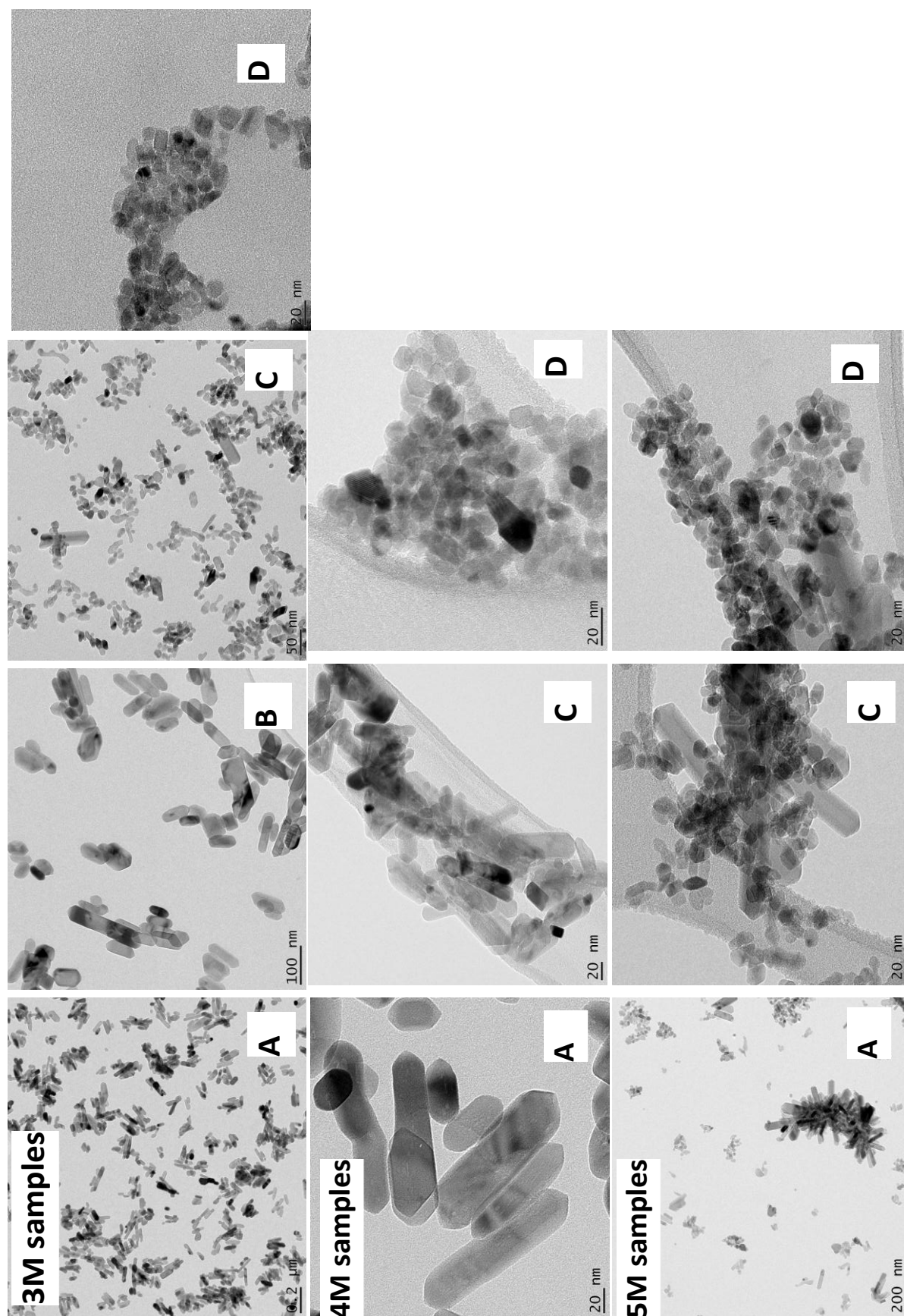
Figure 4.7:Evolution of TiO₂ nanoparticle shape, for a 3M, 4M and 5M HCl concentration, and shortened gel formation time, 72 (A), 48 (B), 24 (C), 12 hours (D)

4.3. Effect of gel formation time and HCl concentration on particle size

Table 4.2 presents a summary of results obtained for average length, average diameter, and the standard deviation determined for gel formation times from 72 to 12 hours, for HCl concentration of 3, 4 and 5 M.

Table 4.2: Average particle size and standard deviation of nanoparticle length and diameter for gel formation times 72 to 12 hours, for HCl concentration of 5 molar

	Average particle length (nm)	STD of length (nm)	Average particle diameter (nm)	STD of diameter (nm)
3M 72 Hours	80	8	28	5
3M 48 Hours	81	9	32	6
3M 24 Hours	19	4	10	3
3M 12 Hours	15	4	9	3
4M 72 Hours	57	8	27	5
4M 24 Hours	27	5	14	3
4M 12 Hours	19	4	10	3
5M 72 Hours	27	5	15	4
5M 24 Hours	20	4	12	3
5M 12 Hours	15	4	12	3

Changes to the size of TiO_2 nanoparticle were observed for changes in HCl concentration and gel formation time. Figure 4.8 presents changes in average particle length for decreasing gel formation time. There is a linear relationship between average particle length and gel formation, irrespective of the HCl concentration.
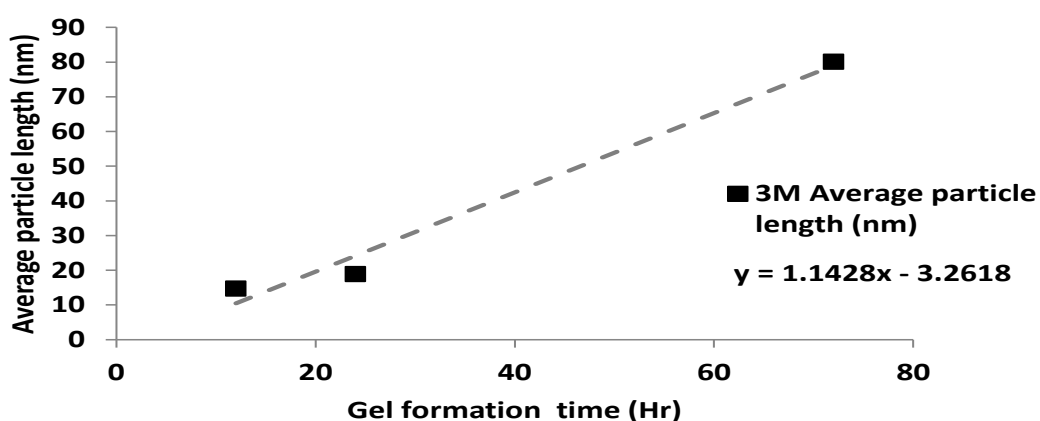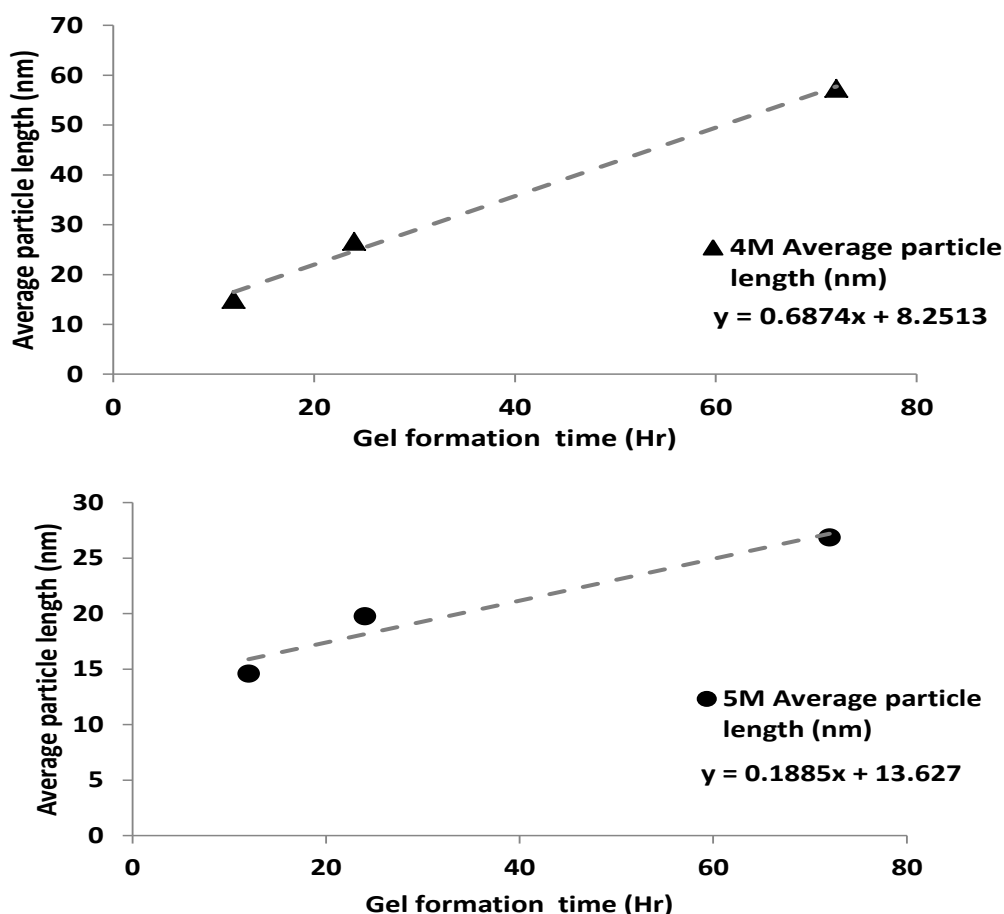
Figure 4.8: Effect to TiO$_2$ average particle length and diameter, for shortening gel formation time from 72 hr to 12 hr at each HCl concentration used

The relationship for 3M, 4M and 5M HCl is presented in Equations 4.1 – 4.3 respectively.

$$A_{length} = 1.028\ t_{gel} + 3$$

Equation 4.1

$$A_{length} = 0.654\ t_{gel} + 10.9$$

Equation 4.2

$$A_{length} = 0.185\ t_{gel} + 14.02$$

Equation 4.3

For a 33% reduction in gel formation time, an 81%, 67% and 44% decrease in average particle length was obtained for 3M, 4M and 5M respectively. HCl concentration can therefore be used to control the growth of average particle length.

Furthermore, this work agrees with findings by Sugimoto et al. (2003), Machesky et al. (2008) and Chen et al. (2011), that increasing the concentration of H^+ and Cl^- ions facilitates protonation of $TiOH_4^+$ gel during hydrothermal treatment, which leads to particle size control. The average particle length for 12-hour gel formation time was equivalent to ≈15 nm. This work agrees with the formation of small particles due to high water content in sol-gel synthesis found by Bischoff and Anderson (1995). Furthermore, high positively charged surfaces due to high HCl concentration affected particle size by the repulsive forces of like-charged particles in bonding, resulting in the formation of smaller particles; this is in agreement with findings by Barnard and Curtiss (2005).

Figure 4.9 shows the average particle size as a function of HCl concentration at different gel formation times. Although a linear relationship was observed at 72 hours where the particle size decreases with increasing acid concentration, this was not the case for 24 hours and 12 hours. The average particle size observed for 3M and 5M HCl was very similar at ≈15 nm in length. At 4M HCl the particle size differed with an average particle length of ≈21 nm. Zhang and Banfield (2000) state that TiO_2 nanoparticle size is dependent on the phase and the size will alter as it transforms between brookite, rutile and anatase.
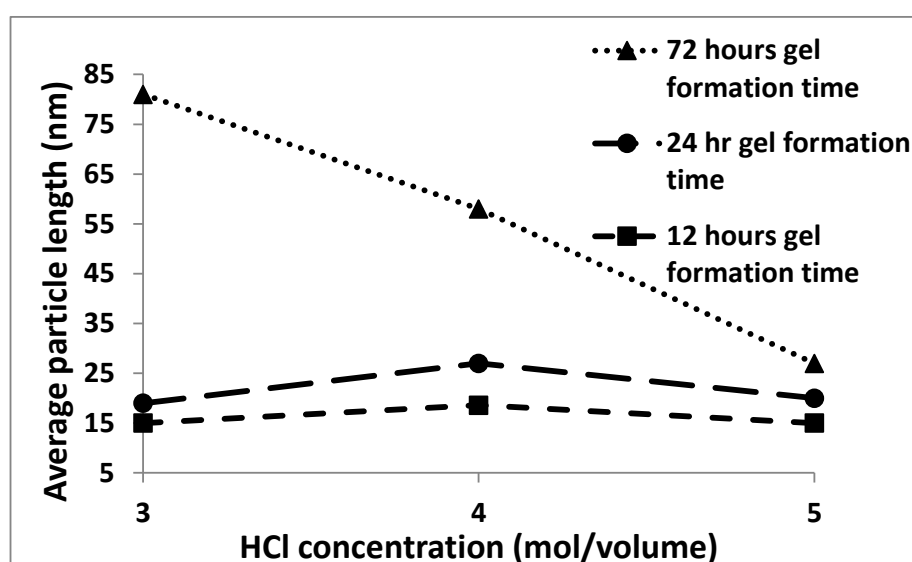
Figure 4.9: Average particle length for 72, 24 and 12 hour gel formation times with increasing HCl concentration

Figure 4.10 presents the changes to TiO_2 average particle length and phase percentage for increasing HCl concentration with decreased gel formation time. Interchanging between phases is shown to have no effect on size, irrespective of HCl concentration; however a decrease is apparent with a decrease in gel formation time. The particle size and phase information are combined in an attempt to find if a relationship exists. Unfortunately no obvious correlation between phase and average particle size emerged. In fact, the particle size at 3M and 5M was similar for very different phase composition. There is also no logical explanation why the particle size at 4M HCl is larger for both 24- and 12- hour gel formation time, as there is no similarity in the phase composition.
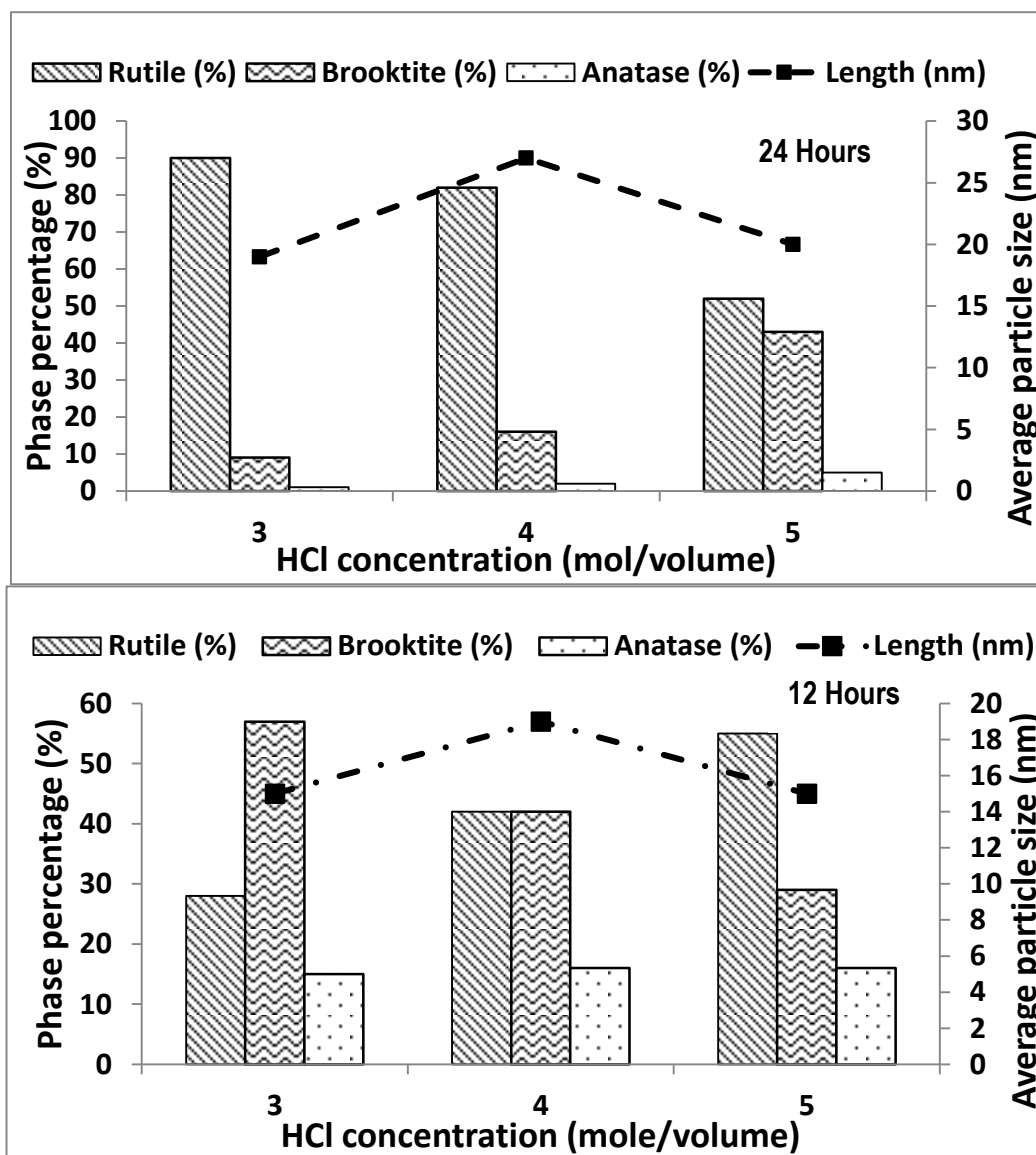
Figure 4.10: Phase percentage and average particle size of TiO₂ nanoparticle gel formation at three HCl acid concentrations for gel formation time 24 hours and 12 hours respectively

TiO$_2$ particle length is a function of gel formation time. For decreased gel formation time, TiO$_2$ nanoparticles tend to become more spherical, irrespective of HCl concentrations, while increasing HCl concentration results in a reduction in particle size. Mixed phases formed for all TiO$_2$ nanoparticles for less than 48 hour gel formation time. Prolonging of hydrothermal treatment promised to favour phase transformation of TiO$_2$, and this was studied.

4.4. TableEffects of prolonged hydrothermal treatment time on TiO₂ nanoparticles

A systematic study was conducted to observe if prolonging hydrothermal treatment time affects the TiO$_2$ phase, particle size and shape. Qualitatively, the percentage of rutile was found to be 55% for the reaction parameters 5M HCl concentration and 12-hour gel formation time. This was the largest percentage of rutile found at the shortest synthesis duration, of the three HCl concentrations used. The times for hydrothermal treatment were

Cape Peninsula
University of Technology

increased by two - hour intervals from 2 to 20 hours. In Appendix E additional TEM images taken can be found, for varying hydrothermal treatment times.

The use of hydrothermal treatment provides amorphous material with the enthalpy needed for phase transformation and controlling particle size as found in Zhang and Banfield (2000). Control over growth kinetics of TiO_2 has received considerable attention (Matthews, 1976; Oskam et al. 2003; Zhang & Banfield 200; Yu et al. 2007; Chen et al., 2011) because size and phase impact the properties and hence the application of TiO_2. This section discusses the effect of hydrothermal time of 1 to 20 hours on TiO_2 prepared in the presence of 5M HCl, with a gel formation time of 12 hours and 1 hour hydrothermal treatment time.

Figure 4.11 presents the evolution in phase for increasing hydrothermal treatment time from 1 hour to 20 hours. It was found for hydrothermal times, mixed phase formed for 1 to 4 hours, with pure rutile forming at 6 hours, mixed phase was again formed for 8 to10 hours and for 12 hours until 20 hours pure rutile was formed. Particle size (Figure 4.12) changed according to changes in phase transformation. This contradicts results by Chen et al. (2011) and Zhang and Banfield (2000), who found an irreversible transformation reaction of brookite and anatase to rutile, and that size increased with increase in time.

Sols formed in this work are classed as unstable sols. The transformation between mixed phase to rutile and rutile to mixed phase can be associated with dissolution and orientated coalescence of particles. Orientated coalescence studied by Yin et al. (2001) and Chen et al. (2011) showed that crystal growth was possible by dehydration in the presence of HF and HCl acid catalysts, at prolonged hydrothermal treatment time and high temperatures. Furthermore, it was suggested that surface chemistry had an effect on phase. Transformation from mixed phase to pure rutile was supported by the findings of Hu et al. (2003); it was observed that brookite provides nucleation sites for anatase particle transformation to rutile particles. Su et al. (2006) suggested that rutile transforms at the expense of anatase particles by forming new nuclei along the [112] twin interface that occurred easily at elevated hydrothermal temperatures and pressures which break bonds and rearrange atoms.

It is therefore suggested in this work that the mechanism for the change in phase consists of reversible reactions of dissolution and orientated coalescence (Isely & Penn, 2006; Chen et al., 2011) caused by unstable sols (So et al.,1997) and strong surface chemistry effects (Barnard & Curtiss, 2005) under prolonged hydrothermal treatment time.
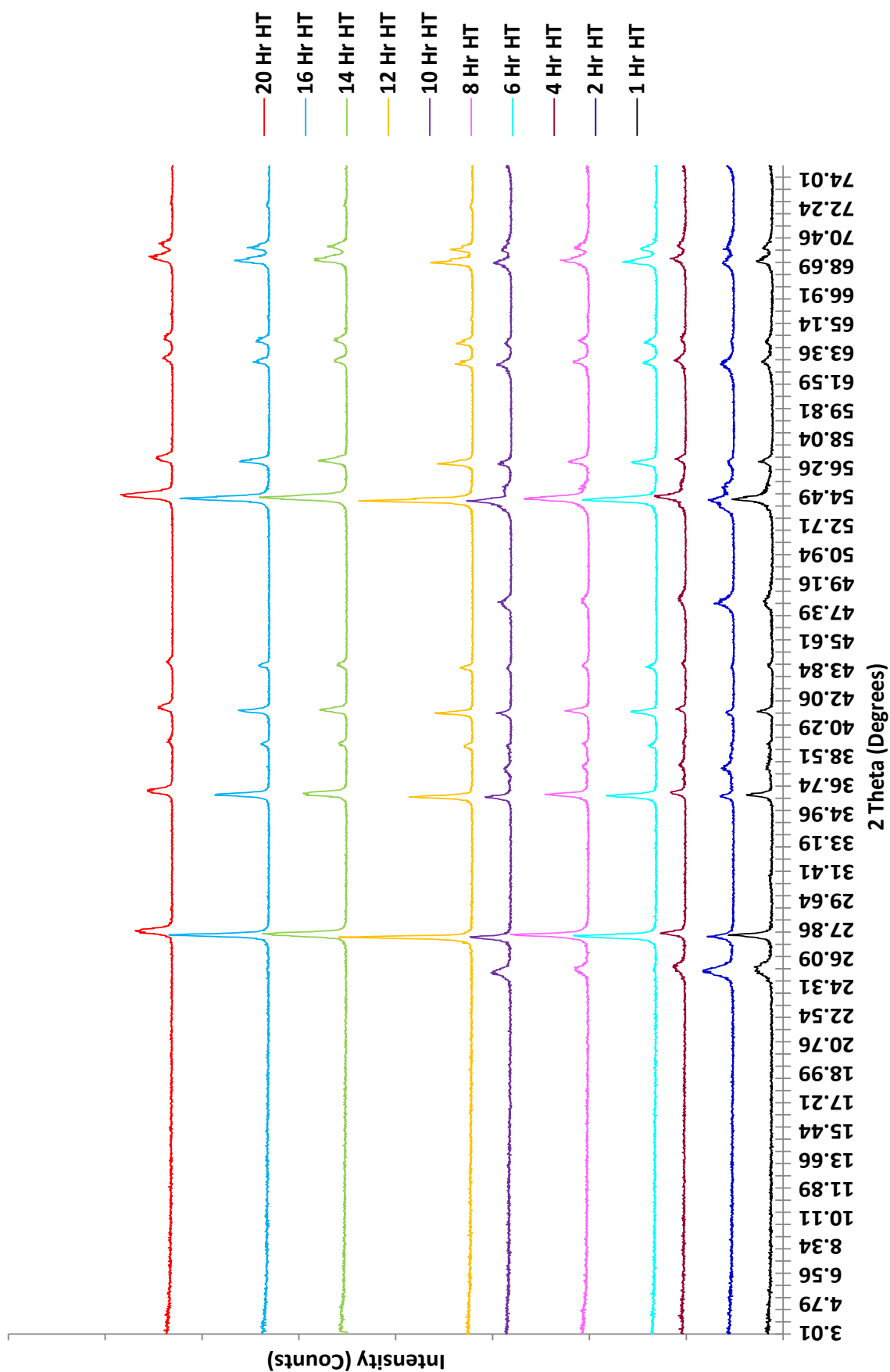
Figure 4.11: Evolution in phase for hydrothermal treatment times ranging from 1 to 20 hours

Table 4.3 presents a summary of results obtained for average length, average diameter, and the standard deviation determined for shortened gel formation time of 12 hours and thereafter hydrothermally treated for 2 to 20 hours.

Table 4.3: Average particle size and standard deviation with regard to nanoparticle length and diameter for 5M 12-hour gel formation time thereafter hydrothermally treated for 2 to 20 hours.

HT duration (hr)	Average particle length (nm)	STD of length	Average particle diameter (nm)	STD of diameter
2	25	5	13	4
4	26	5	15	4
6	89	10	50	7
8	66	8	23	5
10	34	6	19	4
12	133	12	77	9
14	140	12	79	9
16	156	12	46	7
20	66	8	40	6

Figure 4.12 presents the changes in average particle length from 2-hour hydrothermal treatment time to 20 hours. A similar study was done by Su et al. (2006) and Chen et al. (2011) for changes in average particle length, when using 1 to 15 hour and 1 to 24 hour hydrothermal treatment times respectively. For this work, increasing hydrothermal time resulted in an increase in average particle length till 6 hours; thereafter average particle size oscillated with changes in phase with minimum particle sizes observed at 4, 10, and 20 hours and peaks at 6 and 16 hours. A similar pattern for particle size was observed by Su et al. (2006), where increasing hydrothermal time resulted in an increase in size till 5 hours, and thereafter oscillated with minimum particle size observed at 1, 4 and 7 and maximum particle size observed at 5 and 15 hours. On the contrary, Chen et al. (2011) found that average particle size increased with increasing hydrothermal time, forming pure rutile for all samples. In the case of Su et al. (2006), the phase changed from pure anatase (at 1 hour) to mixed rutile to brookite phase (at 3, 4, 5 and 7 hours) and then to rutile (at 15 hours) with increased hydrothermal time. Zhang and Banfield (2000) suggested phase transformation of TiO_2 was dependent on size, and the kinetics for phase transformation was dependent on the surface energy.
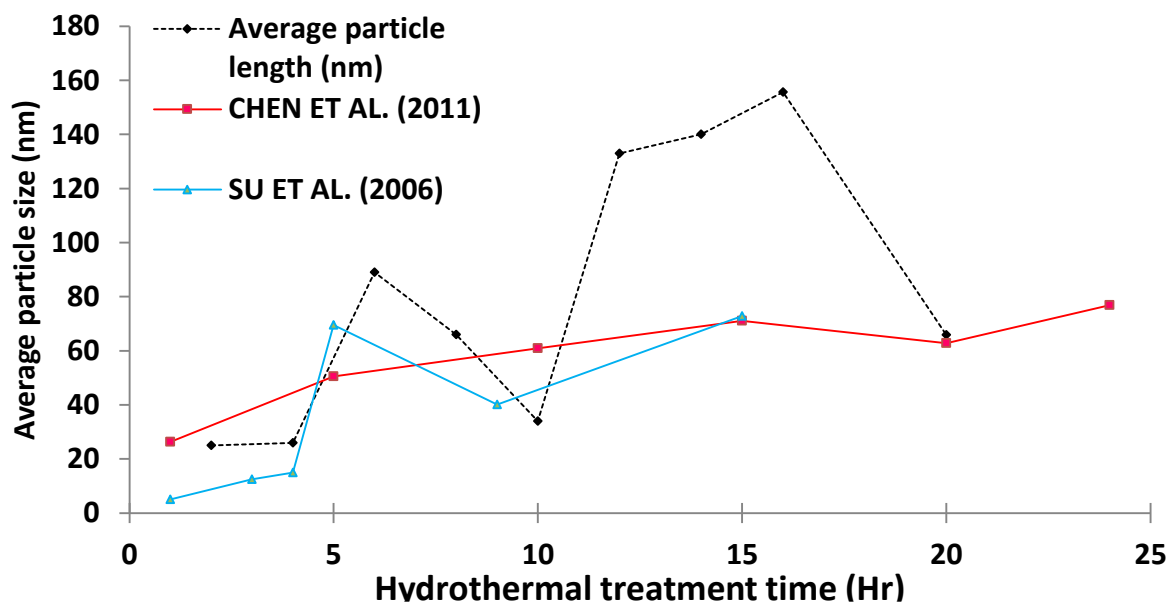
Figure 4.12: Change in average particle length and phase between mixed and pure rutile, for prolonged hydrothermal treatment times and plotted against Chen et al. (2011) and Su et al. (2006)

This work contradicts findings by Cushing et al. (2004) and Yu et al. (2007), where it was found that synthesis of TiO_2 via a sol-gel at lengthening hydrothermal treatment times will follow the Ostwald ripening growth mechanism. Dissolution of particles in terms of size was found to be due to solubility of TiO_2 in acid solutions, and this was in agreement with Bavykin and Walsh (2010). Thereafter free ions reform to a crystal lattice depending on the enthalpy of formation. Large nanorod pure rutile particles that are formed by orientated coalescence from aggregated mixed-phase particles and by surface chemistry bonded and grew by protonation of surface hydroxyl groups, and by dehydration to form large particles. This is in agreement with the findings of Chen et al. (2011).

It is observed that particles can be formed or broken down by changes in surface energy as explained by Bischoff and Anderson (1995), resulting in particles to rupture bonds and have changes in phase, as explained by regions of sol stability by So et al. (1997).

Cape Peninsula
University of Technology
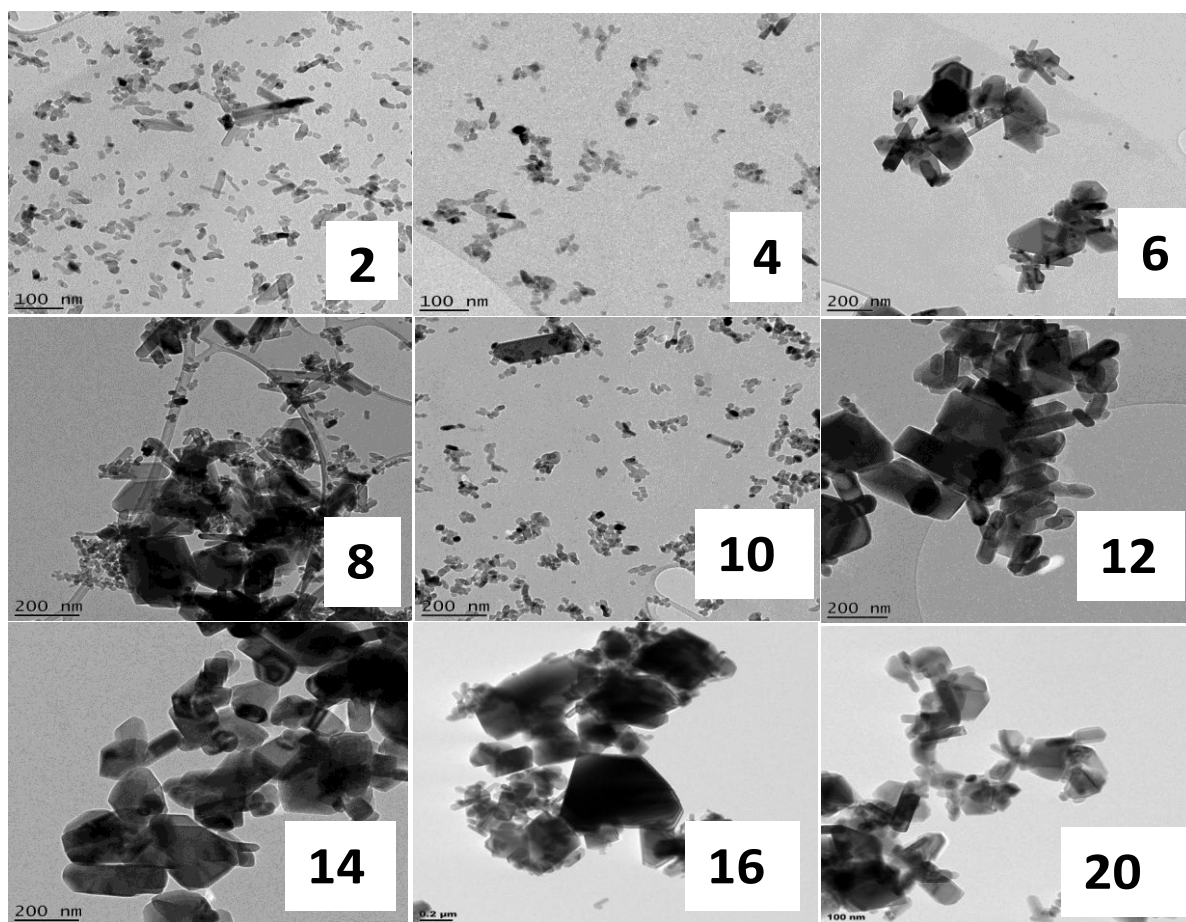
Figure 4.13: HR-TEM images of the particle shapes for prolonged hydrothermal treatment time from 2 to 20 hours

Figure 4.13 presents the change in particle shape over 2 to 20 hours' hydrothermal treatment. The particle shape was found to be mixed, but with distinct rodlike shapes of TiO_2. Three distinct particle shapes of TiO_2 nanoparticles found in this work were similar to results of other studies: ellipsoids, nanorods, spheres, and cubes (Sugimoto et al., 2003). An increase in average particle size from 1 to 20 hours was observed; however particle size oscillated with increasing time and changes in phase.

Manipulation of TiO_2 particle phase and size is possible when using longer hydrothermal treatment times. For longer hydrothermal times, surface chemistry and orientated coalescence are suggested to drive the reversibility reaction between phases, and oscillation of average particle length, respectively. The photocatalytic efficiency of mixed phases formed from selected TiO_2 nanoparticles synthesised for less than 72-hour gel formation time was studied.

4.5. TiO_2 nanoparticle photocatalytic activity, for the application of degrading dye

TiO_2 photocatalytic properties have been extensively researched for the use of degrading pollutants in water (Moreira et al. 2005; Di Paola et al. 2008; Chen et al. 2011; Gupta & Tripathi 2011). Phase and size impact the properties, and hence the application of TiO_2, selected TiO_2 nanoparticle photocatalytic activity of varying phase, size and shape is discussed in this section. This section evaluates the effect on methylene blue (MB)

concentration by photodegradation. Initially the effects of MB degradation by UV light without P25, and P25 without UV light (donated by Evening), were evaluated. The effects of phase, size and shape of pure rutile (synthesised at 3M 72 hours), pure anatase (commercially available from Sigma), P25 and synthesised TiO_2 (synthesised for 3M, 4M and 5M at 24-hour and 12-hour gel formation time) were evaluated thereafter.

Figure 4.14 presents the degradation of methylene blue in the presence of catalysts with and without UV light irradiation, for 120 minutes. Pure rutile, anatase and P25 were used as standards for comparison with synthesised mixed-phase TiO_2. Furthermore, the effects of UV light radiation and catalyst without UV light are presented.
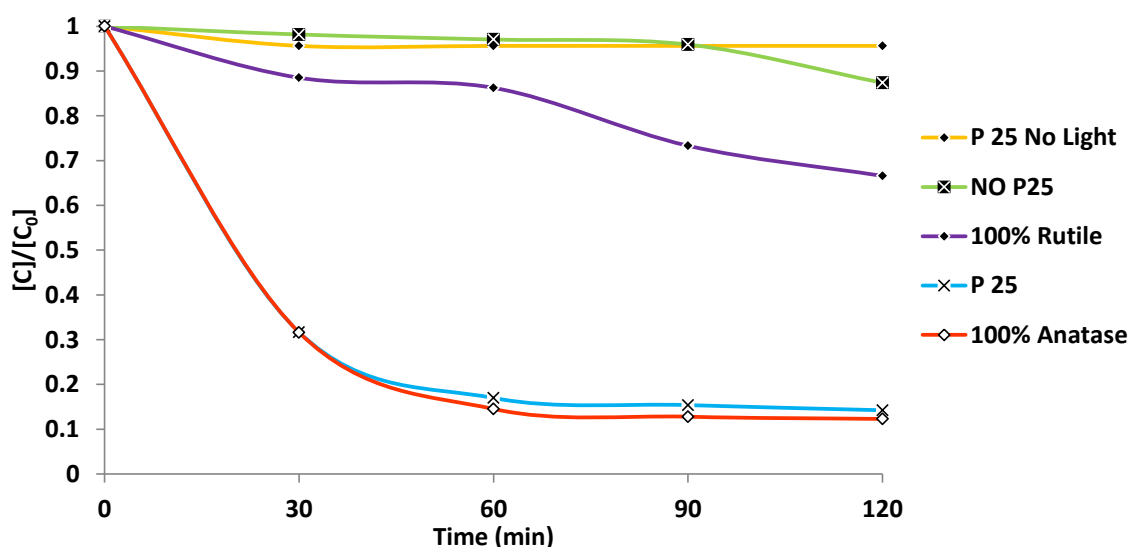
Figure 4.14: Degradation of methylene blue in the presence of three catalysts (in the presence of UV light) and UV light only or no light (in the presence of P25)

Figure 4.15 presents the changes in MB concentration in the presence of pure anatase, pure rutile, P25, and TiO_2 synthesised with mixed-phase percentages, size and shape, for 120 minutes. The effect of UV radiation only showed 13% degradation of MB, with a reaction rate of 0.053 min^{-1}. According to Thomas and Burgess (2007), it was found that degradation of organic dyes in the presence of UV light was possible; however this will take a longer period than when in the presence of a photocatalyst. This work contradicts the findings of Chen et al. (2011), where little changes to MB concentration occurred, when radiated with UV light without a catalyst present. P 25 in the absence of UV light was shown to degrade 5% of MB within 30 minutes and remain constant until 120 minutes, with a reaction rate of 0.0182 min^{-1}. This work is in agreement with the findings of Su et al. (2006), who showed that photocatalysts can absorb a percentage of dye on the particle surface. For degradation of MB in the presence of UV light, the degradation is slow without the presence of a photocatalyst. Furthermore, if a catalyst is present, it is observed that phase and percentage of phase is vital, for improved photocatalytic efficiency.
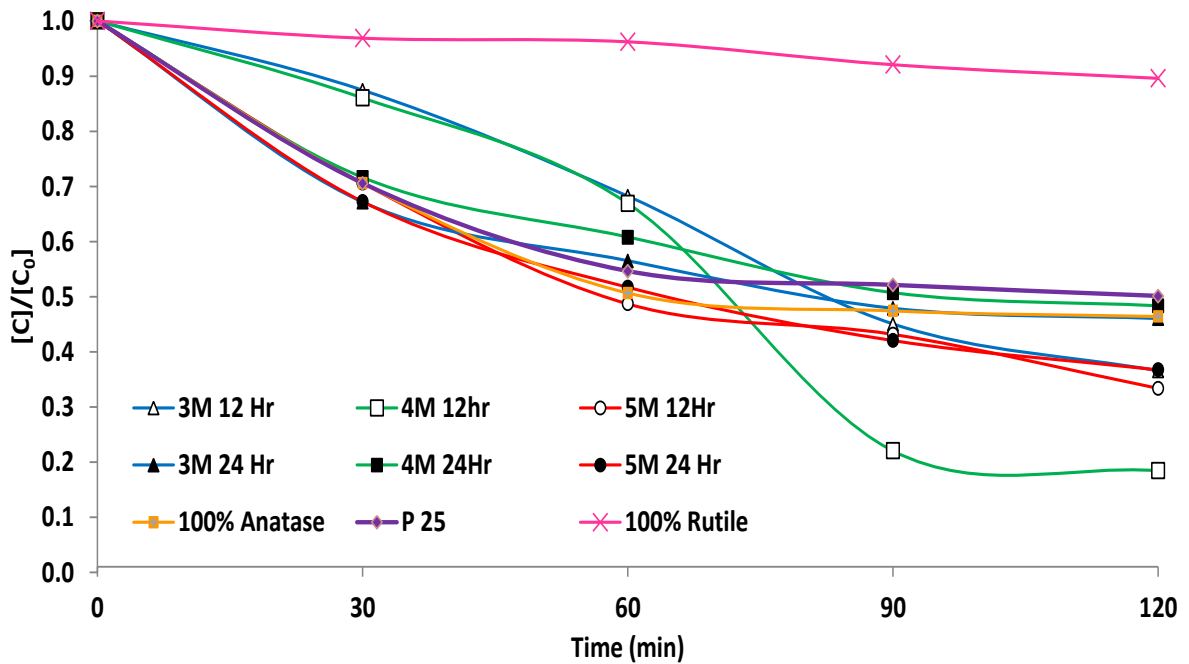
Figure 4.15: Degradation of methylene blue by UV light with synthesised TiO$_2$ of mixed phase percentages, pure Anatase and P25

The effect of pure rutile, pure anatase and P25 in the presence of UV light on the degradation reaction was then evaluated for 120 minutes. A 35% change in MB concentration is observed when irradiating in the presence of pure rutile, with a reaction rate of 0.139 min^{-1}. According to Liao and Liao (2007), the pure rutile phase is known to be least photocatalytically active of the three polymorphs. This can be accounted for by the surface chemistry as found by Bischoff and Anderson (1995), where rutile has low concentration of OH$^-$ ions at the surface of the nanoparticle, which is released as a hydroxide radical on UV light irradiation. This work is in agreement with the findings of Chen et al. (2011) and Su et al. (2006), as rutile nanoparticles possess a lower photocatalytic effect on degradation of MB, and need longer times to decrease the concentration of dye.

An 88% change in MB concentration is observed when irradiating in the presence of pure anatase, with a reaction rate of 0.365 min^{-1}. According to literature (Kim et al., 2005; Liao & Liao, 2007; Scanlon et al., 2013), it was found that the anatase phase is known to be the most photocatalytic active of the three phases. This can be accounted for by the surface chemistry as found by Bischoff and Anderson (1995), where anatase has a high concentration of OH$^-$ ions at the surface of the nanoparticle, which is released as a hydroxide radical on UV light irradiation. According to literature (Andersson et al. 2002; Cozzoli et al. 2003; Su et al., 2006; Dong et al., 2010), it was found that anatase is more photocatalytically active than rutile.

Mixed-phase TiO$_2$ has received great attention as it was found to be more efficient than pure rutile TiO$_2$, for different reaction conditions (Anderson et al. 2002; Lachheb et al. 2002; Testino et al. 2007; Di Paola et al., 2008; Gupta & Tripathi 2011; Gupta & Tripathi 2012; Krivec et al., 2013; Scanlon et al., 2013). An 86% change in MB concentration is observed when irradiating in the presence of P25 (20% rutile and 80% anatase, according to MSDS of Degussa Company), with a reaction rate of 0.357 min^{-1}. Similar results are observed for pure anatase

and P25; this contradicts findings by Testino et al. (2007), where different phase mixture were compared with P25. However, P25 is observed to be more photocatalytically efficient than pure rutile, and similar results were found by Testino et al. (2007) and Di Paola et al. (2008).

Phase percentage and size of synthesised TiO_2 are presented in Table 4.4.

Table 4.4: The phase percentage determined from XRD patterns, TEM average particle size, and photocatalytic activity for the decomposition of MB and initial pH conditions

TiO_2 sample	Average particle size Length x Diameter (nm)	Phase Percentage (%)			Reaction rate constant k_a (min^{-1})	Initial pH
		Rutile	Anatase	Brookite		
3M 72 Hours	81 x 29	100	-	-	0.1393	3.61
3M 48 Hours	60 x 20	100	-	-	-	-
3M 24 Hours	19 x 11	90	1	9	0.3662	3.25
3M 12 Hours	**15 x 10**	**28**	**12**	**60**	**0.3818**	**3.68**
4M 72 Hours	58 x 27	100	-	-	-	-
4M 24 Hours	27 x 14	82	2	16	0.3614	3.38
4M 12 Hours	**19 x 10**	**42**	**16**	**42**	**0.3995**	**3.42**
5M 72 Hours	27 x 15	100	-	-	-	-
5M 24 Hours	20 x 12	52	5	43	0.3816	3.38
5M 12 Hours	**15 x 12**	**55**	**16**	**29**	**0.3859**	**3.55**
P 25	21	25	75	-	0.3574	4.38
Pure anatase	<25	-	100	-	0.3655	6.39

Methylene blue was photodegraded in the presence of three (rutile-rich) catalysts, synthesised using 24-hour gel formation time and varying HCl concentrations. Changes in MB concentration and reaction rates were 88%, 87%, 92% and 0.3662, 0.3614, 0.3816 min^{-1} for TiO_2 synthesised at 3M, 4M, 5M respectively. The change in photocatalytic reaction rate can be accounted for the decrease in rutile percentage from 3M to 5M (90% to 55% and particle size for 3M and 5M, 18 nm to 20 nm), make reference to Figure 4.10 presented. Similar trends for photocatalytic efficiency were found by Yang et al. (2005), as changes in phase percentage of anatase-rich particles with varying particle size were observed. Figure 4.16 shows mixed-phase TiO_2 photocatylysts used to degrade methylene orange. Furthermore, two means of making up photocatalysts were used by Yan et al. (2007): synthesised and physically prepared.
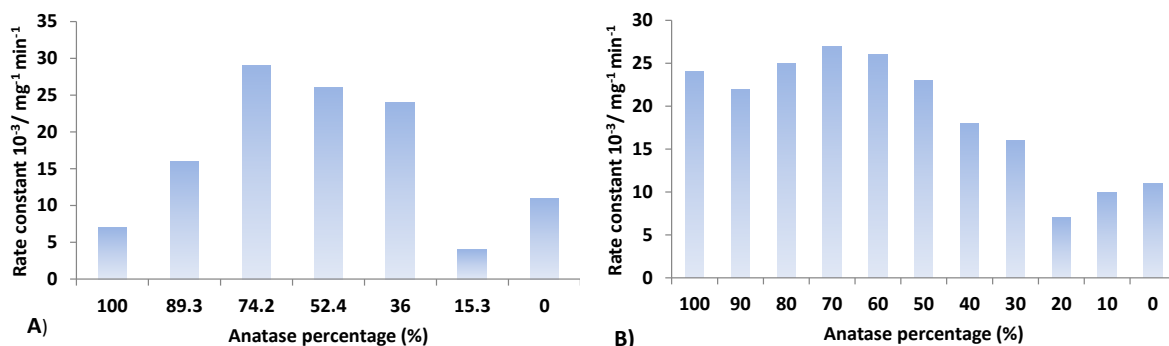
Figure 4.16: Rate constants for the decomposition of methylene orange in the presence of synthesised TiO$_2$ nanoparticles, with varying anatase and rutile phase percentages (reconstructed from Yan et al., (2007)).

Yan et al. (2007) found TiO$_2$ of mixed phased with varying phase percentages to have greater photocatalytic activity than pure phase. This was true for synthesised and physically prepared mixed phase of varying phase percentages.

Rutile-rich mixed-phase TiO$_2$ was found to be more photocatalytic active than P25, pure anatase phase and pure rutile. This can be accounted for greater band gaps available by the three phase of TiO$_2$ for electrons to readily create radicals, as found by Testino et al. (2007) and Yan et al. (2007) and further explained by Li et al. (2007) and Gupta and Tripathi (2011).

In the presence of catalysts synthesised for 12-hour gel formation time at varying HCl concentrations and irradiated for 120 minutes, changes in MB concentration and reaction rates were 92%, 96%, 91% and 0.3818, 0.3995, 0.3859 min^{-1} for TiO$_2$ synthesised at 3M, 4M, 5M HCl respectively. With reference to Figure 4.10 presented earlier, this can be accounted for by the increase of brookite phase by 51%, 26% and 14% for 3M, 4M and 5M respectively. All three samples are observed to have similar average particle size; this can account for the rate of MB being degraded for 120 minutes' radiation. This work is in agreement with the findings by (Jang et al. 2001; Li et al. 2007; Testino et al. 2007), where particle size and phase percentage of the TiO$_2$ nanoparticles will affect the rate of decomposition of bacteria and industrial textile dye respectively. Photocatalytic activity was noted to be dependent on the surface area (for changes in average particle size) and shape.

Figure 4.17 presents the change in photocatalytic activity for increases and decreases in brookite and rutile mixed-phase percentages respectively.

Cape Peninsula
University of Technology
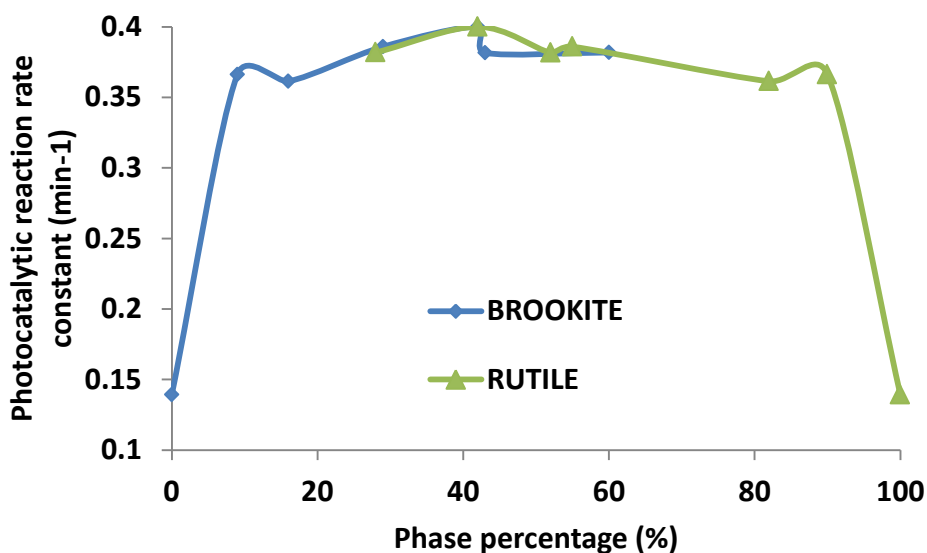
Figure 4.17: Photocatalytic activity for changes between mixed-phased particles with varying rutile and brookite percentages, for anatase phase percentages less than 16% but greater than 0%

For varying mixed phase percentages of rutile and brookite, it is observed that increasing the brookite phase percentage by 9% will dramatically increase the photocatalytic efficiency of rutile. This work is in agreement with that of Testino et al. (2007) and Di Paola et al. (2008), where brookite was found to have high photocatalytic efficiency; however rutile and brookite mixed- phase photocatalysts were more efficient with decreased rutile phase percentage (for photocatalysts consisting of all three phases). This can be due to the synergy of the three-band gap's being available to be excited by UV light as found by Gupta and Tripathi (2011) and Testino et al. (2007). It is noted that the addition of anatase does not equate to a remarkable increase in photocatalytic reactivity. For example, the sample with 1% anatase and 9% brookite improved photocatalytic activity by 55%. The sample with 16% anatase and 29% brookite improved photocatalyst activity by 58%. This work agrees with the findings of Kandiel et al. (2013), where it was found that brookite was more photocatalytically efficient than anatase for degradation of methanol. An increase in photocatalytic activity efficiency is observed when using a mixed-phase photocatalyst, with an increasing brookite percentage and decreased average particle size.

4.6. Conclusion

The effects observed on TiO_2 phase, average particle size and shape for modifications made to HCl concentration, gel formation time and hydrothermal treatment time were presented in this chapter. The synthesis of pure rutile was successfully achieved for shortened synthesis duration of 18 hours. This consisted of 12 hours of gel formation and 6 hours of hydrothermal treatment. Changes in phase, size and shape were discussed for changes made to gel formation time, HCl concentration, lengthening of hydrothermal treatment time. TiO_2 synthesised particles with mixed phase were used to study the photocatalytic activity for the degradation of methylene blue of 0.25 molar concentration and comparisons were made to pure anatase, rutile and P25 TiO_2. An optimum photocatalyst was found and consisted of a mixture of three phases and smaller nanoparticles.

Chapter 5

This chapter presents the findings for TiO_2 nanoparticles synthesised via a sol-gel procedure, where changes to this procedure were made, and how this impacted TiO_2 nanoparticles and their properties. Recommendations for future studies have also been made. This study highlighted the fact that a systematic study relating to reaction parameters , gel formation time, increased HCl concentration and hydrothermal treatment time in the optimisation of the formation of TiO_2 nanoparticles.

5. Conclusion and recommendations

Reaction kinetics was exploited to expedite the synthesis of TiO_2 nanoparticles and the following was found.

5.1. Conclusion

For changes to reaction parameters it could be concluded:

- Pure and mixed phased TiO_2 nanoparticles were successfully synthesised.

- Pure rutile TiO_2 nanoparticles first synthesised at 73 hours (72 hours gel formation time and 1 hour hydrothermal treatment), were synthesised at 18 hours (12 hours gel formation time and 6 hour hydrothermal treatment). Lengthened hydrothermal treatment times assisted in phase transformation.

- Rutile and brookite were favoured for increased HCl acid concentrations.

- The shape of TiO_2 nanoparticles changed from rod to elliptic particles for shortened gel formation time, irrespective of HCl concentration.

- A decrease in size was observed for increased HCl concentration and a decrease in gel formation time.

- Lengthened hydrothermal treatment duration favoured TiO_2 nanoparticle growth and resulted in changes in shape from ellipsis to large rodlike particles (for hydrothermal treatment times 1-6 hours).

- An increase in photocatalytic activity was found for a decrease in the rutile and increase in the brookite (in addition to anatase) phase percentage, but this plateaued after 42% brookite phase.

- An increase in photocatalytic activity was found for decrease in particle size.

- 4M 12 hours synthesised TiO_2 nanoparticles were demonstrated to be the optimum photocatalyst owing to a mixture of percentages; this sample comprised of three phases.

5.2.Contributions

• Reduced time to produce rutile, at the cost of size and shape,

• Confirmed rutile and brookite formed in highly acidic conditions,

• Brookite increased photocatalytic activity of rutile.

5.3.Recommendations

Recommendations for future studies have been provided, as suggestions for and new knowledge of TiO_2 synthesis for altering reaction parameters emerged.

• Kinetic studies of TiO_2 nanoparticle growth by prolonged hydrothermal treatment, for amorphous TiO_2 synthesised via sol-gel.

• Surface chemistry impacts by altering catalyst used, e.g. nitric acid, bromic acid.

• Synthesising amorphous TiO_2 via sol-gel and doping/capping it with additional material.

Cape Peninsula
University of Technology

6. References

Agostini, G. & Lamberti, C. (eds). 2011. *Characterization of semiconductor heterostructures and nanostructures.* Amsterdam: Elsevier Science.

Andersson, M., Österlund, L.L., Jungstroem, S. & Palmqvist, A. 2002. Preparation of nanosize anatase and rutile TiO_2 by hydrothermal treatment of microemulsions and their activity for photocatalytic wet oxidation of phenol. *Journal of Physical Chemistry B*, 106(41):10674-10679.

Archana, J., Navaneethan, M. & Hayakawa, Y. 2013. Hydrothermal growth of monodispersed rutile TiO_2 nanorods and functional properties. *Material Letters*, 98:38-41.

Arora, H., Doty, C., Yuan, Y., Boyle, J., Petras, K., Rabatic, B., Paunesku, T. and Woloschak, G. 2012. Titanium Dioxide Nanocomposites. Nanotechnologies for the Life Sciences.

Bandyopadhyay, A.K. 2008. *Nanomaterials.* New Delhi: New Age International.

Barnard, A.S. & Zapol, P. 2004. Effects of particle morphology and surface hydrogenation on the phase stability of TiO_2. *Physical Review B*, 70:235403.

Barrañón, A. 2009. *New nanotechnology developments.* New York: Nova Science.

Bavykin, D.V. & Walsh, F.C. 2010. *Titanate and titania nanotubes: synthesis, properties and applications.* Cambridge: Royal Society of Chemistry.

Belin, T. & Epron, F. 2005. Characterization methods of carbon nanotubes: a review. *Materials Science and Engineering B*, 119(2):105-118.

Bischoff, B.L. & Anderson, M.A. 1995. Peptization process in the sol-gel preparation of porous anatase (TiO_2). *Chemistry of Materials*, 7(10):1772-1778.

Chang, J.A., Vithal, M., Baek, I.C. & Seok, S.I. 2009. Morphological and phase evolution of TiO_2 nanocrystals prepared from peroxotitanate complex aqueous solution: influence of acetic acid. *Journal of Solid State Chemistry*, 182(4):749-756.

Chen, H., SU, C., Chen, J. L., Yang, T. Y., Hsu, N. M. & Li, W. R. 2011. Preparation and characterization of pure rutile TiO_2 nanoparticles for photocatalytic study and thin films for dye-sensitized solar cells. *Nanomaterials,* 2011, 1-8.

Chen, X. & Mao, S.S. 2007. Titanium dioxide nanomaterials: synthesis, properties, modifications, and applications. *Chemical Reviews*, 107(7):2891-2959.

References

Cozzoli, P.D., Kornowski, A. & Weller, H. 2003. Low-temperature synthesis of soluble and processable organic-capped anatase TiO_2 nanorods. *Journal of the American Chemical Society*, 14539-14548.

Cushing, B.L., Kolesnichenko, V.L. & O'Connor, C.J. 2004. Recent advances in the liquid-phase syntheses of inorganic nanoparticles. *Chemical Reviews*, 104(9):3893-3946.

Di Paola, A., Cufalo, G., Addamo, M., Bellardita, M., Campostrini, R., Ischia, M., Ceccato, R. & Palmisano, L. 2008. Photocatalytic activity of nanocrystalline TiO_2 (brookite, rutile and brookite-based) powders prepared by thermohydrolysis of $TiCl_4$ in aqueous chloride solutions. *Colloids and Surfaces A: Physicochemical and Engineering Aspects*, 317(1):366-376.

Dong, D., Li, P., Li, X., Zhao, Q., Zhang, Y., Jia, C. & Li, P. 2010. Investigation on the photocatalytic degradation of pyrene on soil surfaces using nanometer anatase TiO_2 under UV irradiation. *Journal of Hazardous Materials*, 174(1-3):859-863.

Ede, S., Hafner, L., Dunlop, P., Byrne, J. & Will, G. 2012. Photocatalytic disinfection of bacterial pollutants using suspended and immobilized TiO_2 powders. *Photochemistry and Photobiology*.

Edelstein, A. S. & Cammarata, R. C. 1996. *Nanomaterials: Synthesis, Properties and Applications*. 2nd ed. New York: Taylor & Francis Group.

Ehrampoosh, M.H., Moussavi, G.R., Ghaneian, M., Rahimi, S. & Ahmadian, M. 2011. Removal of methylene blue dye from textile simulated sample using tubular reactor and TiO_2/UV-C photocatalytic process. *Iranian Journal of Environmental Health Science & Engineering*, 8(1):35-40.

Ethayaraja, M. and R. Bandyopadhyaya (2007). Mechanism and modeling of nanorod formation from nanodots. *Langmuir* 23(11): 6418-6423.

Farlex Inc. 2012. *The free dictionary.* Huntingdon Valley, PA: Farlex Inc. htpp://www.thefreedictionary.com [5 June 2012].

Fedlheim, D.L. & Foss, C.A. (eds). 2001. *Metal nanoparticles: synthesis, characterization, and applications.* New York: Taylor & Francis.

Fendler, J.H. (ed.). 2001. *Nanoparticles and nanostructured films: preparation, characterization, and applications.* Weinheim: Wiley-VCH.

Fogler, H.S. 1999. *Elements of chemical reaction engineering.* 3rd ed. Upper Saddle River, NJ: Prentice Hall.

Francisco, M.S.P., Mastelaro, V.R., Nascente, P.A.P. & Florentino, A.O. 2001. Activity and characterization by XPS, HR-TEM, Raman spectroscopy, and BET surface area of CuO/CeO_2-TiO_2 catalysts. *Journal of Physical Chemistry B*, 105(43):10515-10522.

References

Fujishima, A. & Honda, K. 1972. Electrochemical photolysis of water at a semiconductor electrode. *Nature*, 238(1972):37-38.

Gogotsi, Y. 2006. *Nanomaterials handbook.* Boca Roca, FL: Taylor & Francis.

Goossens, A., Maloney, E.L. & Schoonman, J. 1998. Gas phase synthesis of nanostructured anatase TiO_2. *Chemical Vapor Deposition*, 4(3):109-114.

Gopal, M., Chan, W.M. & De Jonghe, L. 1997. Room temperature synthesis of crystalline metal oxides. *Journal of Materials Science*, 32(22):6001-6008.

Granqvist, C.G., Kish, L.B. & Marlow, W.H. (eds). 2004. *Gas phase nanoparticle synthesis.* Dordrecht: Kluwer.

Gupta, S.M. & Tripathi, M. 2011. A review of TiO_2 nanoparticles. *Chinese Science Bulletin*, 56(16):1639-1657.

Gupta, S.M. & Tripathi, M. 2012. A review on the synthesis of TiO_2 nanoparticles by solution route. *Central European Journal of Chemistry*, 10(2):279-294.

Han, F., Kambala, V.S.R., Srinivasan, M., Rajarathnam, D. & Naidu, R. 2009.Tailored titanium dioxide photocatalysts for the degradation of organic dyes in wastewater treatment: a review. *Applied Catalysis A: General*, 359(1-2):25-40.

Hannavy, J. 2013. *Encyclopedia of nineteenth-century photography.* New York: Routledge.

Hsu, J.P. & Nacu, A. 2003. On the factors influencing the preparation of nanosized titania sols. *Langmuir*, 19(10):4448-4454.

Hu, Y., Tsai, H.L. & Huang, C.L. 2003. Effect of brookite phase on the anatase–rutile transition in titania nanoparticles. *Journal of the European Ceramic Society*, 23(5):691-696.

Ilyas, H., Qazi, I.A., Asgar, W., Awan, M.A. & Khan, Z. 2011. Photocatalytic degradation of nitro and chlorophenols using doped and undoped titanium dioxide nanoparticles. *Journal of Nanomaterials*, 21, 1-7.

Isley, S. L. and R. L. Penn (2006). Relative brookite and anatase content in sol-gel-synthesized titanium dioxide nanoparticles. *The Journal of Physical Chemistry B,* 110(31): 15134-15139.

Jiang, B., Yin, H., Jiang, T., Jiang, Y., Feng, H., Chen, K., Zhou, W. & Wada, Y. 2006. Hydrothermal synthesis of rutile TiO_2 nanoparticles using hydroxyl and carboxyl group-containing organics and modifiers. *Materials Chemistry and Physics*, 98(2-3):231-235.

Jang, H. D., S.-K. Kim, et al. (2001). Effect of particle size and phase composition of titanium dioxide nanoparticles on the photocatalytic properties. *Journal of Nanoparticle Research* 3(2-3): 141-147.

Cape Peninsula
University of Technology

References

Kandiel, T.A., Robben, L., Alkaim, A. & Bahnmann, D. 2013. Brookite versus anatase Tio$_2$ photocatalysts: phase transformations and photocatalytic activities. *Photochemical & Photobiological Sciences*, 12(4):602-609.

Kelton, K.F. & Greer, A.L. 2010. *Nucleation in condensed matter: applications in materials and biology.* Amsterdam: Elsevier Science.

Kim, J.H., Noh, B.H., Lee, G.D. & Hong, S.S. 2005. Hydrothermal synthesis of titanium dioxide using acid peptizing agents and their photocatalytic activity. *Korean Chemical Engineering,* 22, 370-374.

Kolen'ko, Y.V., Kovnir, K.A., Gavrilov, A.I., Garshev, A.V., Frantti, J., Lebedev, O.I., Churagulov, B.R., Van Tendeloo, G. & Yoshimura, M. 2006. Hydrothermal synthesis and characterization of nanorods of various tinanates and tinanium dioxide. *Journal of Physical Chemistry B*, 100(9):4030-4038.

Krivec, M., Segundo, R.A., Faria, J.L., Silva, A.M.T. & Dražić, G. 2013. Low-temperature synthesis and characterization of rutile nanoparticles with amorphous surface layer for photocatalytic degradation of caffeine. *Applied Catalysis B: Environmental*, 140:19-15.

Kroschwitz, J.I. & Seidel, A. 2007. *Kirk-Othmer encyclopedia of chemical technology.* 5th ed. Hoboken, NJ: Wiley.

Kuzmany, H., Plank, W., Hulman, M., Kramberger, C., Grüneis, A., Pichler, T., Peterlik, H., Kataura, H. & Achiba, Y. 2001. Determination of SWCNT diameters from the Raman response of the radial breathing mode. *European Physical Journal B: Condensed Matter and Complex Systems*, 22(3):307-320.

Lachheb, H., Puzenat, E., Houas, A., Ksibi, M., Elaloui, E., Guillard, C. & Herrmann, J.M. 2002. Photocatalytic degradation of various types of dyes (Alizarin S, Crocein Orange G, Methyl Red, Congo Red, Methylene Blue) in water by UV-irradiated titania. *Applied Catalysis B: Environmental*, 39(1):75-90.

Lakshmi, B.B., Dorhout, P.K. & Martin, C.R. 1997. Sol-gel template synthesis of semiconductor nanostructures. *Chemistry of Materials*, 9(3):857-862.

Leng, Y. 2009. *Materials characterization: introduction to microscopic and spectroscopic methods.* Hoboken, NJ: Wiley.

Levenspiel, O. 1972. *Chemical reaction engineering.* New York: Wiley.

Li, J.-G., T. Ishigaki, et al. (2007). Anatase, brookite, and rutile nanocrystals via redox reactions under mild hydrothermal conditions: phase-selective synthesis and physicochemical properties. *The Journal of Physical Chemistry C,* 111, 4969-4976.

Li, G., Li, L., Boerio-Goates, J. & Woodfield, B.F. 2003. Grain-growth kinetics of rulile TiO$_2$ nanocrystals under hydrothermal conditions. *Journal of Materials Research*, 18(11):2664-2669.

References

Liao, D. & Liao, B. 2007. Shape, size and photocatalytic activity control of TiO_2 nanoparticles with surfactants. *Journal of Photochemistry and Photobiology A: Chemistry*, 187(2-3):363-369.

Limmer, S.J., Chou, T.P. & Cao, G.Z. 2004. A study on the growth of TiO_2 nanorods using sol electrophoresis. *Journal of Materials Science*, 39(3):895-901.

Livraghi, S., Paganini, M.C. Giamello, E., Selloni, A., Di Valentin, C. & Pacchioni, G. 2006. Origin of photoactivity of nitrogen-doped titanium dioxide under visible light. *Journal of the American Chemical Society*, 128(49):15666-15671.

Machesky, M.L., Wesolowski, D.J., Ridley, M.K., Palmer, D.A., Rosenqvist, J., Lvov, S., Fedkin, M., Předota, M. & Vlcek, L. 2008. The protonation behaviour of metal oxide surfaces to hydrothermal conditions. *ECS Transactions*, 11(27):151-166.

Mahshid, S., Askari, M. & Ghamsari, M.S. 2007. Synthesis of TiO_2 nanoparticles by hydrolysis and peptization of titanium isopropoxide solution. *Journal of Materials Processing Technology*, 189(1):296-300.

Mahshid, S., Ghamsari, M.S., Askari, M., Afshar, N. & Lahuti, S. 2006. Synthesis of TiO_2 nanoparticles by hydrolysis and peptization of titanium isopropoxide solution. *Semiconductor Physics, Quantum Electronics and Optoelectronics*, 9(2):65-68.

Masterton, W.L. Hurley, C.N. & Neth, E.J. 2011. *Chemistry: principles and reactions.* 7th ed. Pacific Grove, CA: Brooks/Cole.

Matthews, A. 1976. The crystallization of anatase and rutile from amorphous titanium dioxide under hydrothermal conditions. *American Minerologist*, 61:419-424.

Megawati, Sediawan, W.B., Sulistyo, H. & Hidayat, M. 2011. Kinetics of sequential reaction of hydrolysis and sugar degradation of rice husk in ethanol production: effect of catalyst concentration. *Bioresource Technology*, 102(2):2062-2067.

Monreal, H.A., Chacón-Nava, J.G., Arce-Colunga, U., Martínez, C.A., Casillas, P.G. & Martínez-Villañe, A. 2009. Sol-gel preparation of titanium dioxide nanoparticles in presence of a linear polysaccharide. *Micro & Nano Letters*, 4(4):187-191.

Moreira, R. De F. P.M., Sauer, T.P., Casaril, L. & Humeres, E. 2005. Mass transfer and photocatalytic degradation of leather dye using TiO_2/UV. *Journal of Applied Electrochemistry*, 35(7-8):821-829.

Moritz, T., Reiss, J., Diesner, K., Su, D. & Chemseddine, A. 1997. Nanostructured crystalline TiO_2 through growth control and stabilization of intermediate structural building units. *Journal of Physical Chemistry B*, 101(41):8052-8053.

References

Nagarajan, R. & Alan Hatton, T. (eds). 2008. *Nanoparticles: synthesis, stabilization, passivation, and functionalization.* Washington, DC: American Chemical Society.

Nayak, P.S. & Singh, B.K. 2007. Instrumental characterization of clay by XRF, XRD and FTIR. *Bulletin of Building Materials Science*, 30(3):235-238.

Nian, J.N. & Teng, H. 2006. Hydrothermal synthesis of single-crystalline anatase TiO_2 nanorods with nanotubes as the precursor. *Journal of Physical Chemistry B*, 110(9):4193-4198.

Niederberger, M. & Pinna, N. 2009. *Metal oxide nanoparticles in organic solvents: synthesis, formation, assembly and application.* Heidelberg: Springer.

Novikov, V. 2002. *Concise dictionary of materials science: structure and characterization of polycrystalline materials.* Boca Raton, FL: CRC Press.

Oskam, G., Nellore, A., Penn, R.L. & Searson, P.C. 2003. The growth kinetics of TiO_2 nanoparticles from titanium (IV) alkoxide at high water/titanium ratio. *Journal of Physical Chemistry B*, 107(8):1734-1738.

Patil, K.C, Hedge, M.S., Rattan, T. & Aruna, S. 2008. *Chemistry of nanocrystalline oxide materials: combustion synthesis, properties and applications.* Singapore: World Scientific.

Pavasupree, S., Ngamsinlapasathian, S., Suzuki, Y. & Yoshikawa, S. 2006. Synthesis and dye-sensitized solar cell performance of nanorods/nanoparticles TiO_2 from high surface area nanosheet TiO_2. *Nanoscience and Nanotechnology*, 6(12):3685-3692.

Porter, D.A., Easterling, K.E. & Sherif, M.Y. 2009. *Phase transformations in metals and alloys.* 3rd ed. Boca Roca, FL: CRC Press.

Pottier, A., C. Chanéac, et al. (2001). Synthesis of brookite TiO_2 nanoparticlesby thermolysis of $TiCl_4$ in strongly acidic aqueous media. Journal of material chemistry 11(4): 1116-1121.

Ramesh, K.T. 2009. *Nanomaterials: mechanics and mechanisms.* Dordrecht: Springer.

Reyes-Coronado, D., Rodriguez-Gattorno, G., Espinosa-Pesqueira, M.E., Cab, C. De Coss, R. & Oskam, G. 2008. Phase-pure TiO_2 nanoparticles: anatase, brookite and rutile. *Nanotechnology*, 19(4): 1-10.

Rocco, R.M. 2006. *Landmark papers in clinical chemistry.* Amsterdam: Elsevier Science.

Rotello, V.M. 2004. *Nanoparticles: building blocks for nanotechnology.* New York: Kluwer Academic/Plenum.

Ryu, Y.B., Lee, G.D., Park, S.S. & Hong, S.S. 2006. Synthesis of nanosized titanium dioxide using a hydrothermal method and their photocatalytic activity. *Industrial and Engineering Chemistry*, 12(2):289-294.

References

Sakka, S. (ed.). 2005. *Handbook of sol-gel science and technology, Vol. 1: Sol-gel processing.* Dordrecht: Kluwer.

Scanlon, D.O., Dunnill, C.W., Buckeridge, J., Shevlin, S.A., Logsdail, A.J., Woodley, S.M., Catlow, C.R.A., Powell, M.J., Palgrave, R.G., Parkin, I.P., Watson, G.W., Keal, T.W., Sherwood, P., Walsh, A. & Sokol, A.A. 2013. Band alignment of rutile and anatase TiO_2. *Nature Materials*, 12(9):798-801.

So, W.W., Park, S.B., Kim, K.J. & Moon, S.J. 1997. Phase transformation behavior at low temperature in hydrothermal treatment of stable and unstable titania sol. *Journal of Colloid and Interface Science*, 191(2):398-406.

Su, C., Tseng, C.M., Chen, L.F., You, B.H., Hsu, B.C. & Chen, S.S. 2006. Sol-hydrothermal preparation and photocatalysis of titanium oxide. *Thin Solid Films*, 498(1-2):259-265.

Sugimoto, T., Zhou, X. & Muramatsu, A. 2003. Synthesis of uniform anatase TiO_2 nanoparticles by gel-sol method: 4. Shape control. *Journal of Colloid and Interface Science*, 259(1):53-61.

Svishchev, I.M. & Nahtigal, I. 2008. Simulating hydrothermal nucleation of ionic nanoparticles. Paper presented at the 15th ICPWS (International Conference on the Properties of Water and Steam) Conference, Berlin, 7–11 September, 2008.

Tahir, M.N., Theato, P., Oberle, P., Melnyk, G., Faiss, S., Kolb, U., Janshoff, A., Stepputat, M. & Tremel, W. 2006. Facile synthesis and characterization of functionalized, monocrystalline rutile TiO_2 nanorods. *Langmuir*, 22(12):5209-5212.

Testino, A., Bellobono, I.R., Buscaglia, V., Canevali, C., D'Arienzo, M., Polizzi, S., Scotti, R. & Morazzoni, F. 2007. Optimizing the photocatalytic properties of hydrothermal TiO_2 by the control of phase composition and particle morphology. A systematic approach. *Journal of the American Chemical Society*, 129(12):3564-3575.

Thomas, O. & Burgess, C. (eds). 2007. *UV-visible spectrophotometry of water and wastewater.* Amsterdam: Elsevier Science.

Transparency Market Research. 2012. *Nanoparticle titanium dioxide (TiO_2): global industry size, market share, trends, analysis, and forecasts 2012–2018*. http://www.transparencymarketresearch.com/nanoparticle-titanium-dioxide-tio2-market.html [6 July 2012].

Tzikalos, N., Belessi, V. & Lambropoulou, D. 2013. Photocatalytic degradation of Reactive Red 195 using anatase/brookite TiO_2 mesoporous nanoparticles: optimization using response surface methodology (RSM) and kinetics studies. *Environmental Science and Pollution Research*, 20(4):2305-2320.

Vogel, A.I. & Jeffery, G.H. 1989. *Vogel's textbook of quantitative chemical analysis.* 5th ed. Harlow: Longman Scientific & Technical.

References

Vorkapic, D. & Matsoukas, T. 1998. Effect of temperature and alcohols in the preparation of titania nanoparticles from alkoxides. *Journal of the American Ceramic Society*, 81(11):2815-2820.

Wang, Y., Zhang, L., Deng, K., Chen, X. & Zou, Z. 2007. Low temperature synthesis and photocatalytic activity of rutile TiO_2 nanorod superstructures. *Journal of Physical Chemistry C*, 111(6):2709-2714.

Wang, C.-C. and J. Y. Ying (1999). Sol-gel synthesis and hydrothermal processing of anatase and rutile titania nanocrystals. Chemistry of materials 11(11): 3113-3120.

Winkler, J. 2003. *Titanium dioxide*, Germany, Vincentz Network.

Wiggers, H. 2009. Novel material properties based on flame-synthesized nanomaterials. *KONA Powder and Particle Journal*, 27:186-194.

Wu, M., Lin, G., Chen, D., Wang, G., He, D., Feng, S. & Xu, R. 2002. Sol-hydrothermal synthesis and hydrothermally structural evolution of nanocrystal titanium dioxide. *Chemistry of Materials*, 14(5):1974-1980.

Yan, M., F. Chen, et al. (2005). Preparation of controllable crystalline titania and study on the photocatalytic properties. The Journal of Physical Chemistry B 109(18): 8673-8678.

Yang, Y., Wang, H., Li, J., He, B., Wang, T. & Liao, S. 2012. Novel functionalized nano-TiO_2 loading electrocatalytic membrane for oily wastewater treatment. *Environmental Science & Technology*, 46(12):6815-6821.

Yin, H., Y. Wada, et al. (2001). Hydrothermal synthesis of nanosized anatase and rutile TiO_2 using amorphous phase TiO_2. Journal of materials chemistry 11(6): 1694-1703.

Yoldas, B.E. 1986. Hydrolysis of titanium alkoxide and effects of hydrolytic polycondensation parameters. *Journal of Materials Science*, 21(3):1087-1092.

Yu, J., Wang, G., Cheng, B. & Zhou, M. 2007. Effects of hydrothermal temperature and time on the photocatalytic activity and microstructures of bimodal mesoporous TiO_2 powders. *Applied Catalysis B: Environmental*, 69(3-4):171-180.

Yu, Y., Wang, J. & Parr, J.F. 2012. Preparation and properties of TiO_2/fumed silica composite photocatalytic materials. *Procedia Engineering*, 27:448-456.

Zhang, H. and J. F. Banfield (2000). Understanding polymorphic phase transformation behavior during growth of nanocrystalline aggregates: insights from TiO_2. The journal of physical chemistry B 104(15): 3481-3487.

Zhang, H. and J. F. Banfield (2005). Size dependence of the kinetic rate constant for phase transformation in TiO_2 nanoparticles. Chemistry of materials 17(13): 3421-3425.

Appendix A: Pump curves
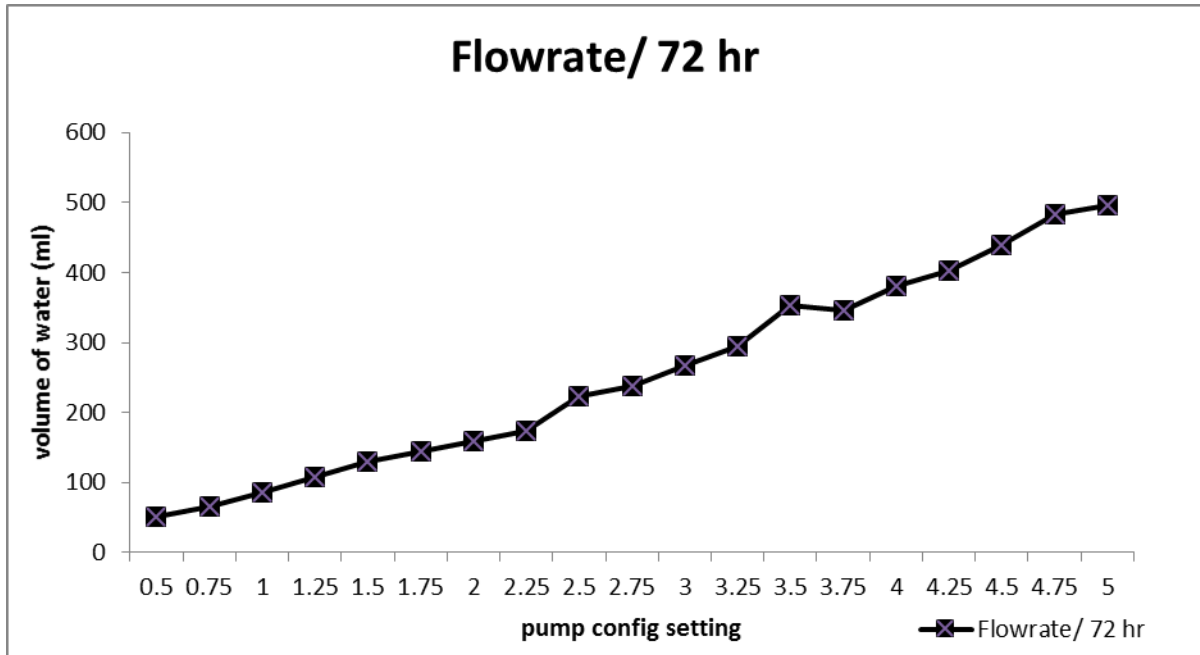
Figure A.1: Pumping flow curve for peristaltic pump used in experimentation, for the desired water ageing durations 72 hours
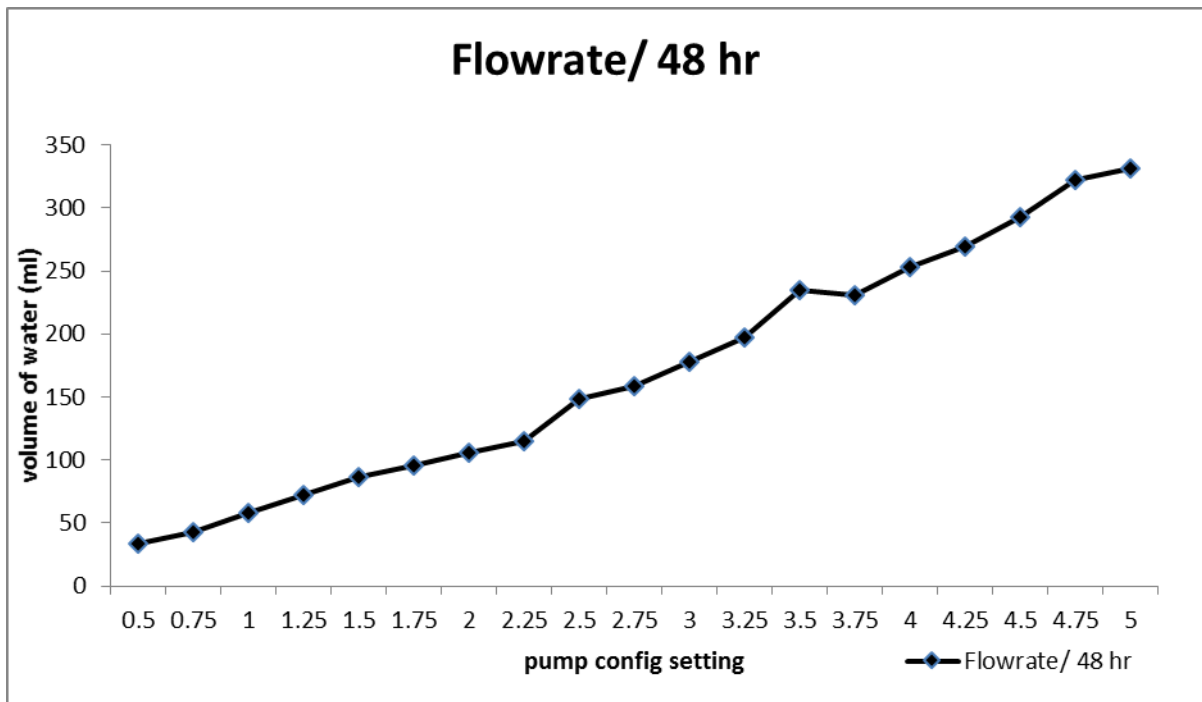
Figure A.2: Pumping flow curve for peristaltic pump used in experimentation, for the desired water ageing durations 48 hours

Cape Peninsula
University of Technology
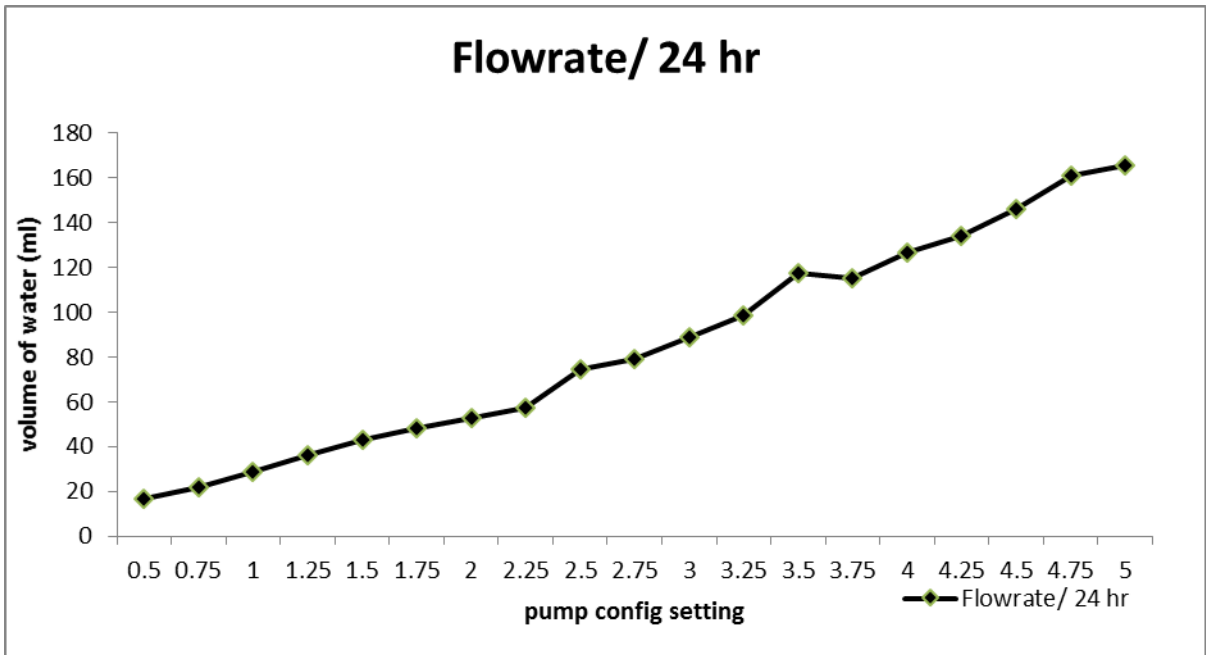
Figure A.3: Pumping flow curve for peristaltic pump used in experimentation, for the desired water ageing durations 24 hours
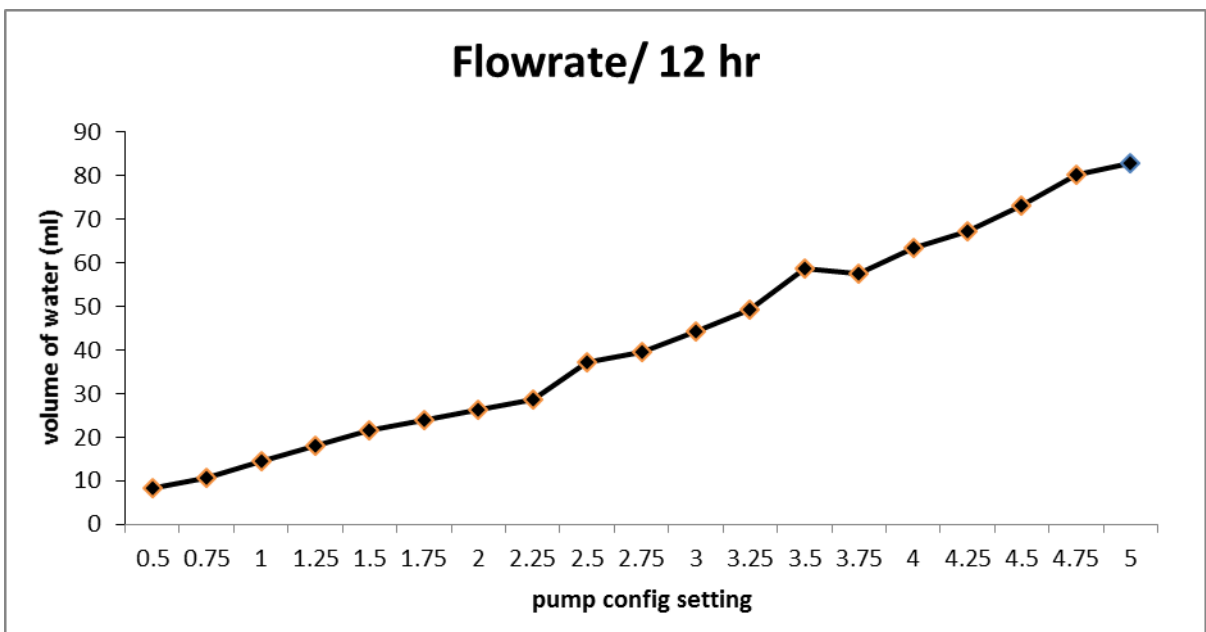
Figure A.4: Pumping flow curve for peristaltic pump used in experimentation, for the desired water ageing durations 12 hours

Table A.1: Pump test data for pump curve construction

needed pumping rates		24 hour	48 hour	72 hour	
	(ml/hr)	6.3	3.2		2.1
PUMP CONFIG. TESTS					
Pump configure	ml/ hr	ml / 12 hr	ml / 24 hr	ml / 48 hr	ml / 72 hr
0.5	0.7	8.4	16.8	33.6	50.4
0.75	0.9	10.8	21.6	43.2	64.8
1	1.2	14.4	28.8	57.6	86.4
1.25	1.5	18	36	72	108
1.5	1.8	21.6	43.2	86.4	129.6
1.75	2	24	48	96	**144**
2	2.2	26.4	52.8	105.6	158.4
2.25	2.4	28.8	57.6	115.2	172.8
2.5	3.1	37.2	74.4	**148.8**	223.2
2.75	3.3	39.6	79.2	158.4	237.6
3	3.7	44.4	88.8	177.6	266.4
3.25	4.1	49.2	98.4	196.8	295.2
3.5	4.9	58.8	117.6	235.2	352.8
3.75	4.8	57.6	115.2	230.4	345.6
4	5.28	63.36	126.72	253.44	380.16
4.25	5.6	67.2	134.4	268.8	403.2
4.5	6.1	73.2	**146.4**	292.8	439.2
4.75	6.7	80.4	160.8	321.6	482.4
5	6.9	**82.8**	165.6	331.2	496.8

Cape Peninsula
University of Technology

Appendix B: Samples of Characterization tools

Table B.1: A sample of 200 TiO₂ nanoparticles measured with the use of ImageJ software

Measured particles	length (nm)	Diameter (nm)	Measured particles	length (nm)	Diameter (nm)
1	20.664	12.283	40	36.422	19.765
2	16.014	13.886	41	24.305	20.468
3	18.43	11.684	42	25.565	8.709
4	23.166	11.022	43	57.828	17.77
5	14.391	20.759	44	21.485	18.503
6	27.6	8.294	45	25.668	13.451
7	20.005	8.549	46	13.737	13.951
8	21.575	7.258	47	23.458	12.209
9	22.647	10.209	48	15.918	11.295
10	18.786	10.209	49	28.688	11.818
11	12.952	13.336	50	25.526	12.384
12	35.337	25.261	51	15.655	20.161
13	35.571	10.156	52	14.431	14.826
14	28.646	11.39	53	22.862	17.258
15	22.711	16.889	54	23.831	16.068
16	20.044	11.152	55	20.008	15.054
17	18.018	13.573	56	23.509	17.154
18	10.633	9.953	57	19.784	21.826
19	8.274	11.908	58	23.961	19.459
20	19.834	14.251	59	31.383	13.733
21	31.845	11.798	60	21.999	14.256
22	21.473	15.392	61	14.955	13.165
23	35.046	14.135	62	23.272	9.195
24	18.731	13.451	63	12.472	11.756
25	27.45	14.277	64	35.679	16.94
26	13.12	14.307	65	17.817	16.882
27	21.699	8.933	66	23.207	17.506
28	25.88	17.498	67	26.409	17.455
29	27.368	21.316	68	37.957	20.92
30	16.059	13.652	69	37.731	19.476
31	26.932	9.711	70	31.597	11.469
32	23.205	13.374	71	11.602	14.521
33	18.363	13.404	72	11.798	17.672
34	15.5	14.021	73	27.475	12.157
35	29.571	11.143	74	24.566	12.263
36	16.714	10.568	75	33.319	8.657
37	40.502	7.477	76	15.558	19.696
38	32.327	11.076	77	23.384	12.655

Measured particles	length (nm)	Diameter (nm)	Measured particles	length (nm)	Diameter (nm)
39	20.066	10.584	78	32.182	17.672
79	16.723	12.083	122	23.638	12.181
80	16.884	16.413	123	30.42	16.427
81	32.288	22.827	124	21.656	18.518
82	37.585	19.488	125	35.346	10.648
83	19.044	14.716	126	39.748	14.246
84	21.455	14.204	127	33.309	19.512
85	24.263	13.403	128	32.094	0
86	20.659	20.305	129	18.906	11.89
87	68.318	13.3	130	33.761	17.404
88	30.2	11.461	131	37.436	12.088
89	20.961	11.988	132	18.189	17.778
90	17.136	13.904	133	39.07	11.688
91	24.55	13.602	134	51.361	11.446
92	18.572	18.968	135	39.931	19.662
93	13.171	18.899	136	42.69	15.873
94	26.55	13.403	137	21.82	26.46
95	20.114	14.476	138	41.95	19.31
96	34.3	21.473	139	28.347	23.262
97	20.174	17.225	140	31.473	20.607
98	22.904	19.358	141	71.938	15.261
99	23.671	0	142	46.428	16.563
100	19.816	16.781	143	24.956	12.272
101	24.511	15.684	144	23.553	17.588
102	22.516	14.538	145	27.735	14.451
103	30.718	15.559	146	15.836	21.485
104	35.816	16.625	147	22.969	20.001
105	28.041	17.728	148	50.079	14.899
106	13.738	15.301	149	22.994	7.196
107	18.763	16.058	150	36.051	11.709
108	23.028	17.686	151	55.74	12.963
109	13.916	14.476	152	19.815	13.055
110	21.547	7.829	153	23.217	13.243
111	38.596	15.992	154	30.983	10.681
112	12.755	16.066	155	29	18.331
113	54.952	10.273	156	16.632	9.785
114	54.952	18.639	157	23.022	15.34
115	42.317	26.713	158	22.369	19.633
116	22.987	13.767	159	18.038	13.231
117	15.572	21.815	160	18.618	8.447
118	34.328	27.457	161	25.875	12.257
119	39.906	21.4	162	24.43	14.845
120	33.583	16.23	163	61.111	9.569

	121	32.986	10.635		164	37.302	13.425
Measured particles	length (nm)	Diameter (nm)					
165	15.437	17.555					
166	23.418	12.334					
167	17.805	12.8					
168	30.48	20.262					
169	31.635	11.505					
170	23.091	11.012					
171	22.324	13.636					
172	22.594	15.985					
173	28.607	9.972					
174	25.699	10.43					
175	16.564	10.802					
176	29.131	12.96					
177	28.281	13.128					
178	20.043	29.888					
179	15.442	23.046					
180	21.183	13.114					
181	38.449	14.576					
182	13.596	11.936					
183	32.333	8.896					
184	12.674	11.153					
185	19.571	14.652					
186	33.939	17.928					
187	20.833	10.621					
188	21.522	16.033					
189	18.511	12.605					
190	25.61	9.174					
191	19.034	9.839					
192	15.254	16.608					
193	16.76	12.245					
194	46.181	14.644					
195	34.729	13.519					
196	31.842	18.69					
197	29.373	16.492					
198	13.771	22.137					
199	17.448	12.382					
200	19.173	22.405					
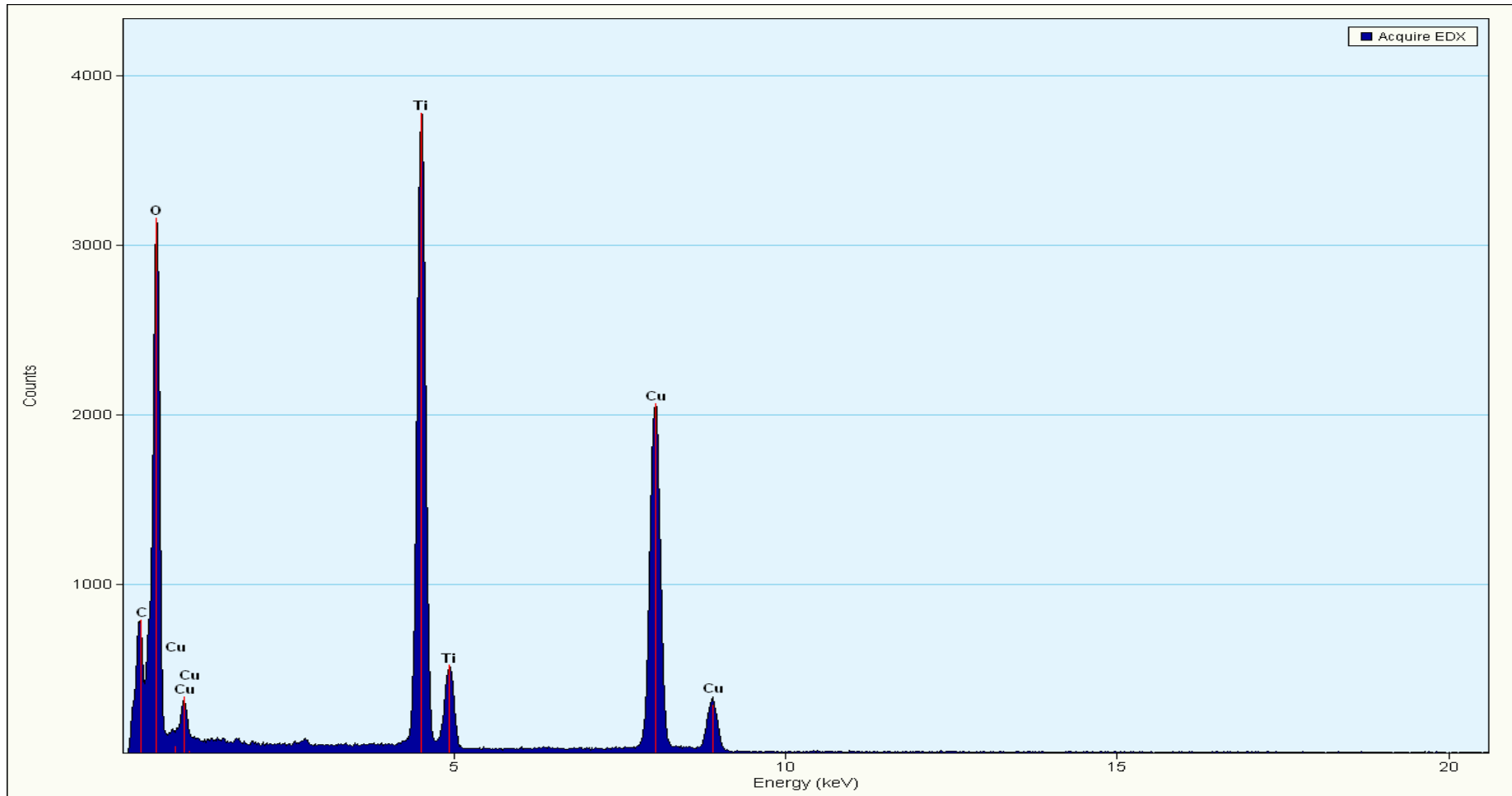
Figure B.1: EDS scan on a copper grid, of TiO$_2$ prepared at 4M 24 Hr.
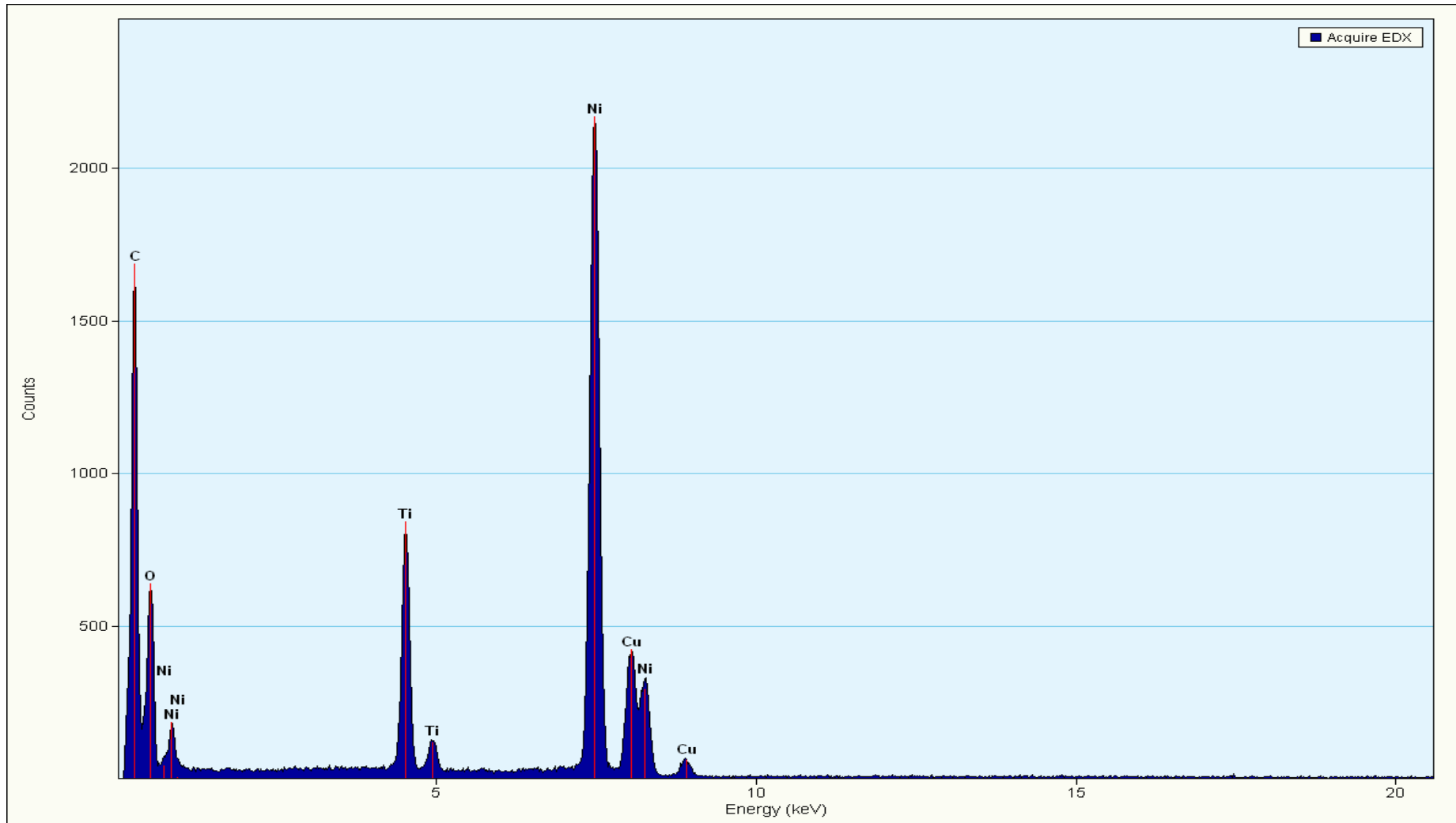
Figure B.2: EDS scan on a nickel grid, of TiO$_2$ prepared at 5M 12 Hr.

Appendix C: Additional TEM images for 3 Molar samples
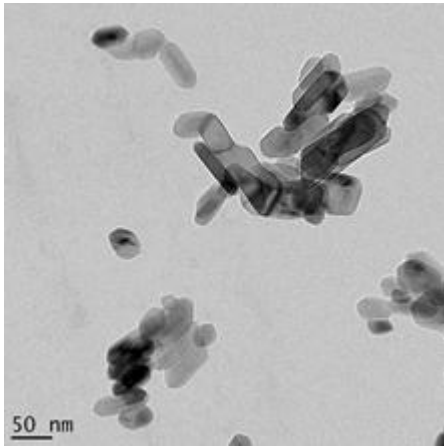
Figure C.1: TEM images of TiO$_2$ prepared for gel formation time of 3M 72 hours
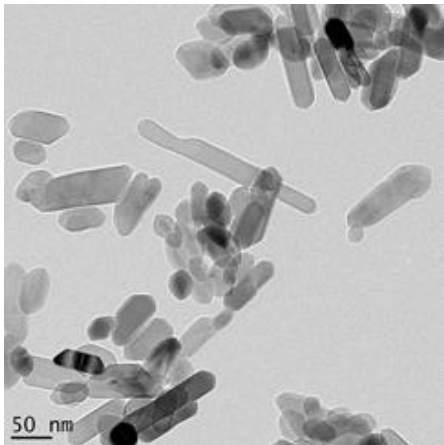
Figure C.2: TEM images of TiO$_2$ prepared for gel formation time of 3M 72 hours
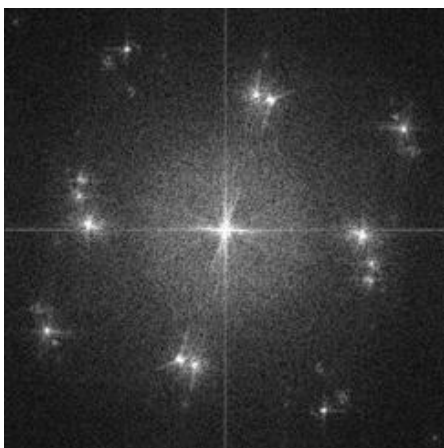
Figure C.3: FFT live feed when preforming TEM characterization, this image validates that nanoparticles synthesised at 3 M 72 hours were crystalline
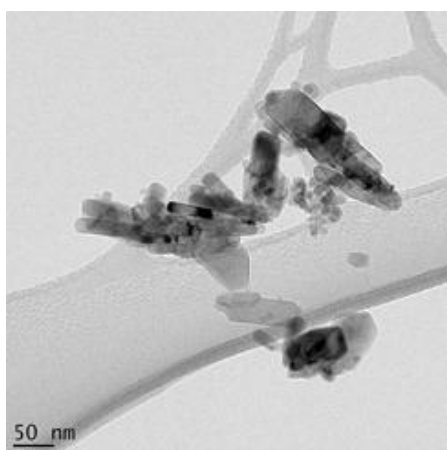
Figure C.4: TEM images of TiO$_2$ prepared for gel formation time of 3M 48 hours
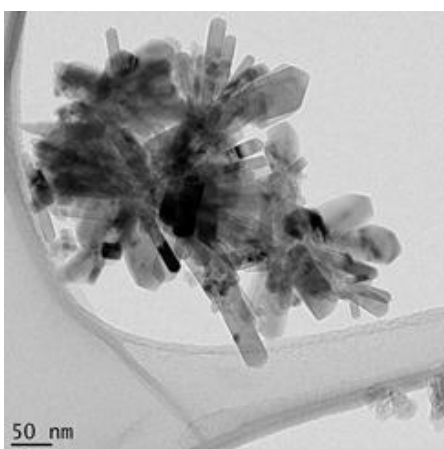
Figure C.5: TEM images of TiO$_2$ prepared for gel formation time of 3M 48 hours
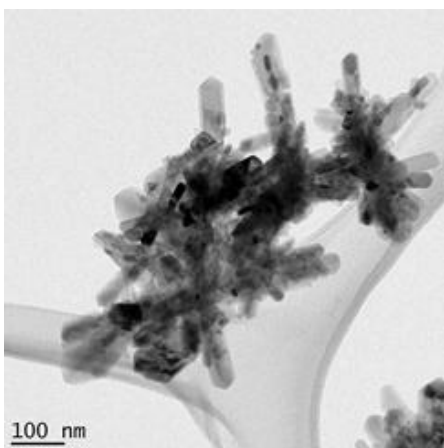
Figure C.6: TEM images of TiO$_2$ prepared for gel formation time of 3M 48 hours

Cape Peninsula
University of Technology
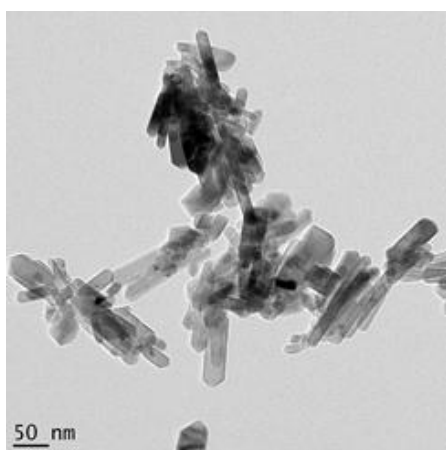
Figure C.7: TEM images of TiO$_2$ prepared for gel formation time of 3M 24 + 16 hours
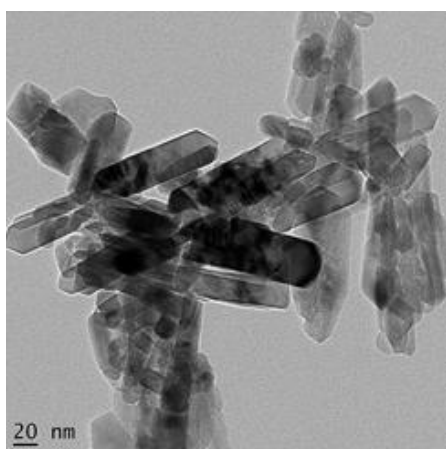
Figure C.8: TEM images of TiO$_2$ prepared for gel formation time of 3M 24 + 16 hours
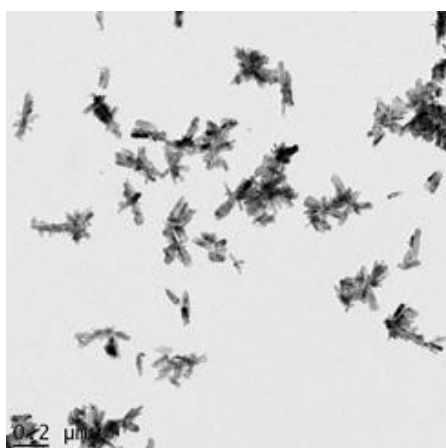
Figure C.9: TEM images of TiO$_2$ prepared for gel formation time of 3M 24 + 16 hours

Cape Peninsula
University of Technology
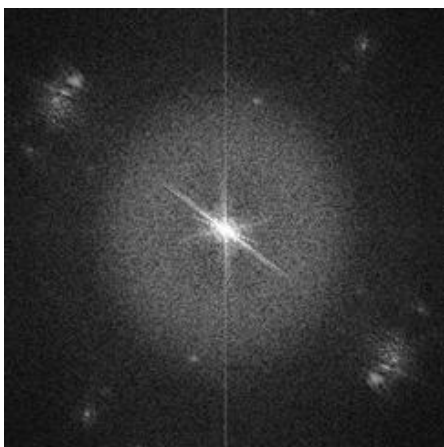
Figure C.10: FFT live feed when preforming TEM characterization, this image validates that nanoparticles synthesised at 3 M 24 + 16 hours were crystalline
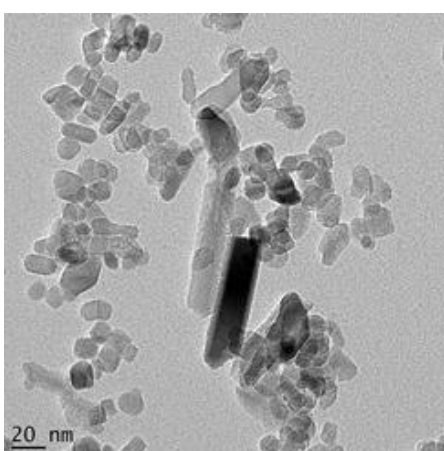
Figure C.11: TEM images of TiO$_2$ prepared for gel formation time of 3M 24 hours
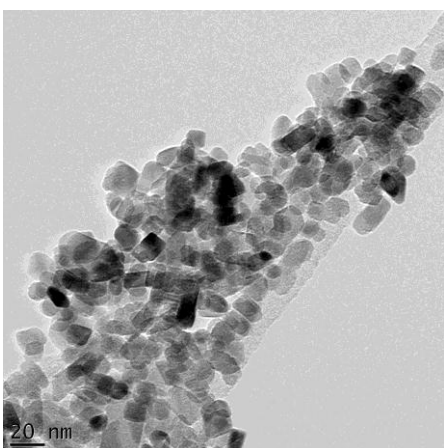
Figure C.12: TEM images of TiO$_2$ prepared for gel formation time of 3M 24 hours
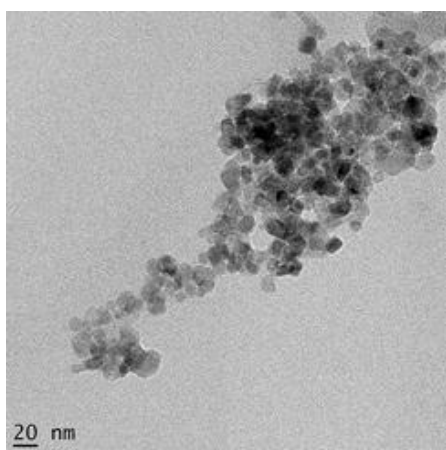
Figure C.13: TEM images of TiO$_2$ prepared for gel formation time of 3M 24 hours
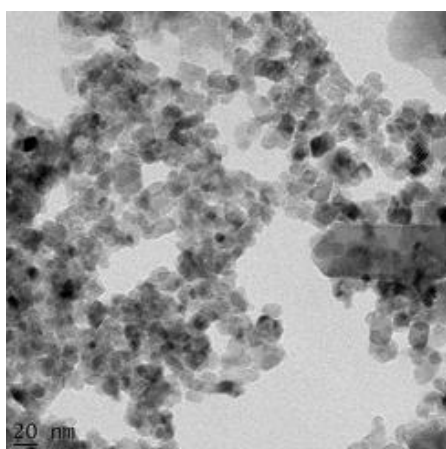
Figure C.14: TEM images of TiO$_2$ prepared for gel formation time of 3M 12 hours
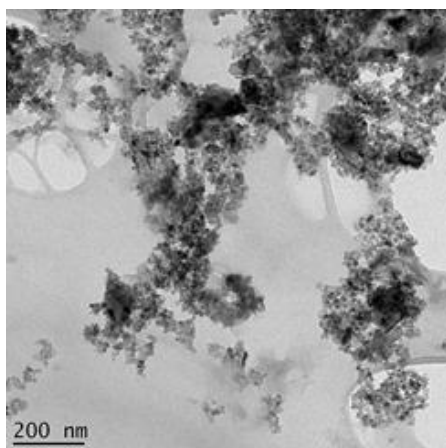
Figure C.15: TEM images of TiO$_2$ prepared for gel formation time of 3M 12 hours
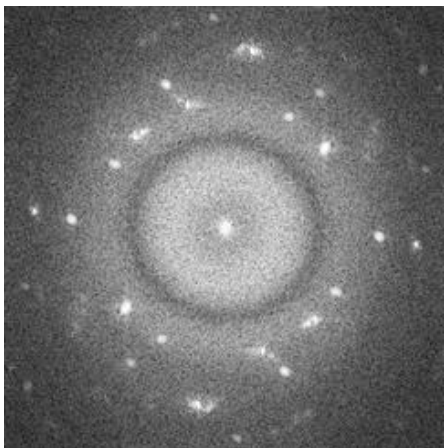
Figure C.16: FFT live feed when preforming TEM characterization, this image validates that nanoparticles synthesised at 3 M 12 hours were crystalline

Appendix D: Additional TEM images for 4 Molar samples
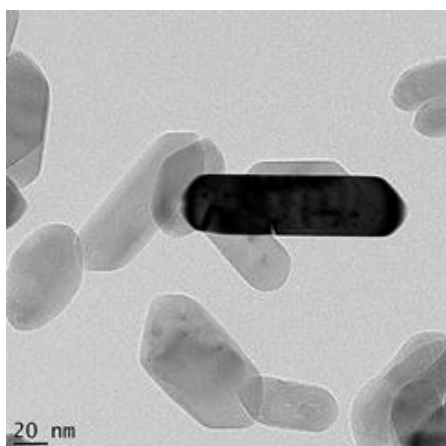
Figure D.1: TEM images of TiO$_2$ prepared for gel formation time of 4M 72 hours
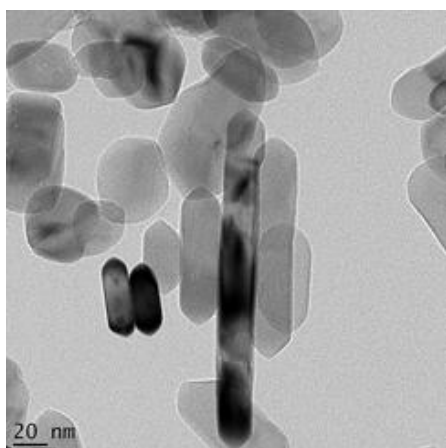
Figure D.2: TEM images of TiO$_2$ prepared for gel formation time of 4M 72 hours
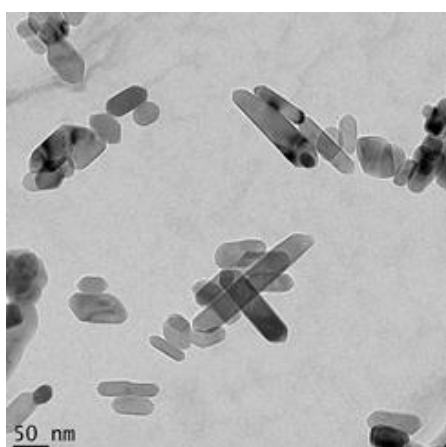
Figure D.3: TEM images of TiO$_2$ prepared for gel formation time of 4M 72 hours

Cape Peninsula
University of Technology
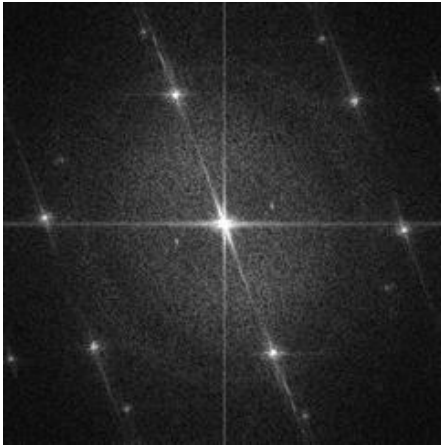
Figure D.4: FFT live feed when preforming TEM characterization, this image validates that nanoparticles synthesised at 4 M 72 hours were crystalline
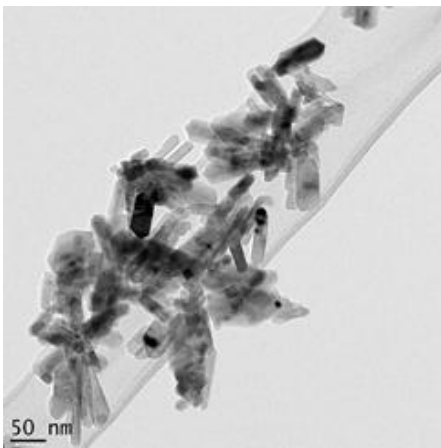
Figure D.5: TEM images of TiO$_2$ prepared for gel formation time of 4M 24hours
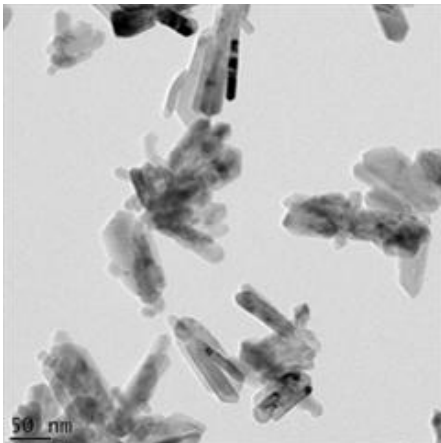
Figure D.6: TEM images of TiO$_2$ prepared for gel formation time of 4M 24 hours
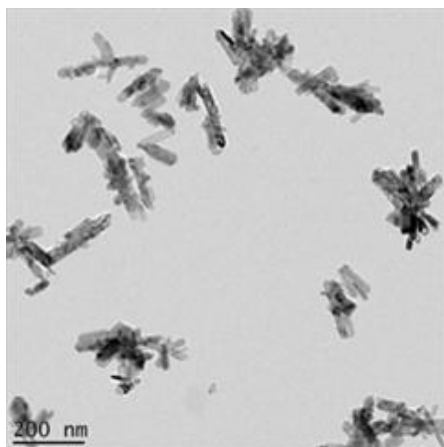
Figure D.7: TEM images of TiO$_2$ prepared for gel formation time of 4M 24 hours
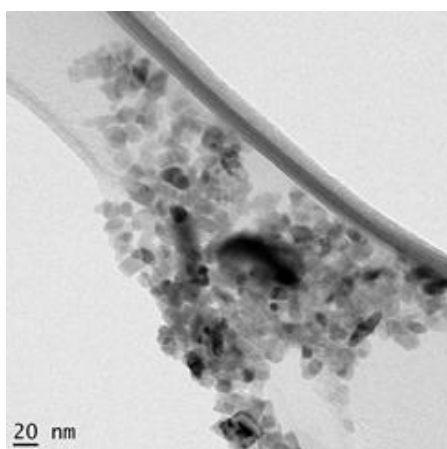
Figure D.8: TEM images of TiO$_2$ prepared for gel formation time of 4M 12 hours
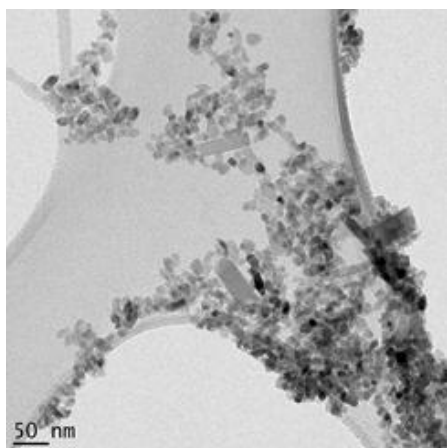
Figure D.9: TEM images of TiO$_2$ prepared for gel formation time of 4M 12 hours

Cape Peninsula
University of Technology

Appendix E: Additional TEM images for 5 Molar samples and prolonged hydrothermal treatment
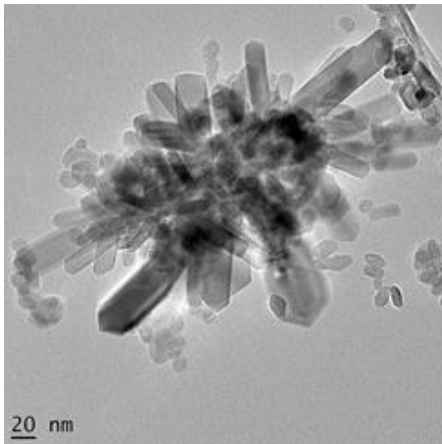
Figure E.1: TEM images of TiO$_2$ prepared for gel formation time of 5M 72 hours
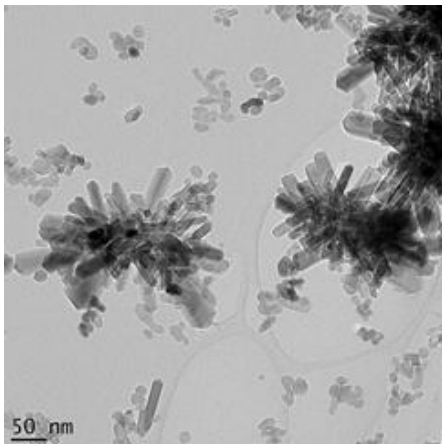
Figure E.2: TEM images of TiO$_2$ prepared for gel formation time of 5M 72 hours
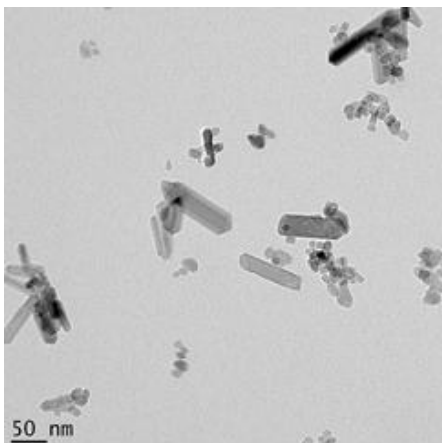
Figure E.3: TEM images of TiO$_2$ prepared for gel formation time of 5M 72 hours

Cape Peninsula
University of Technology
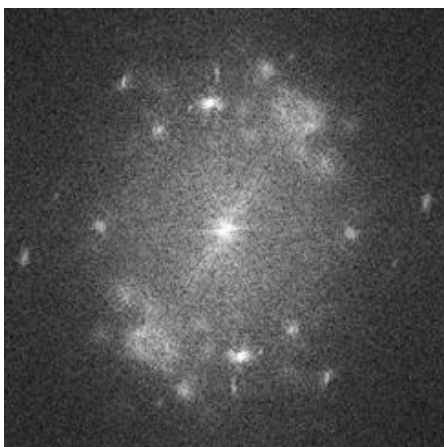
Figure E.4: FFT live feed when preforming TEM characterization, this image validates that nanoparticles synthesised at 5 M 72 hours were crystalline
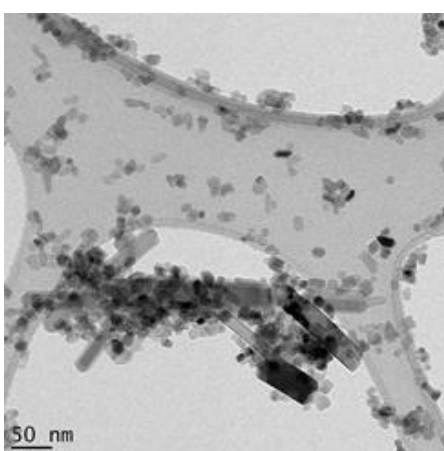
Figure E.5: TEM images of TiO$_2$ prepared for gel formation time of 5M 24 hours
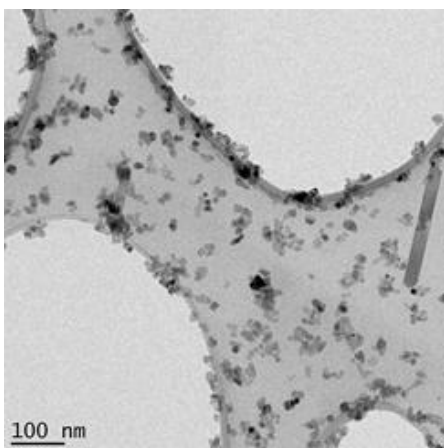
Figure E.6: TEM images of TiO$_2$ prepared for gel formation time of 5M 24 hours
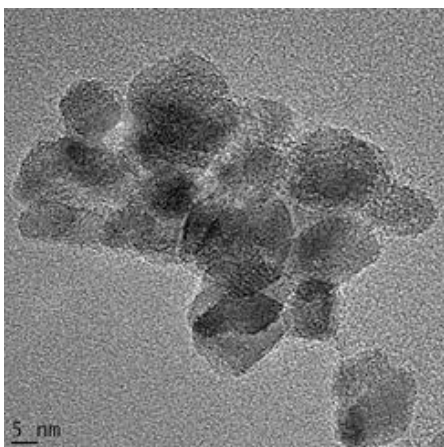
Figure E.7: TEM images of TiO$_2$ prepared for gel formation time of 5M 12 hours
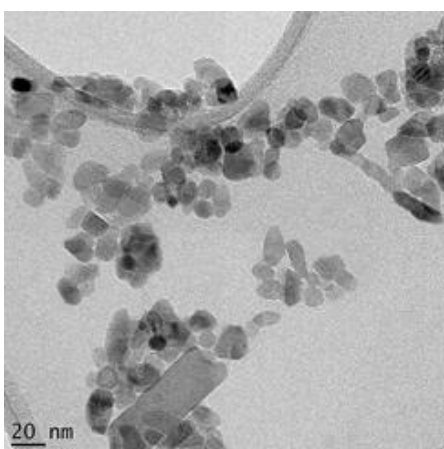
Figure E.8: TEM images of TiO$_2$ prepared for gel formation time of 5M 12 hours
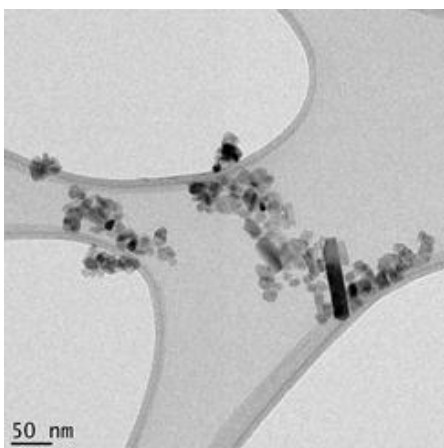
Figure E.9: TEM images of TiO$_2$ prepared for gel formation time of 5M 12 hours
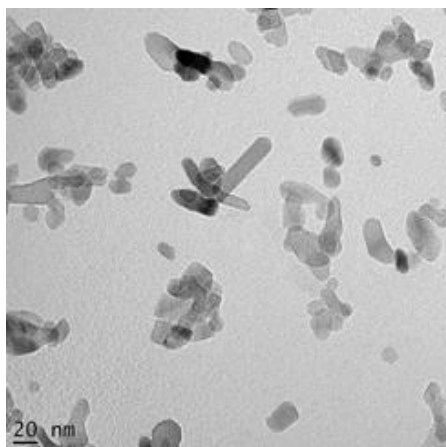
Figure E.10: TEM image of TiO₂ nanoparticles prepared in 5M concentration of HCl and water aged for a duration of 12 hr, thereafter hydrothermally treated for 2 hour
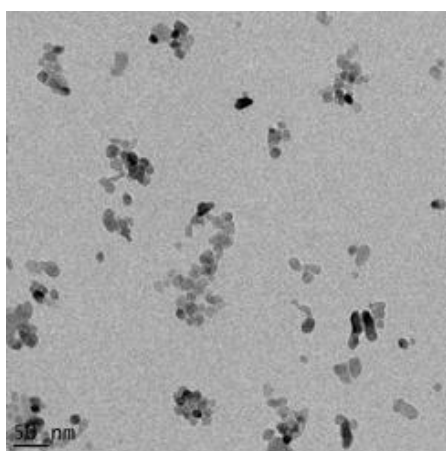
Figure E.11: TEM image of TiO₂ nanoparticles prepared in 5M concentration of HCl and water aged for a duration of 12 hr, thereafter hydrothermally treated for 3 hour
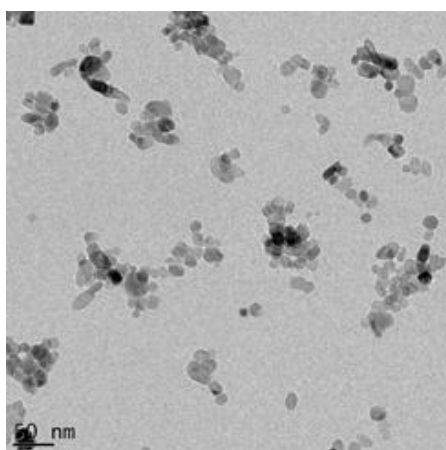
Figure E.12: TEM image of TiO₂ nanoparticles prepared in 5M concentration of HCl and water aged for a duration of 12 hr, thereafter hydrothermally treated for 3 hour

Cape Peninsula
University of Technology
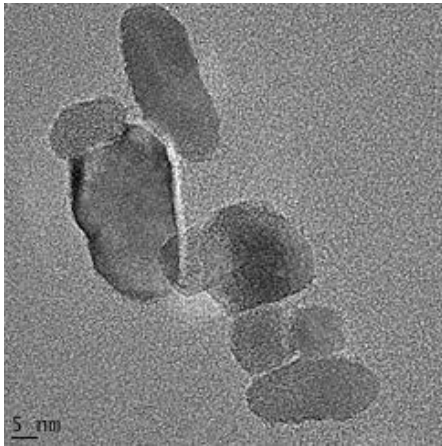
Figure E.13: TEM image of TiO₂ nanoparticles prepared in 5M concentration of HCl and water aged for a duration of 12 hr, thereafter hydrothermally treated for 3 hour
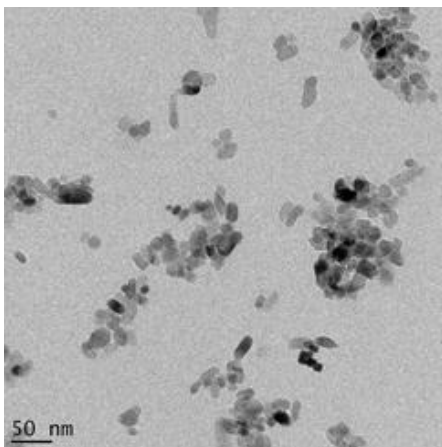
Figure E.14: TEM image of TiO₂ nanoparticles prepared in 5M concentration of HCl and water aged for a duration of 12 hr, thereafter hydrothermally treated for 4 hour
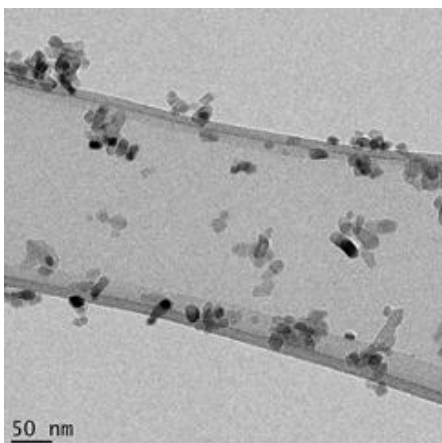
Figure E.15: TEM image of TiO₂ nanoparticles prepared in 5M concentration of HCl and water aged for a duration of 12 hr, thereafter hydrothermally treated for 4 hour
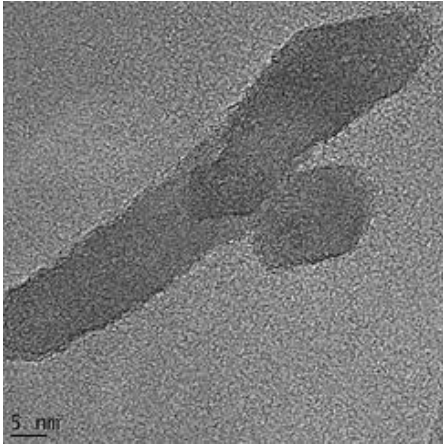
Figure E.16: TEM image of TiO₂ nanoparticles prepared in 5M concentration of HCl and water aged for a duration of 12 hr, thereafter hydrothermally treated for 4 hour
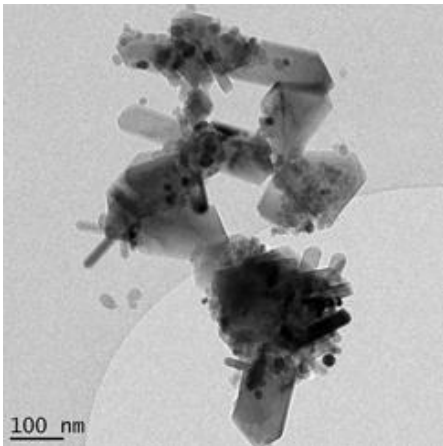
Figure E.17: TEM image of TiO₂ nanoparticles prepared in 5M concentration of HCl and water aged for a duration of 12 hr, thereafter hydrothermally treated for 5 hour
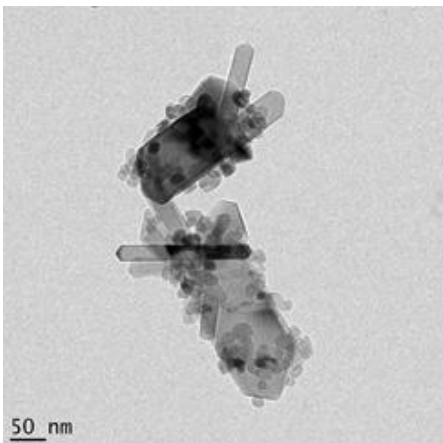
Figure E.18: TEM image of TiO₂ nanoparticles prepared in 5M concentration of HCl and water aged for a duration of 12 hr, thereafter hydrothermally treated for 5 hour

Cape Peninsula
University of Technology
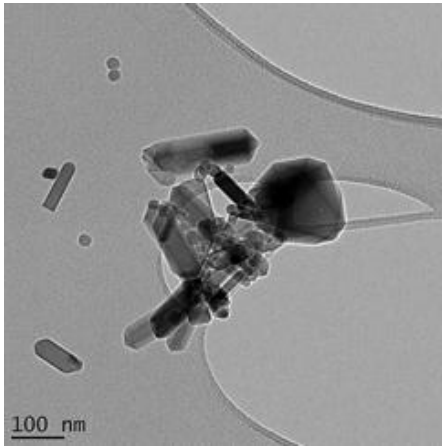
Figure E.19: TEM image of TiO₂ nanoparticles prepared in 5M concentration of HCl and water aged for a duration of 12 hr, thereafter hydrothermally treated for 6 hour
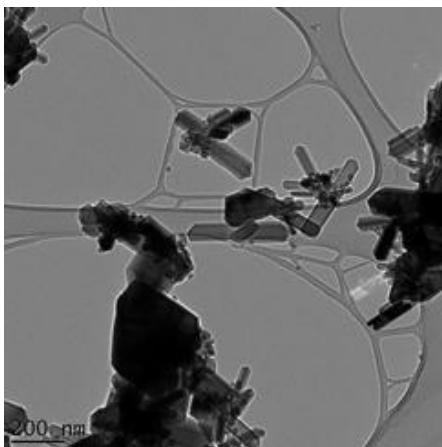
Figure E.20: TEM image of TiO₂ nanoparticles prepared in 5M concentration of HCl and water aged for a duration of 12 hr, thereafter hydrothermally treated for 6 hour
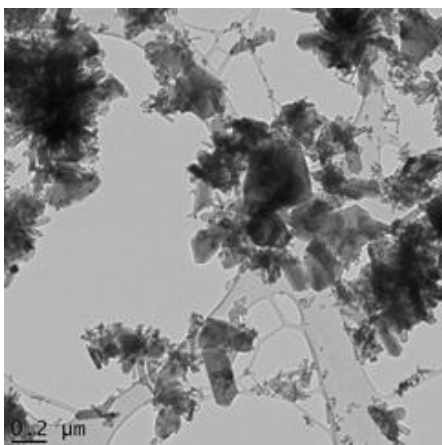
Figure E.21: TEM image of TiO₂ nanoparticles prepared in 5M concentration of HCl and water aged for a duration of 12 hr, thereafter hydrothermally treated for 8 hour
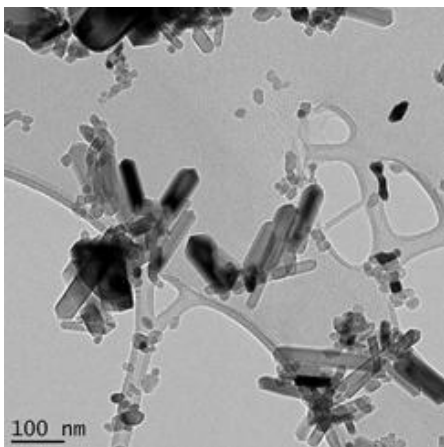
Figure E.22: TEM image of TiO₂ nanoparticles prepared in 5M concentration of HCl and water aged for a duration of 12 hr, thereafter hydrothermally treated for 8
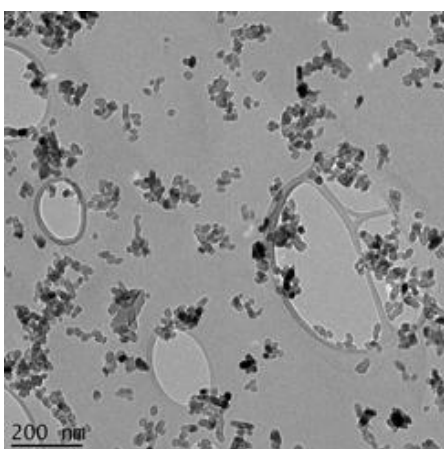
Figure E.23: TEM image of TiO₂ nanoparticles prepared in 5M concentration of HCl and water aged for a duration of 12 hr, thereafter hydrothermally treated for 10 hour
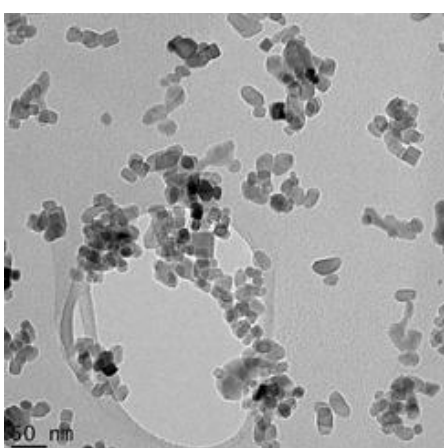
Figure E.24: TEM image of TiO₂ nanoparticles prepared in 5M concentration of HCl and water aged for a duration of 12 hr, thereafter hydrothermally treated for 10

Cape Peninsula
University of Technology
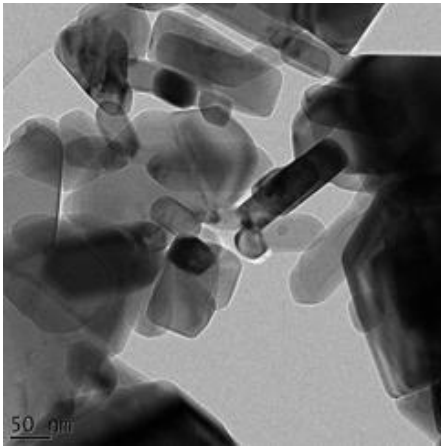
Figure E.25: TEM image of TiO₂ nanoparticles prepared in 5M concentration of HCl and water aged for a duration of 12 hr, thereafter hydrothermally treated for 12 hour
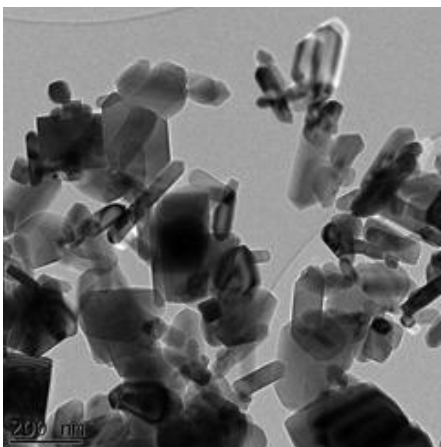
Figure E.26: TEM image of TiO₂ nanoparticles prepared in 5M concentration of HCl and water aged for a duration of 12 hr, thereafter hydrothermally treated for 12 hour
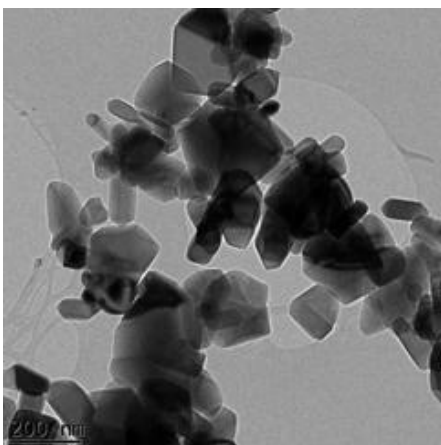
Figure E.27: TEM image of TiO₂ nanoparticles prepared in 5M concentration of HCl and water aged for a duration of 12 hr, thereafter hydrothermally treated for 14 hour
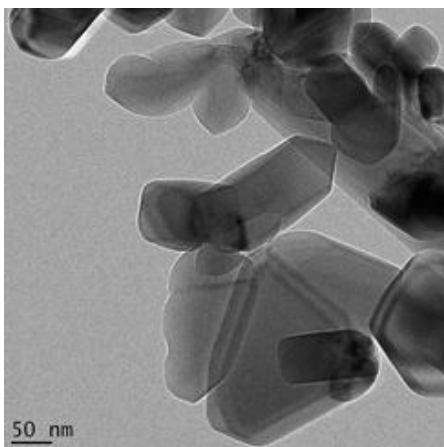
Figure E.28: TEM image of TiO₂ nanoparticles prepared in 5M concentration of HCl and water aged for a duration of 12 hr, thereafter hydrothermally treated for 14 hour